NASA CONTRACTOR REPORT 177325

Passive Orbital Disconnect Strut (PODS III) Structural Test Program

R.T. Parmley

CONTRACT NAS2– 10848
JANUARY, 1985

NASA

NASA CONTRACTOR REPORT 177325

Passive Orbital Disconnect Strut (PODS III) Structural Test Program

R.T. Parmley
Lockheed Missiles & Space Company
Palo Alto, CA 94304

Prepared for
Ames Research Center
Under Contract NAS2-10848

National Aeronautics and
Space Administration

Ames Research Center
Moffett Field, California 94035

FOREWORD

This work was conducted for the National Aeronautics and Space Administration through the Ames Research Center, Moffett Field, California, Dr. Peter Kittel, Program Manager.

The Lockheed Palo Alto Research Laboratory conducted the program within the Cryogenic Technology Group of the Thermal Sciences Laboratory. Key individuals who contributed to the success of this program and their contributions are as follows:

Ed Cavey - Designed the PODS-III support and test fixtures
J. Nickel - Assembled the PODS-III struts
J. Skogh - Performed the structural analyses
R. Boorn - Performed the structural tests
R. Wedel - Performed the thermal analyses

R. T. Parmley
Principal Investigator

CONTENTS

ILLUSTRATIONS

TABLES

Section 1
INTRODUCTION AND SUMMARY

1.1 INTRODUCTION

A prior study (Ref. 1) has shown that the support conductance is reduced by greater than a factor of 10 and the weight of a 3-year lifetime superfluid helium (SFHe) dewar is cut in half if passive orbital disconnect strut (PODS) supports are used in place of nondisconnect, state-of-the-art, fiberglass tension-band supports. The objective of this program is to design, build, and structurally test (down to 78 K) an advanced concept of this support (PODS-III). The test data are then compared with the strut's predicted performance to verify that the projected improvement in dewar performance is real. The thermal test data down to 4 K were reported previously in Ref. 2.

The PODS-III strut design described in Ref. 2 was reexamined based on new thermal and structural data obtained on boron/epoxy and graphite/epoxy composites. The boron/epoxy is a candidate to replace the fiberglass/epoxy launch tube; the graphite/epoxy is a candidate to replace the orbit fiberglass/epoxy tube.

The fiberglass/epoxy launch tube was retained, although for higher temperature cryogens and larger tanks the boron/epoxy tube should be reconsidered. The small orbit fiberglass/epoxy tube was replaced with a graphite/epoxy tube due to a heat rate that is lower by a factor of 2, a higher resonance caused by a higher modulus value, superior fatigue life at low temperature, and a lower thermal expansion value.

1.2 SUMMARY

A description of how the PODS-III support concept works is followed by a rationale for selecting S-2 glass/epoxy for the launch tube and graphite/epoxy for the orbit tube. Detailed design drawings, structural analysis, and

thermal analysis of the strut tested on this program are presented. Development tests were performed on both the S-2 glass/epoxy and graphite/epoxy tubes to verify the suitability of their selection and provide information needed for the strut design.

A detailed assembly procedure was written and updated as required to assemble one strut. Side load, axial load, evacuation, and fatigue tests were performed on this strut to verify its structural performance. Six more struts were assembled based on these results. A dewar simulator was fabricated that allowed the following tests to be performed on the six struts as a support system: (1) installation tests, (2) load tests in both the launch and orbit configurations, and (3) simulated temperature change tests including the effect of asymmetric temperature gradients around the vacuum shell. Shorting loads and design limit loads were measured and compared with results obtained previously on individual struts.

The structural test results from this program plus the thermal test results from Reference 2 verify the adequacy of the design concept. Consequently, superfluid helium dewar lifetimes of 3 years are obtainable as predicted previously in Reference 1. The struts perform structurally as designed under all load conditions from ground hold through launch and orbit environments.

Section 2
PODS-III DESIGN CONCEPT

2.1 DESIGN

The PODS-III support concept is shown in Fig. 2-1. A minimum of six struts (three pairs) is required to support a cryogen tank. (Six struts provide a statically determinate support system in all axes.) As the tank diameter changes due to cooldown or pressurization, the angled pinned-end struts are free to move in and out as the tank moves up or down slightly a value of H. A similar adjustment occurs automatically as the vacuum shell changes diameter in orbit due to temperature changes.

For purposes of installation, the warm end of the strut provides a length adjustment feature. The threads on the rod-end fitting and length adjustment are a different pitch; consequently, by rotating the adjustment hex, precise length adjustments can be made during strut installation without rotating the strut. This feature allows length adjustments after the vapor-cooled shields are attached to the struts.

The cold end of the strut provides the passive orbital disconnect feature. The cold rod-end fitting/stem is connected to the body by a thin-wall graphite/epoxy tube and adjustment bushing. The conical stem load-bearing surfaces are separated from the nut (tension) and body (compression) by an axial gap of ~0.076 mm (0.003 in.) at operating temperature. (At ambient temperature, the gaps are set to take into account the differential shrinkage between the various parts.) During one-g thermal testing or orbital flight, the conical surfaces do not touch. Consequently, heat is transferred from the body to the thin-wall graphite tube/stem/rod-end fitting subassembly by radiation and by conduction along the graphite tube. At the operating temperatures of the body (typically 20 to 30 K when vapor cooled), radiation

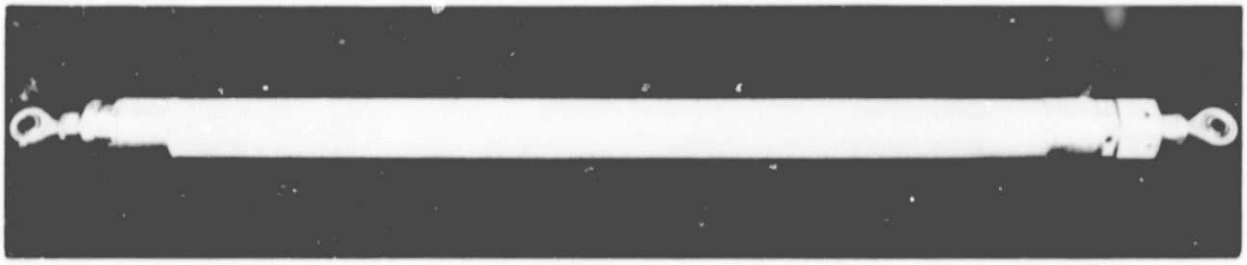

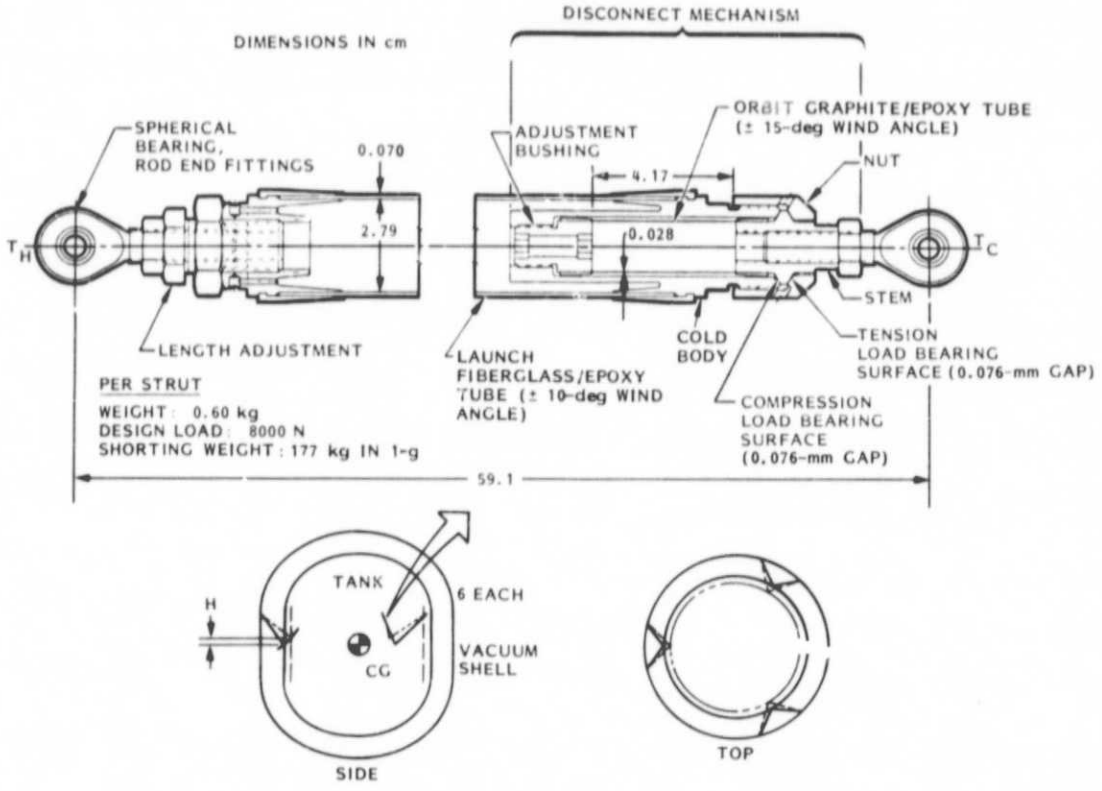

Fig. 2-1 PODS-III Support Concept

heat transfer is negligible. Essentially all heat is transferred by conduction.

During launch, the g load elastically deforms the graphite/epoxy tube along its axis; the stem's conical shoulder rests hard on the body (compression) or nut (tension). The load path bypasses the graphite/epoxy tube. The major thermal resistance and load path during launch is now the fiberglass epoxy tube. Upon achieving orbit, the stem's conical shoulder passively disconnects

from the body or nut, and the major thermal resistance is again the thin-wall graphite/epoxy tube.

This design combines the desirable features of a thermal disconnect during ground hold and orbit with the high reliability of a completely passive design. Since the struts do not short out in one-g, the orbital performance of the struts can be demonstrated in one-g thermal qualification tests and the ground hold heat leak is lower. These are both highly desirable features.

2.2 MATERIALS SELECTION CRITERIA

This section describes the rationale for using Invar parts and filament-wound fiberglass/epoxy and graphite/epoxy tubes in the design. Typical operating temperature ranges and resonance requirements for the launch and orbit tubes are shown in Table 2-1.

Table 2-1 PODS-III OPERATING TEMPERATURE RANGES AND RESONANCE REQUIREMENTS

Tube	Typical Operating Temp. Range (K)			Typical Minimum Resonance Requirements (Hz)
	Vacuum Bakeout	Ground Hold and Launch	Orbit	
Launch Tube	340	300-4	200-20	35
Orbit Tube	340	4-2	20-2	20

Both tubes must be able to withstand 340 K during prolonged vacuum bakeout (weeks) of the dewar without degradation and operate over the temperature ranges shown during ground hold and orbit flight.

For both tubes, it is desirable to use a material that has the lowest thermal conductivity (heat leak), highest modulus (high resonance), and appropriate fatigue life at the design stress levels. The launch tube is designed

structurally by Euler column buckling (where the buckling load varies directly with the modulus).

The orbit tube is designed structurally by shell buckling; again, the crippling load varies directly with the modulus. Consequently, the material with the lowest k/E ratio over the temperature range of interest is the optimum choice.

Filament-wound tubes of S-2 glass/epoxy, graphite/epoxy, and boron/epoxy are the leading candidates as shown in Tables 2-2 and 2-3 and Figs. 2-2 through 2-6. Figures 2-2 and 2-4 show that graphite/epoxy is the optimum selection for the orbit tube over the range 2 to 35 K based on the lowest conductivity and the lowest integral value of the k/E ratio. For the launch tube, the two top choices are S-2 glass/epoxy and boron/epoxy as shown in Fig. 2-4. If the k/E ratios are integrated over the orbit temperature range of 200 to 20 K, the boron/epoxy ratio is slightly superior (lower) than glass/epoxy by 6 percent.

Other factors enter the launch tube selection process, however. The minimum practical wall thickness for an unbalanced filament wrap is approximately 0.3 mm (0.011 in.) or two layers. However, because of the loads sustained by the launch tube, the minimum thickness should be at least 0.5 mm (0.020 in.) or four equivalent layers. For the tank weights being considered for instrument cooling applications, the wall thickness is normally near the minimum gage. For example, the wall thickness for the fiberglass/epoxy tube being tested on this program is 0.7 mm (0.028 in.). Consequently, it does not pay to go to the higher modulus boron/epoxy composite because the minimum tube cross-sectional area is fixed and the heat rate is higher than for an S-glass epoxy tube.

An application where boron/epoxy launch tubes are attractive is in supporting large heavy NF_3 (153 K) or LO_2 (90 K) tanks where the k/E ratio is lower than for glass/epoxy and wall gages for launch struts are above the minimum values. Boron/epoxy should also be considered for launch struts on

Table 2-2 TYPICAL PROPERTIES OF FILAMENTS

Properties	S-2 Glass (Ref. 3)	Graphite Thornel 300 WYP 30 I/O (Ref. 4)	Boron (Ref. 5)
Tensile Strength GN/m^2 (ksi)	4.6 (665)	3.10 (450)	2.8 (400)
Tensile Modulus GN/m^2 (10^6 psi)	87 (12.6)	230 (33.2)	414 (60)
Density g/cm^3 ($lb/in.^3$)	2.49 (0.090)	1.77 (0.064)	2.60 (0.094)
Filament Diameter μm (mils)	10 (0.39)	7 (0.28)	100 to 200 (4 to 8)
~Minimum Bend Radius* cm (in.)	0.01 (0.004)	0.1 (0.04)	0.6 (0.25)

* Affects possible filament winding patterns. Unlike S-2 glass or graphite, boron cannot be interwoven.

Table 2-3 COMPOSITE ELASTIC MODULUS VALUES GN/m^2 (10^6 psi)

Composite	300 K	77 K	20 K	4 K
Epoxy	2.4 (Ref. 7) (0.35)			8.5 (Ref. 13) (1.24)
S-2 Glass (Ref. 3)	87 (12.6)			
Graphite (Thornel 300) (Ref. 4)	230 (33)			
Boron (Ref. 5)	414 (60)			
S-2 Glass/Epoxy (10-deg Wind Angle, 64 Vol percent)	54 (7.8)	54 (7.8)	54 (7.8)	54 (7.8)
S-2 Glass/Epoxy (30-deg Wind Angle, 64 Vol percent) (Ref. 2)	34 (5.0)	52 (7.5)	52 (7.5)*	52 (7.5)*
Graphite/Epoxy (15-deg Wind Angle, 60 Vol percent)	110 (15.9)	104 (15.1)	104 (15.1)*	104 (15.1)*
4-mil Boron/Epoxy (0-deg Wind Angle, 50 Vol percent) (Ref. 6)	207 (30)	221 (32)	228 (33)	228 (33)

* Extrapolated

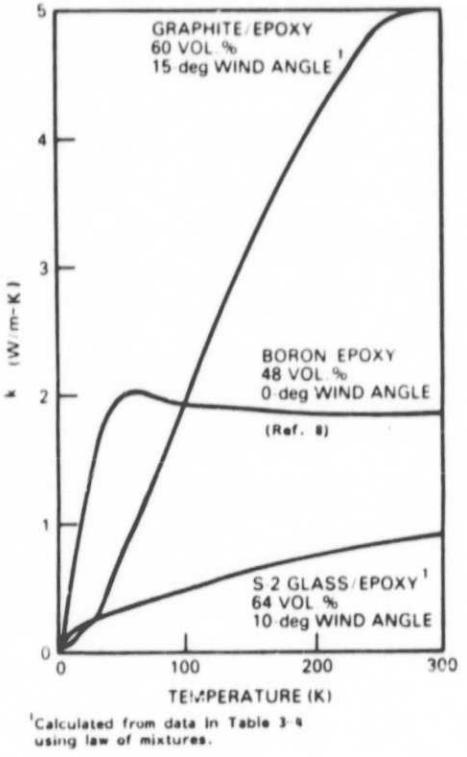

[1]Calculated from data in Table 3-4 using law of mixtures.

Fig. 2-2 Composite Thermal Conductivity Values

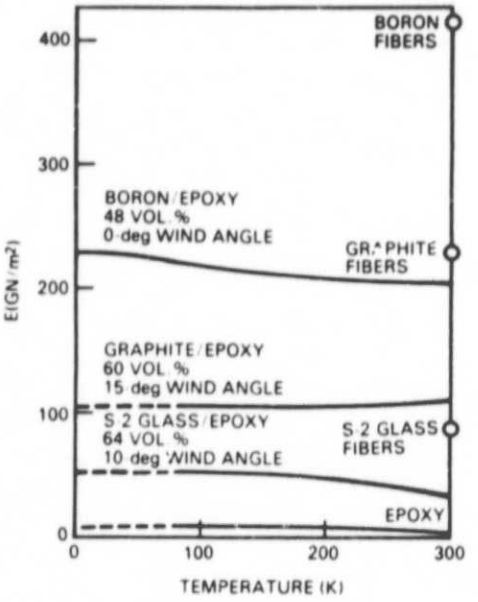

Fig. 2-3 Composite Modulus Values

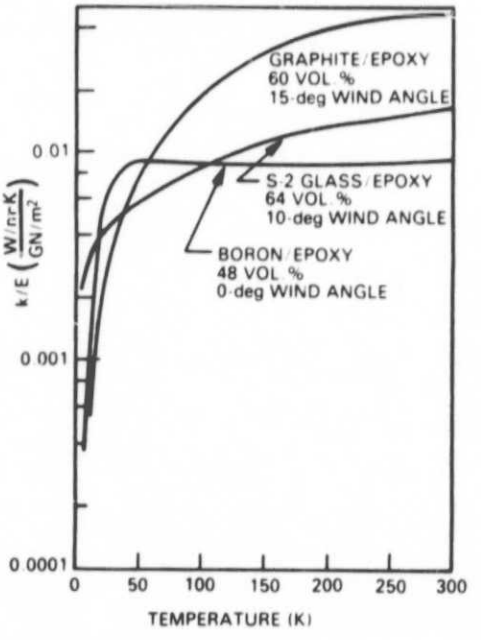

Fig. 2-4 Composite Conductivity/ Modulus Ratios

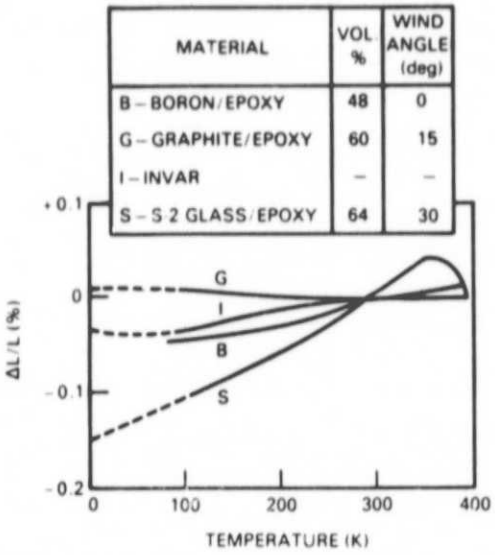

Fig. 2-5 Comparison of Composite and Invar Thermal Expansion Values

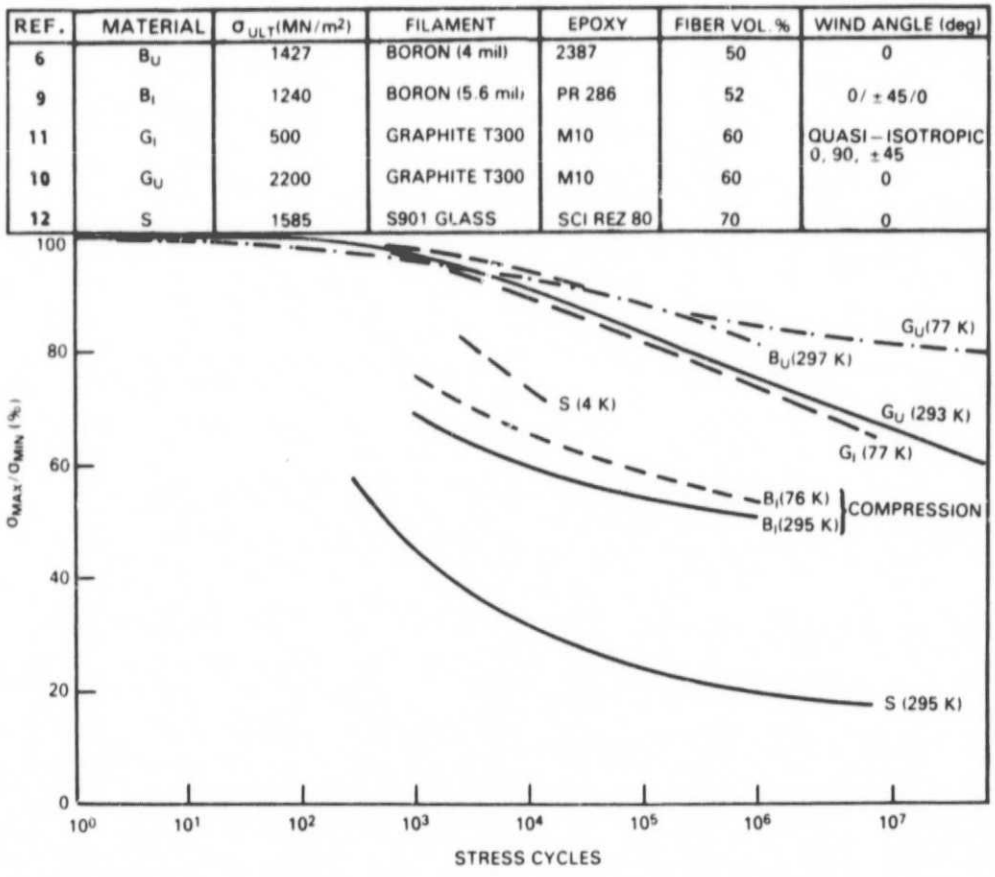

Fig. 2-6 Composite Fatigue Life

any cryogen tank that is very heavy where the minimum wall gage is not approached.

Fatigue life is also an important criterion for dynamically loaded structures. Both the graphite/epoxy and boron/epoxy composites have superior fatigue properties as compared to S-glass/epoxy (Fig. 2-6).

The orbit graphite/epoxy tube is cold at launch (4 to 2 K), so its fatigue life is excellent (Fig. 2-6). The S-glass/epoxy launch tube has a temperature gradient of 300 to 4 K. Consequently, the ambient temperature fatigue properties (warm end of the strut) designs this tube.

However, the 35-Hz resonance requirement during shuttle launch (rather than launch loads) normally drives the tube design as discussed in Ref. 1. This keeps the maximum tube stresses low. For example, the S-glass/epoxy tube stress levels in Ref. 1 for a SFHe system fall below $\sigma_{max}\ 100/\sigma_{ult} =$ 15 percent because the tube dimensions are sized by the resonance requirements. At this low stress level, the S-glass/epoxy tube has reasonable fatigue life.

The axial thermal expansion of the three composites is compared to Invar in Fig. 2-5. Gold-coated Invar is used for the end fittings. The low expansion Invar matches the composites more closely than other metal candidates such as beryllium, molybdenum, or titanium. Consequently, it induces lower thermal stresses in the bond joints. The low thermal expansion Invar also minimizes the required load gap offset at ambient temperature (see the discussion later in Section 4.1.4). All Invar parts are gold-coated to reduce the infrared emissivity and protect the Invar from corrosion.

Section 3
PODS-III STRUT TEST ARTICLE

3.1 DESIGN

The assembly drawing of the PODS-III strut is shown in Fig 3-1. Detail drawings of the parts are shown in Figs. 3-2 through 3-13. The design is identical to that recommended for flight struts.

3.2 STRUCTURAL ANALYSIS

Different parts of the PODS-III support are affected by the following design criteria:

Criterion	Design Affected
Launch Loads	• Large fiberglass/epoxy tube • Stem wedge area
Launch Resonance and Launch Thermal Resistance	• Large fiberglass/epoxy tube
Orbit Resonance, Orbit Thermal Resistance, and 1-g Thermal Test Requirement	• Thin-wall graphite/epoxy tube and gap spacing

The launch requirements design the large fiberglass/epoxy tube, while orbit requirements and 1-g thermal test requirements design the thin-wall graphite/epoxy tube. This feature is highly desirable because it allows the dimensions of each tube to be optimized separately. This optimization, performed on the PANDA-DEWAR program, considers the relationships shown in Table 3-1.

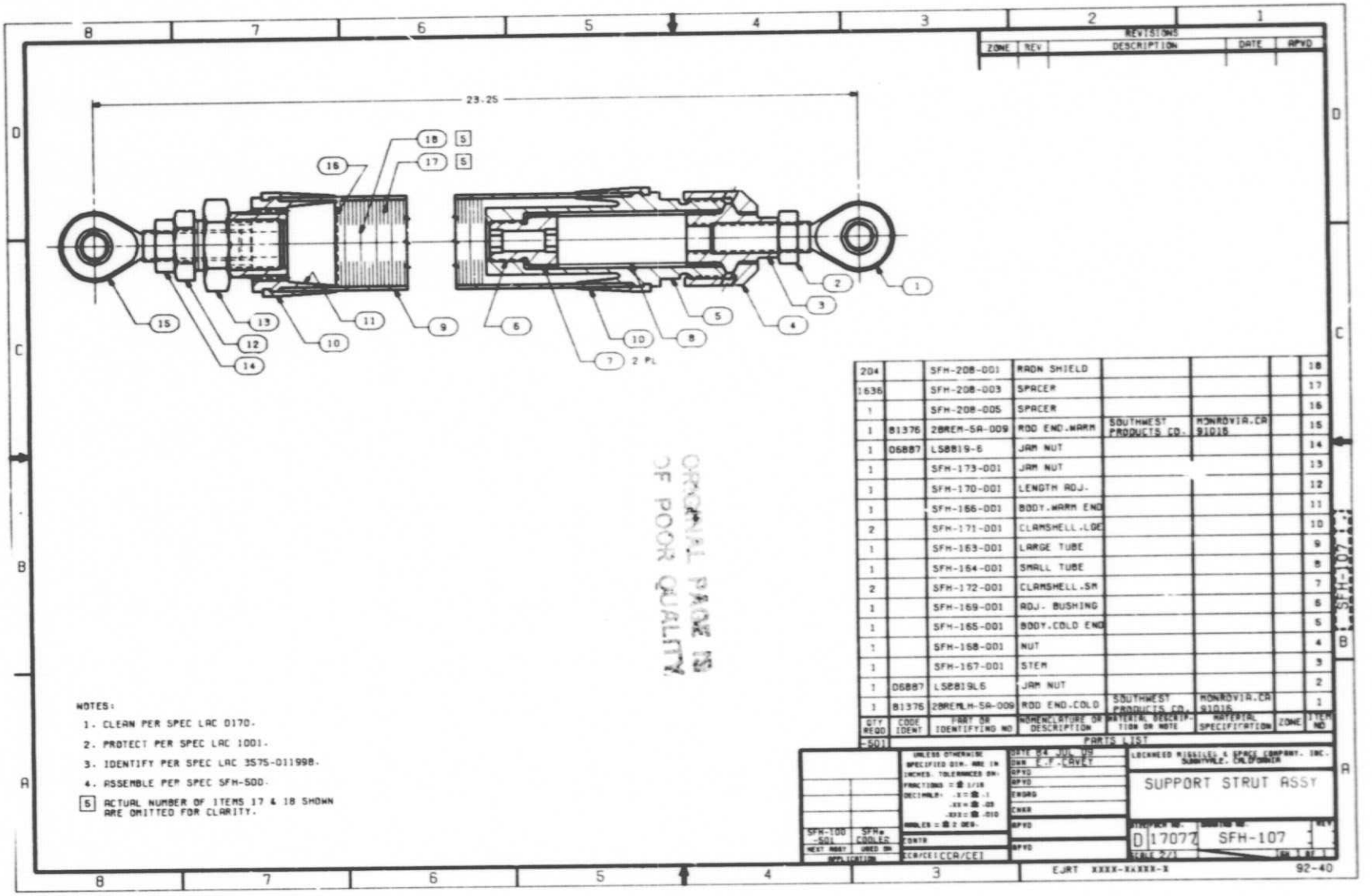

Fig. 3-1 Support Strut Assembly

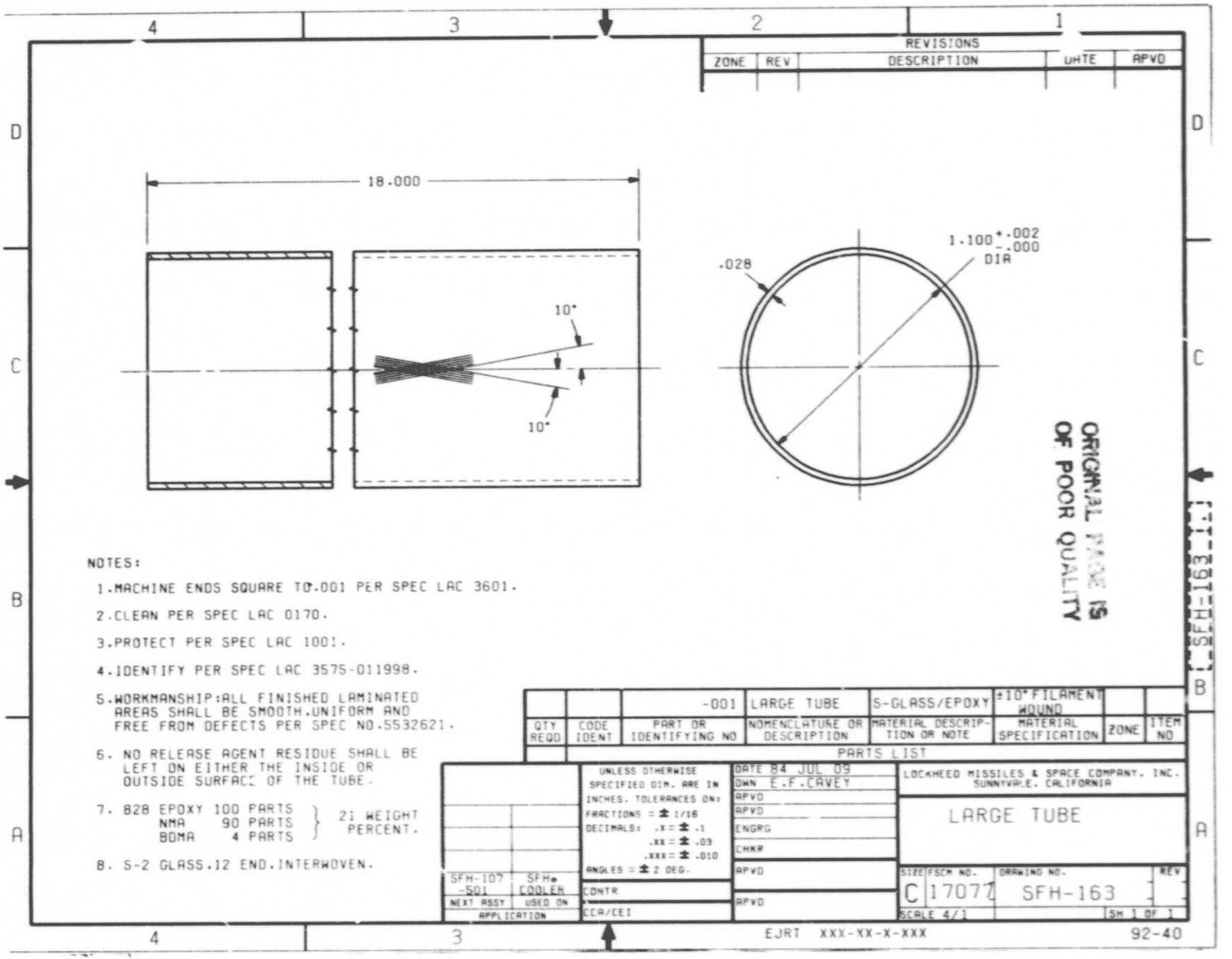

Fig. 3-2 Launch Tube

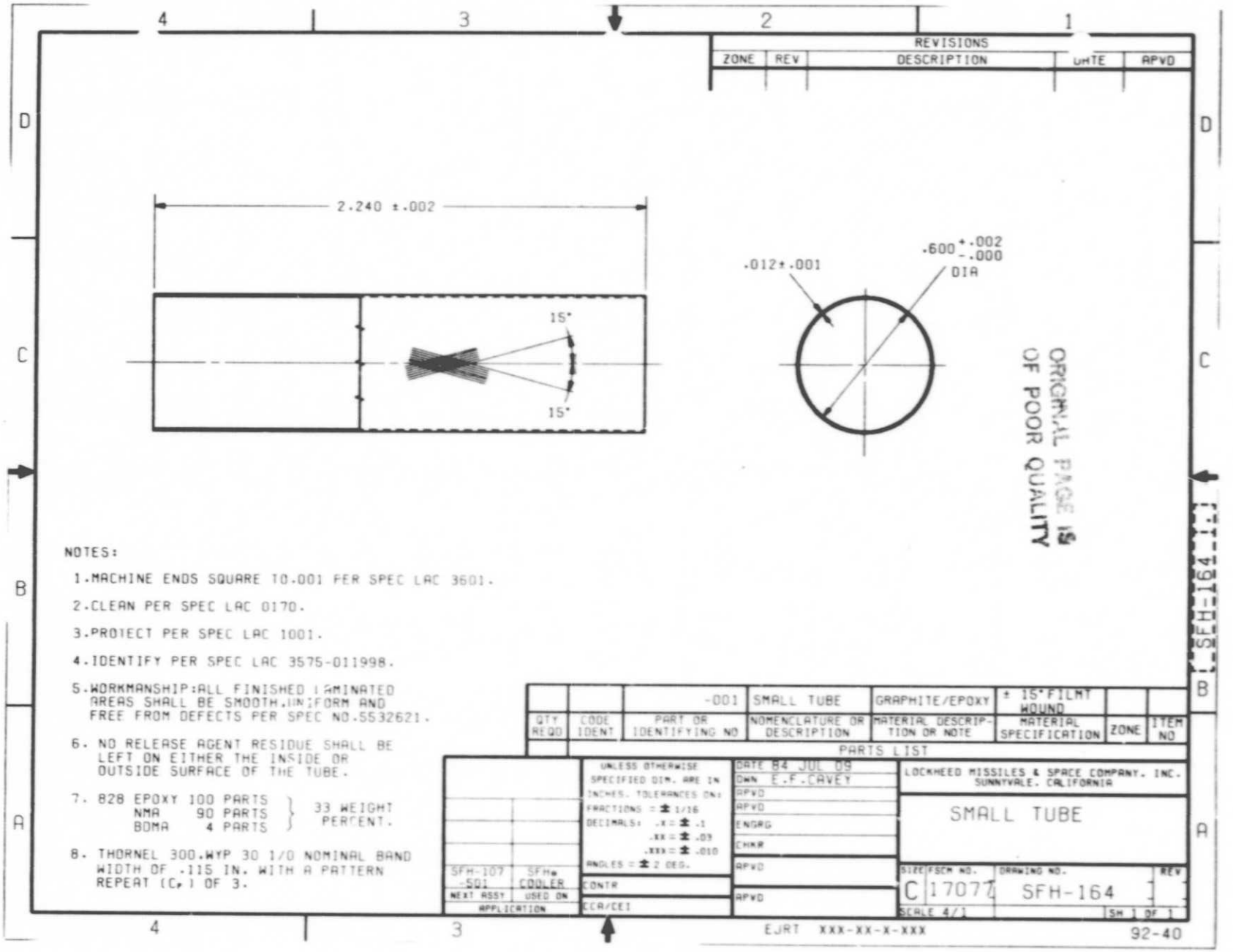

Fig. 3-3 Orbit Tube

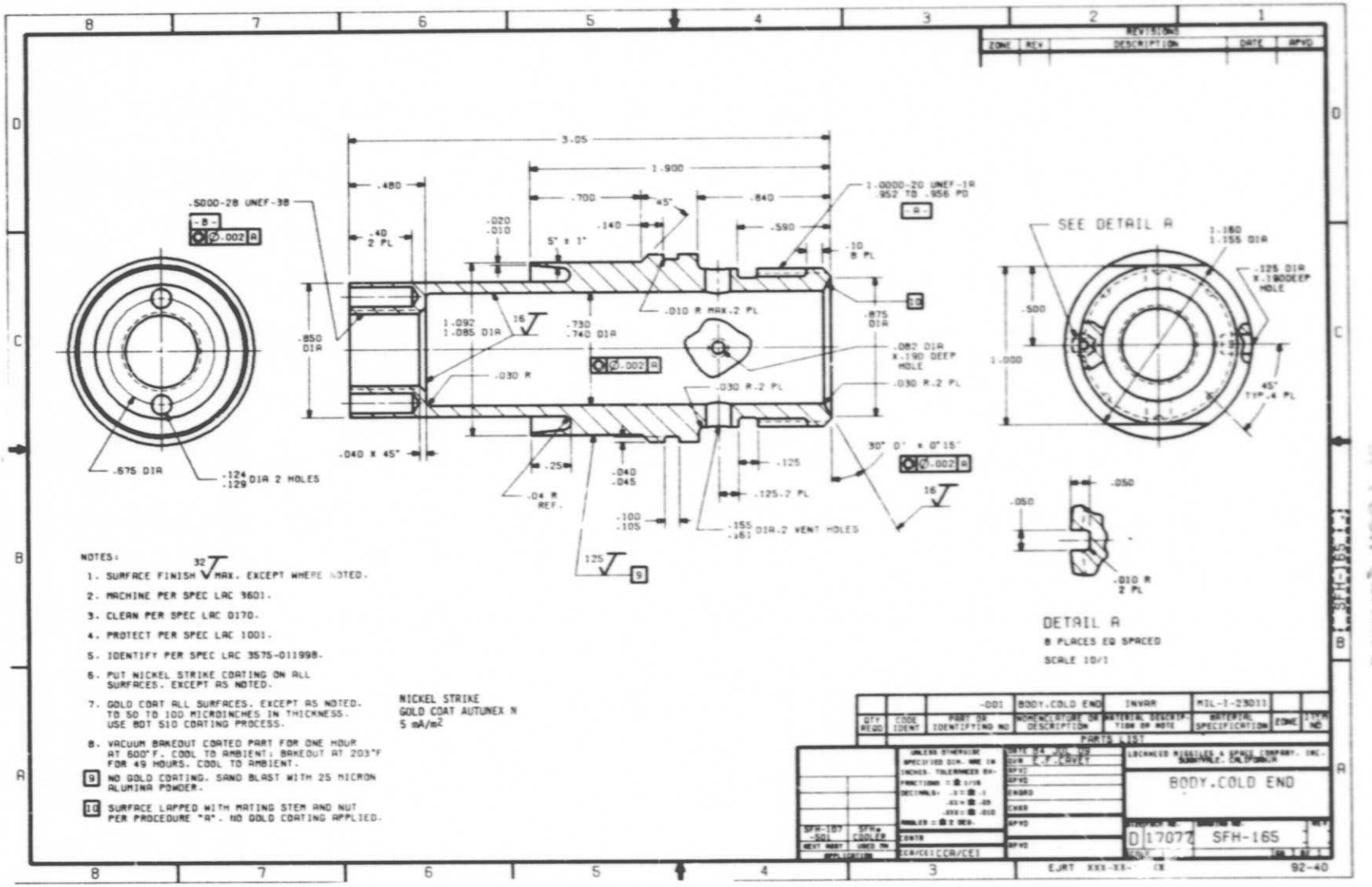

Fig. 3-4 Body, Cold End

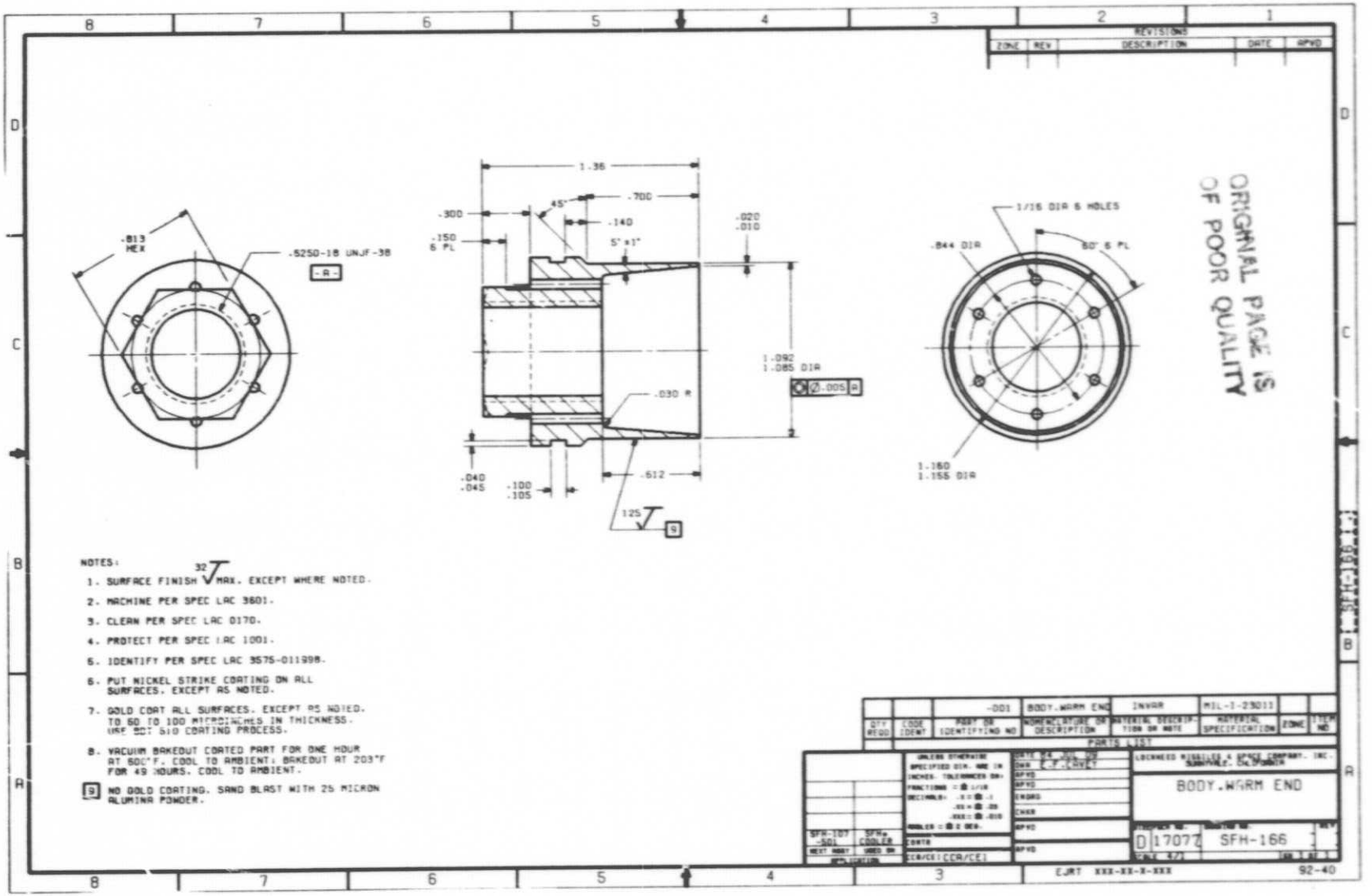

Fig. 3-5 Body, Warm End

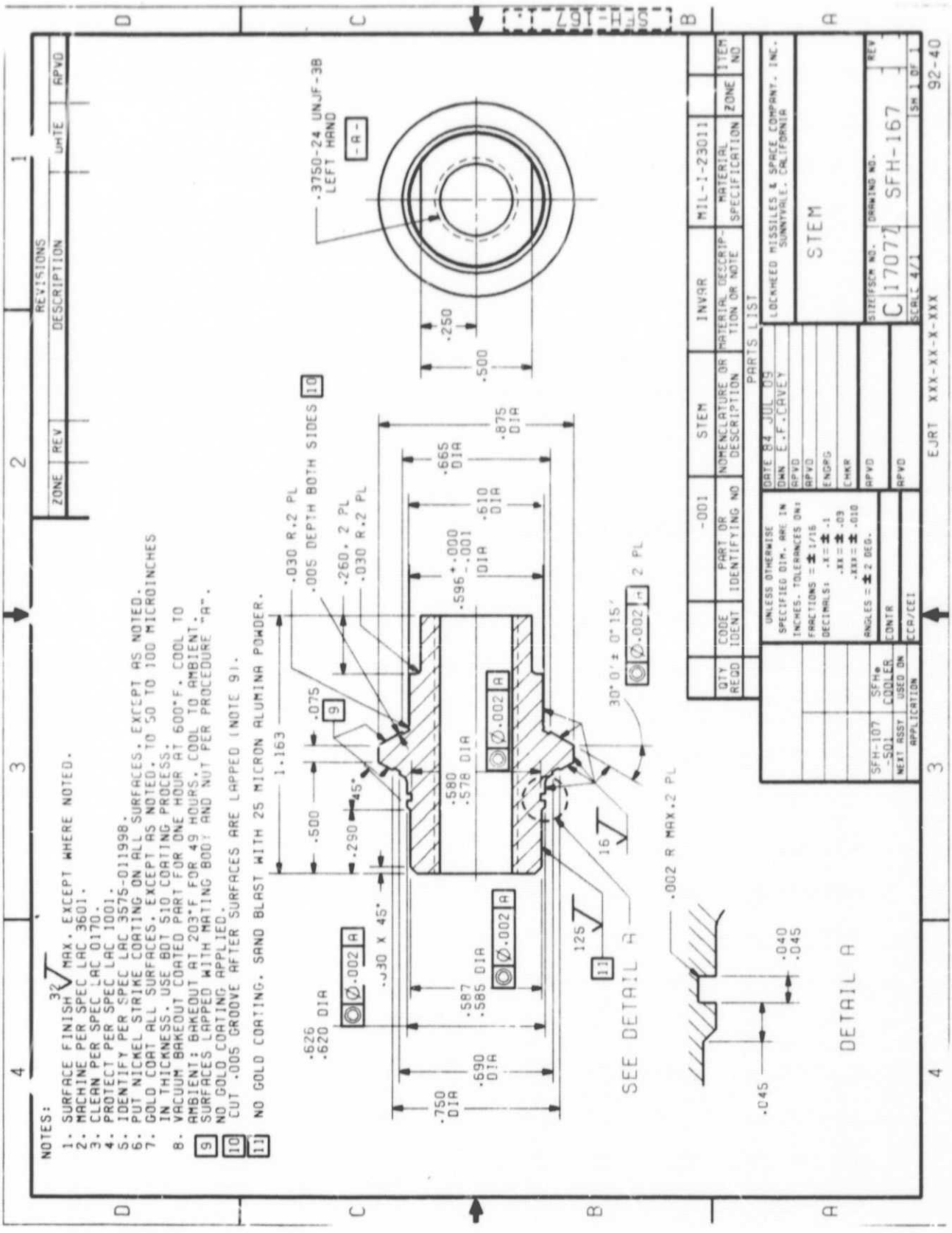

Fig. 3-6 Stem

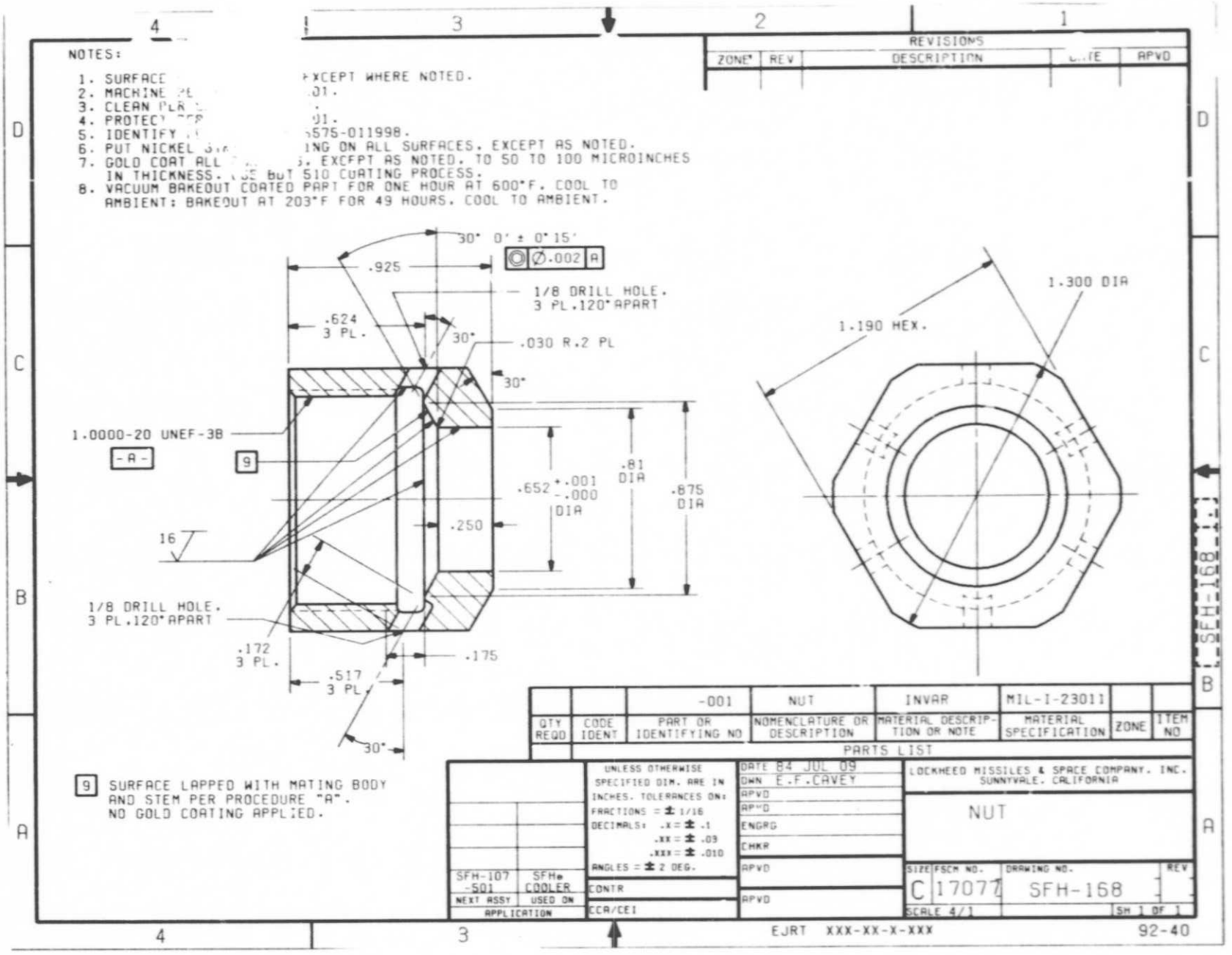

Fig. 3-7 Nut

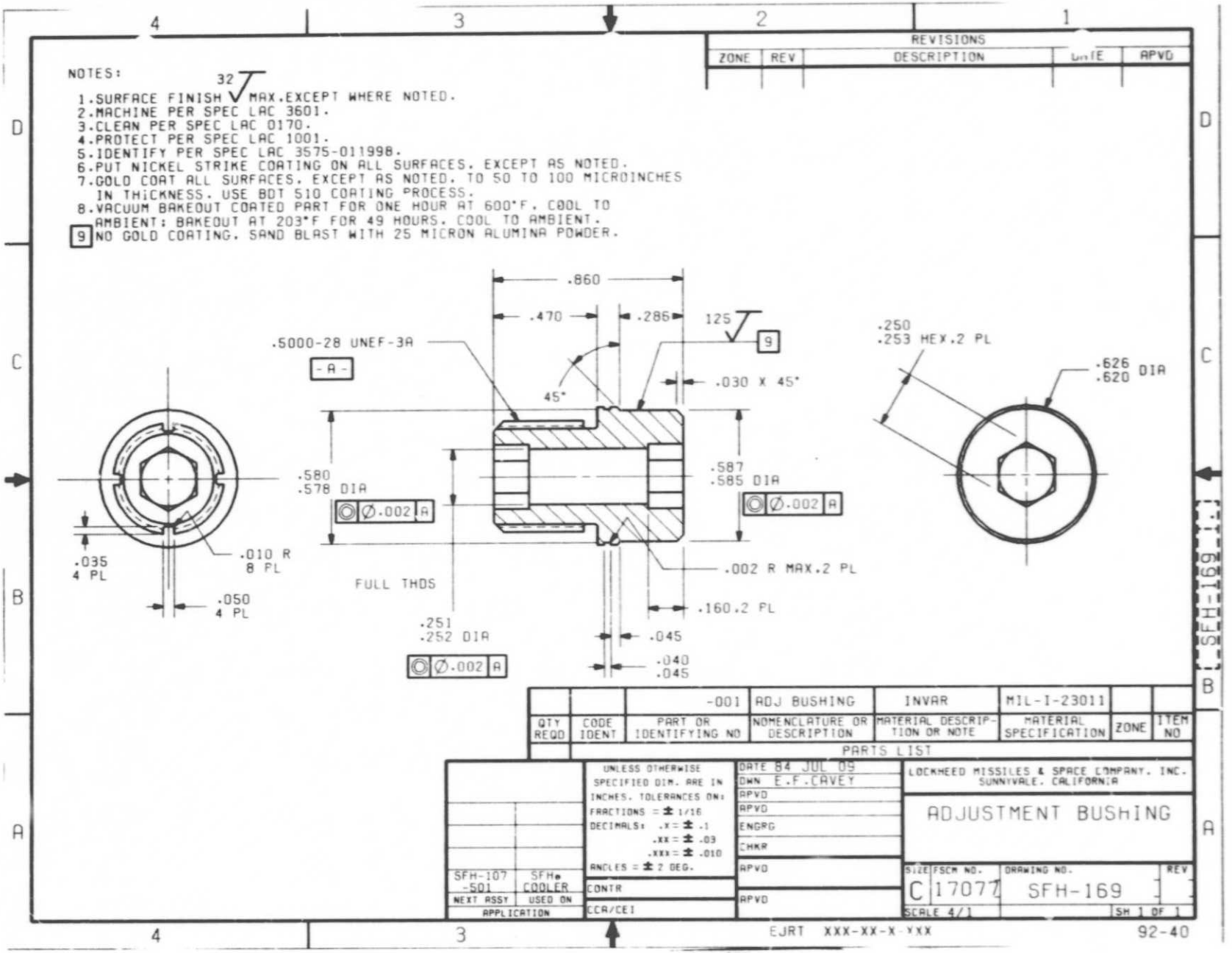

Fig. 3-8 Adjustment Bushing

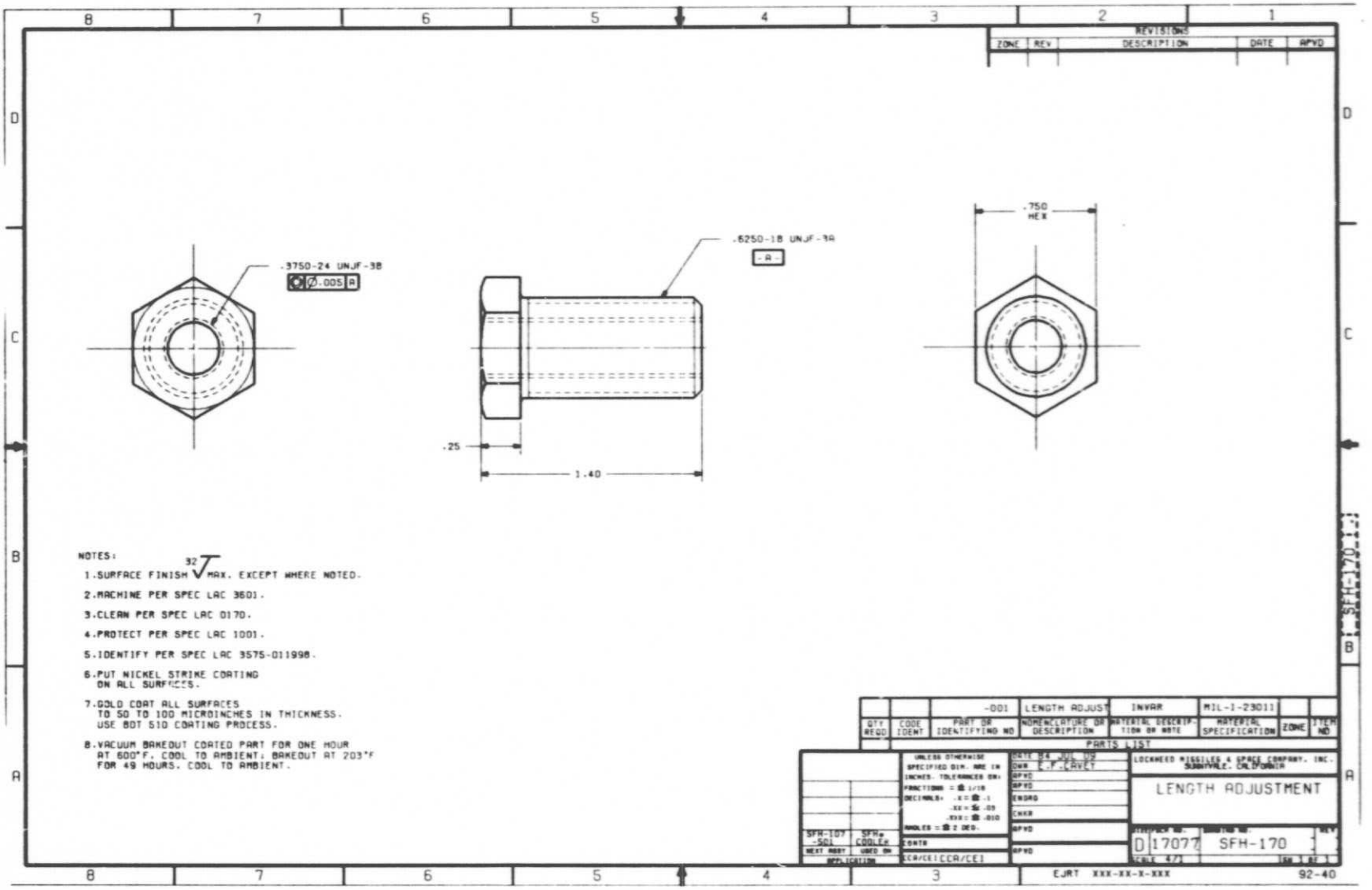

Fig. 3-9 Length Adjustment

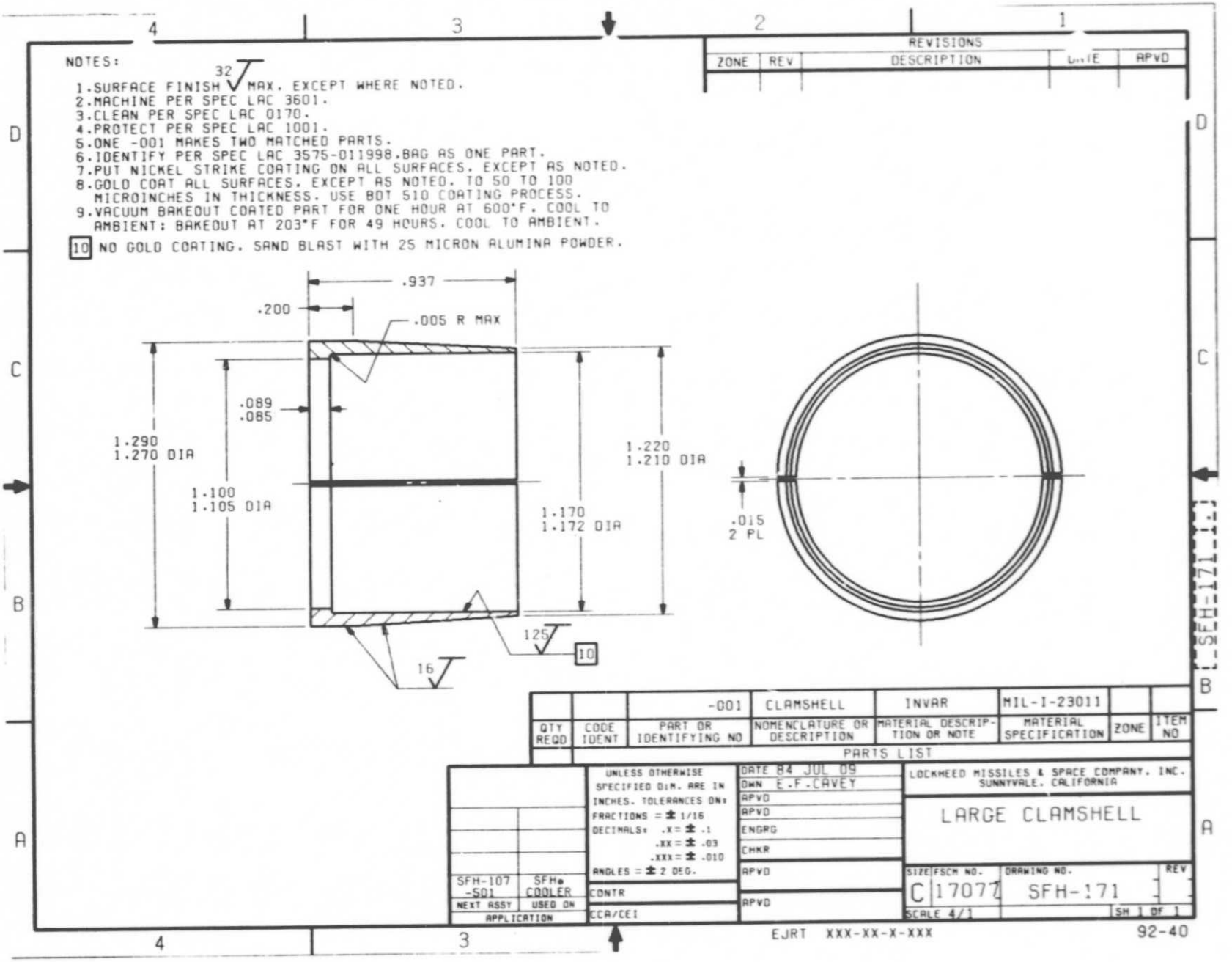

Fig. 3-10 Large Clamshell

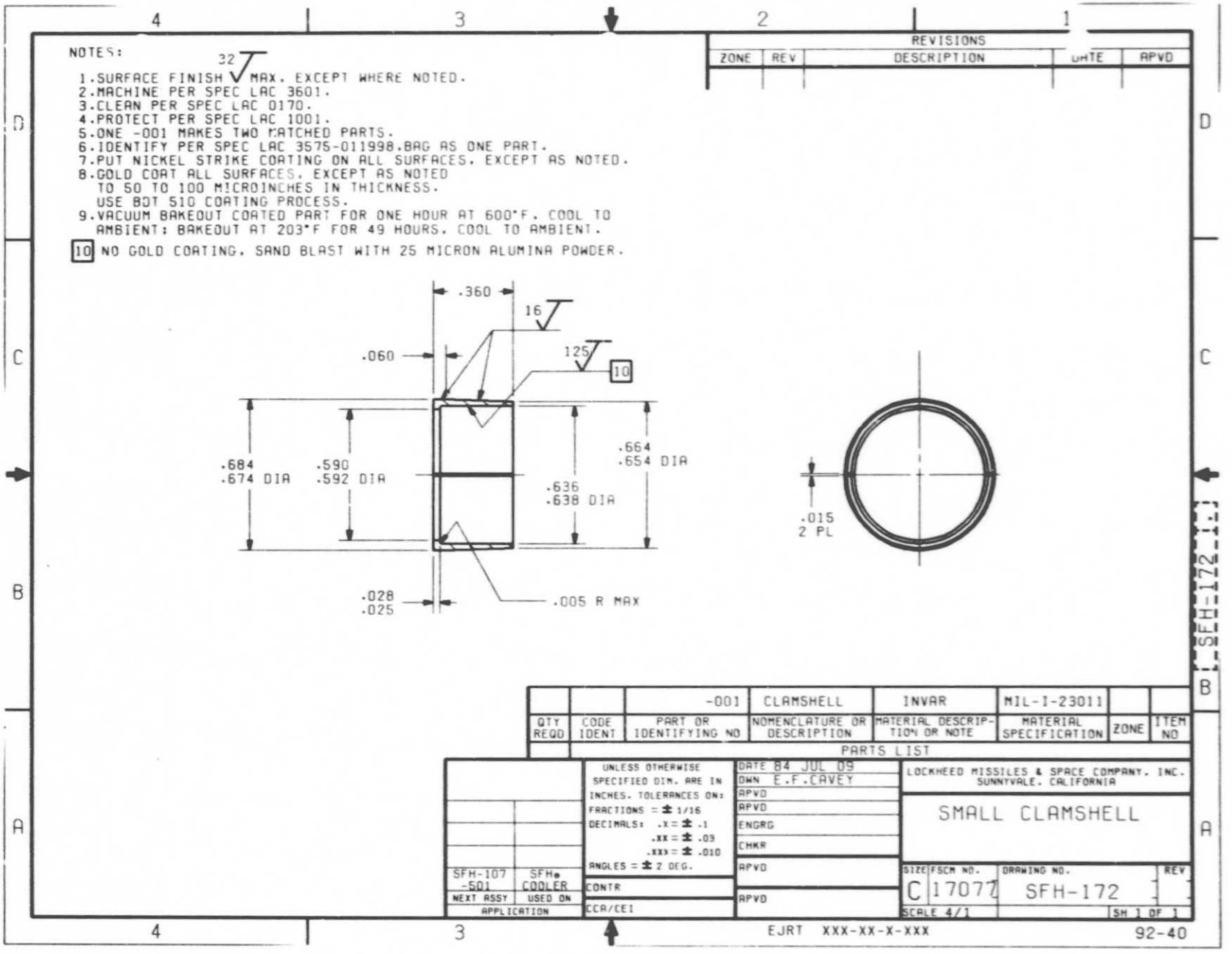

Fig. 3-11 Small Clamshell

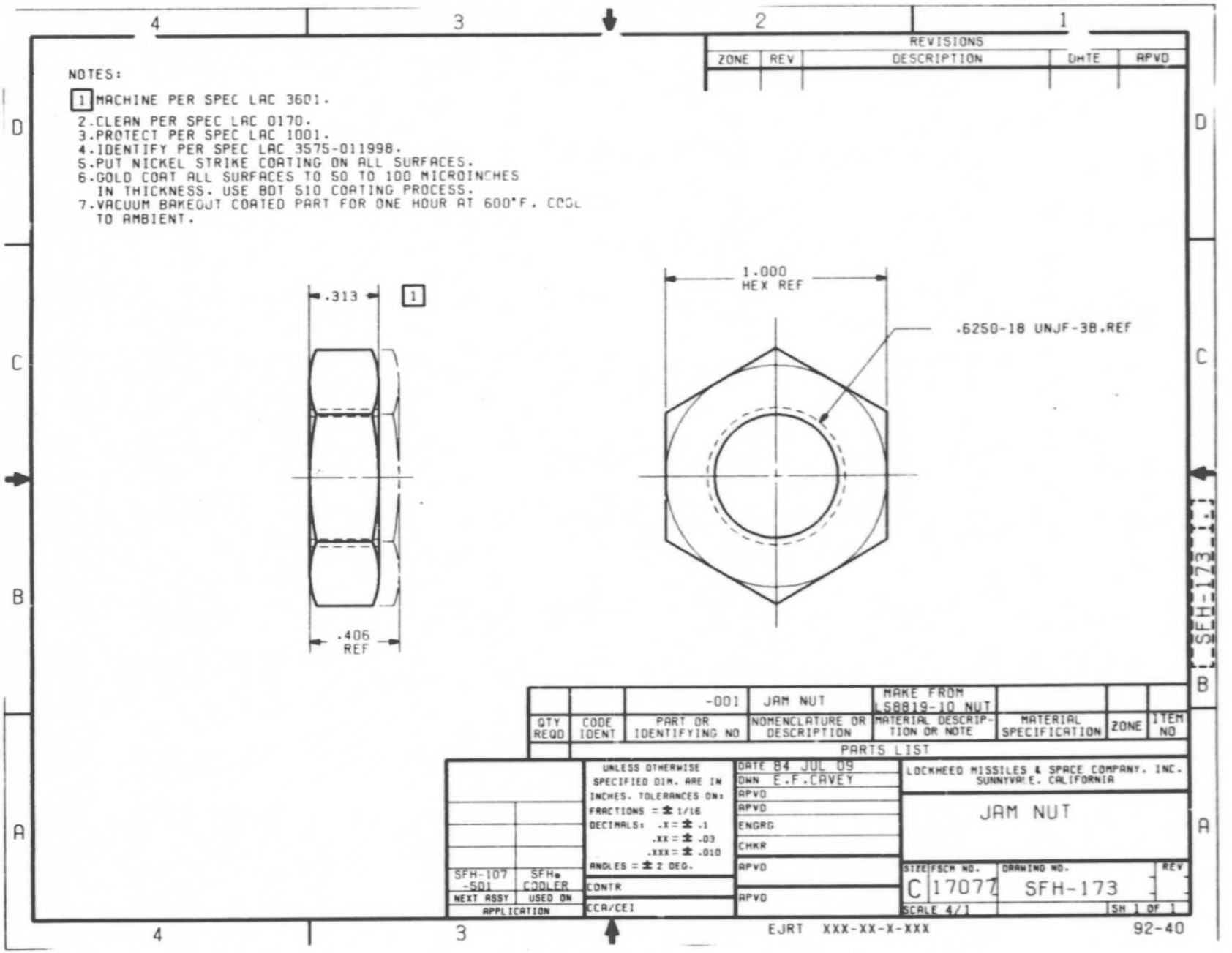

Fig. 3-12 Jam Nut

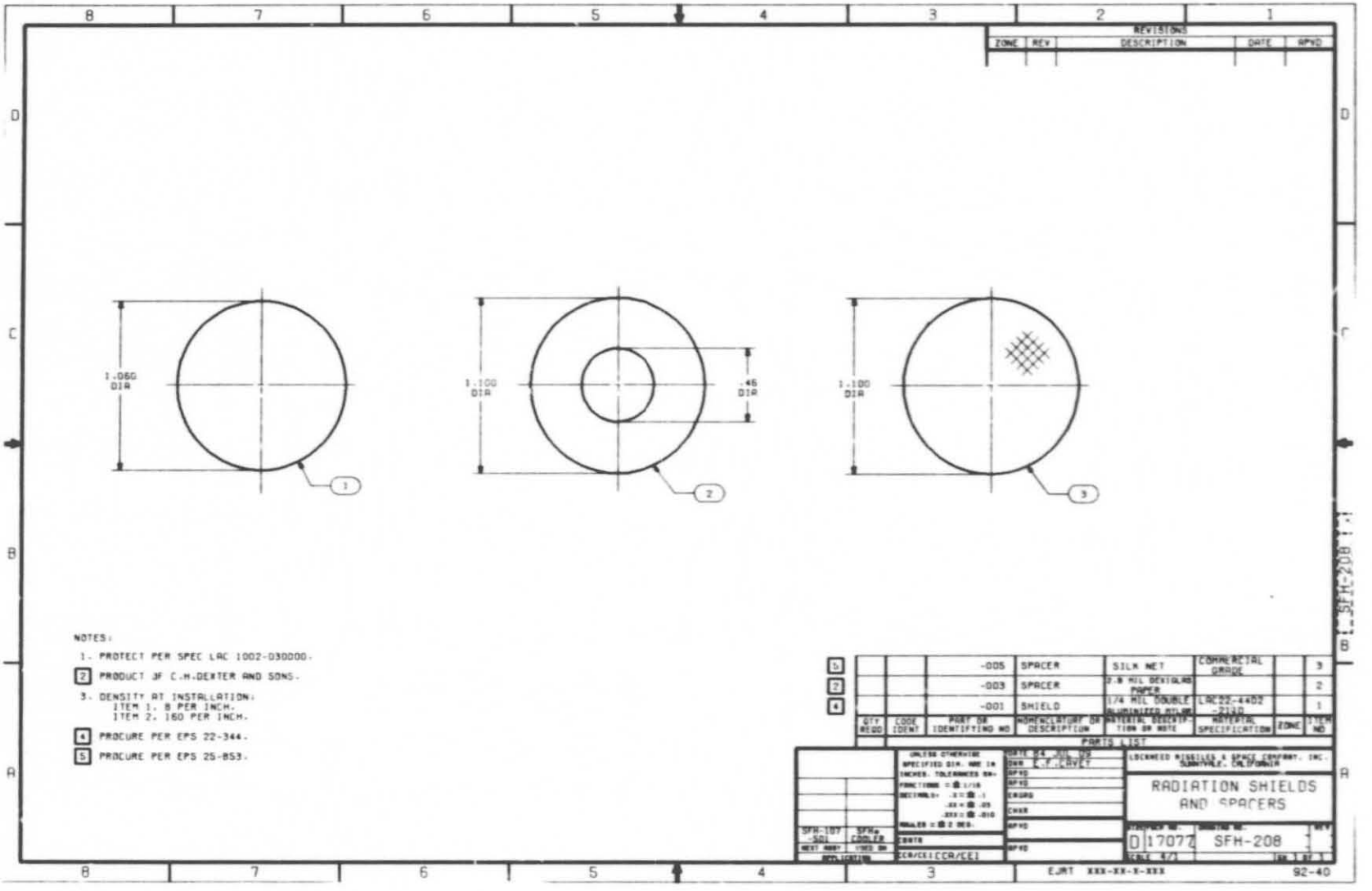

Fig. 3-13 Radiation Shields and Spacers

Table 3-1 STRUCTURAL AND THERMAL RELATIONSHIPS

	Property	Tube Radius	Wall Thickness	Length	Modulus
Structural	Resonance	$\sqrt{R}$	$\sqrt{t}$	$1/\sqrt{L}$	$\sqrt{E}$
	Tensile Strength	R	t	-	-
	Column Buckling Strength	R3	t	$1/L^2$	E
	Local Crippling Strength	1/R	t	-	E
	Side Load Resistance	R3	t	$1/L^3$	E
Thermal	Conduction Resistance	1/R	1/t	L	-
	Radiation Resistance	1/R	-	1/L	-

It is desirable to have the highest value possible for each property shown: (1) resonance, (2) tensile strength, (3) column buckling strength, (4) local crippling strength, (5) side load capability, and (6) both conduction and radiation resistance. As usual, the structural requirement of a large-radius, thick-walled, short tube is in direct opposition to the thermal requirement of a small-radius, thin-walled, long tube. This is not true in all cases; local crippling capability goes up as the radius goes down, and the radiation heat transfer goes down with smaller diameters and shorter lengths (less radiating area between the tube and gold-coated Invar body).

For column buckling, increasing the radius proportionately increases the buckling strength faster than decreasing the length. Radiation resistance increases when both the tube radius and length go down. Resonance, side load, and conduction resistance values do not change when the changes in R and L are proportionally opposite and equal.

The PANDA-DEWAR program previously optimized the large fiberglass/epoxy tube dimensions (Ref. 1) using the criteria discussed above. The thin-wall graphite/epoxy tube dimensions were set based on the following criteria:

- Six struts must support 431 kg (950 lb) in 1-g without shorting (same as Ref. 1)
- The orbit resonance is $\geq$ 20 Hz (same as Ref. 1)
- A minimum wall thickness is used based on manufacturing considerations
- Side load resistance to shorting is > 13 N (3 lb_f) based on side loads possible from vapor-cooled shields
- The orbit heat rate for six struts is approximately the same as that given in Ref. 1 for 12 PODS-I struts
- The thin-wall tube length is kept short relative to the radius to maximize column buckling strength

3.2.1 Compression and Tension Limits

Euler column buckling designs the fiberglass/epoxy launch tube.

$$P_C = \pi^2 E_C A_C / (L/\rho_C)^2$$

where

P_C = elastic column buckling load
E_C = axial compression modulus
A_C = cross-sectional area of fiberglass tube
L = strut length, center to center of rod end fittings
ρ_C = (0.707)(tube outer diameter/2) = 0.409

The optimum wind angle for the fiberglass/epoxy tube is 10 deg. (Fig. 3-14). The optimum wind angle for the graphite/epoxy tube is 15 deg. (Fig. 3-15).

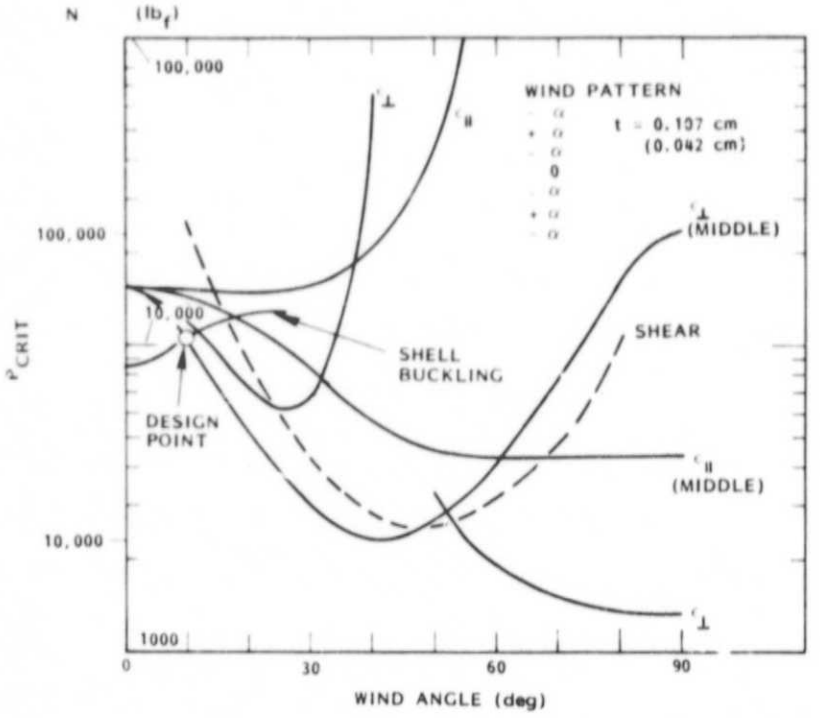

Fig. 3-14 Optimum Wind Angle for the Fiberglass/Epoxy Tube

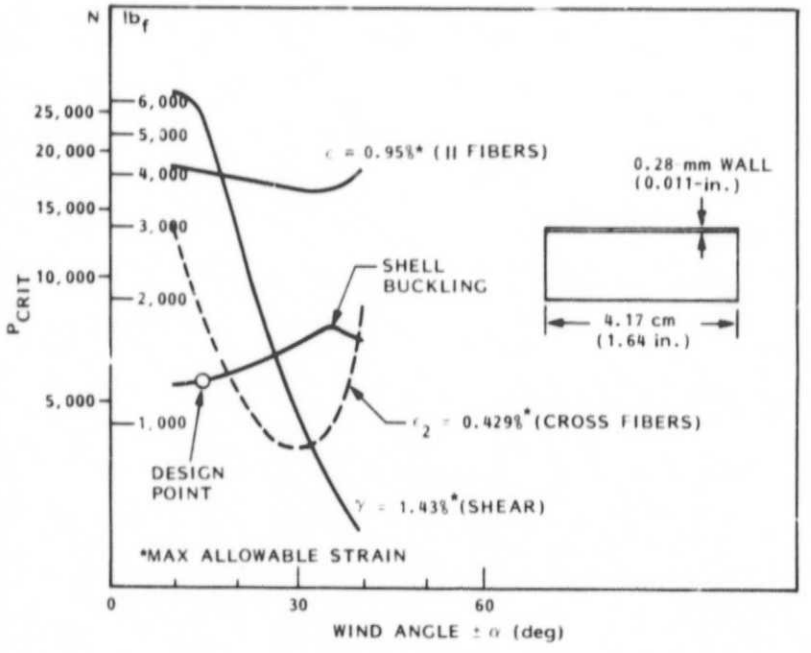

Fig. 3-15 Optimum Wind Angle for the Graphite/Epoxy Tube

NOTE: The ultimate strain ϵ is calculated versus wind angle and critical load parallel ($\parallel$) to the fibers, perpendicular ($\perp$) to the fibers, and in shear between fibers. The shell buckling mode of failure is also shown. The design points chosen provide near maximum critical load capability for each tube. The wind angle was also chosen nearer to 0 than 90 deg to maximize the axial modulus for column buckling loads yet provide enough of a wind angle for hoop stability.

The ultimate tension load L_T equals

$$L_T = F_{tu}A_c$$

where

F_{tu} = ultimate tensile strength of tube
A_c = cross-sectional area of tube

The epoxy bond shear strengths L_s are calculated as follows

$$L_s = F_{ts}A$$

where

F_{ts} = epoxy shear strength
A = epoxy bond area

Based on the dimensions and material properties shown in Table 3-2, the ultimate loads were calculated as shown in Table 3-3. For the most critical loads in compression, tests were performed, and the results were compared to the predicted values. The epoxy-bond areas were set so the bond shear strengths exceed the ultimate tension loads for either tube.

3.2.2 Shorting Weight

Based on the modulus and dimensions of the Invar parts in the passive orbital disconnect mechanism and the graphite/epoxy tube, the shorting weight was calculated as a function of the gap spacing as shown in Fig. 3-16. The average measured values for six struts (from Section 7) are also shown. Additional compliance in the system, i.e., epoxy bonds, may account for the difference between predicted and measured values.

Table 3-2 STRUT PROPERTIES

Rod End to Rod End Length, m (in.)	0.59	(23.25)
S-Glass/Epoxy Tube Properties		
Inside Diameter, m (in.)	0.0279	(1.100)
Wall Thickness, m (in.)	0.00071	(0.028)
Cross-Sectional Area, m^2 ($in.^2$)	0.000064	(0.099)
Bond Area, Each End, m^2 ($in.^2$)	0.0032	(4.96)
Modulus, N/m^2 (psi)	5.4410^{10}	(7.8×10^6)
Tensile Ultimate, N/m^2 (psi)	1.4×10^9	(200,000)
$\sigma_{MAX}/\sigma_{ULT}$, 10^6 cycles	0.20	
Graphite/Epoxy Tube Properties		
Inside Diamter, m (in.)	0.0152	(0.600)
Wall Thickness, m (in.)	0.00029	(0.0113)
Cross-Sectional Area, m^2 ($in.^2$)	0.000014	(0.0217)
Bond Area, Each End, m^2 ($in.^2$)	0.00064	(0.99)
Modulus, 77 K, N/m^2 (psi)	1.0×10^{11}	(15.1×10^6)
Tensile Ultimate, 4 K, N/m^2 (psi)	1.72×10^9	(250,000)
$\sigma_{MAX}/\sigma_{ULT}$, 10^6 cycles	0.73	
1210 A/9615-10 Epoxy Adhesive with 5 percent by Weight 4-mil Glass Beads Added		
Shear Strength, N/m^2 (psi)		
300 K	22×10^6	(3200)
77 K	16×10^6	(2300)
4 K	15×10^6	(2200)

Table 3-3 CALCULATED VERSUS MEASURED ULTIMATE LOADS

Material	Calculated N (lb_f)	Measured[3] N (lb_f)
S-Glass/Epoxy Tube		
Column Buckling	10,264 (2308)[1]	12,317 (2769)
Tension	32,000 (7200)	-
Graphite/Epoxy Tube		
Shell Buckling	5650 (1270)	4272 (961)[2]
Tension	8000 (1800)	-
Epoxy Bonds		
S-Glass to Invar	44,000 (9900)	-
Graphite to Invar	8800 (1980)	-

1 Assumes tube length is rod end to rod end length
2 78 K
3 See sections 4.1.3 and 4.4

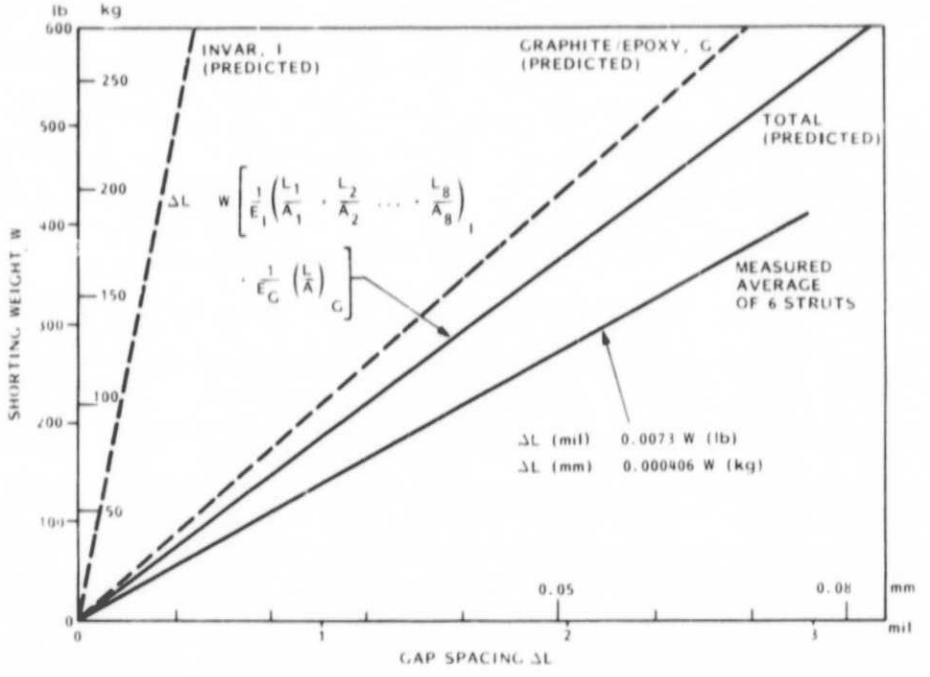

Fig. 3-16 Shorting Weight Versus Gap Spacing

3.2.3 Dimensional Stability of the Graphite/Epoxy Tube

Different strut loads and environments prior to flight can change the load gap setting by altering the length of the graphite/epoxy tube. These include: (1) moisture content, (2) creep under load prior to tank fill and after tank fill, and (3) microcracking due to thermal cycling between 300 and 2 K. The ADVLAM composite laminate analysis code was used to analyze each of these conditions as shown in Fig. 3-17. The weights used in the creep analysis per strut were 7 kg for an empty tank and 14.7 kg for a full tank based on a 200-L tank volume and a strut angle of 55 deg from the horizontal.

Two of the effects can be eliminated by processing procedures. Vacuum baking out the graphite/epoxy tube at 340 K for 1 week and storing the tube in a dessicator eliminates the moisture effect. The rate at which moisture is readsorbed back into the composite is slow enough (Fig. 3-18) so the gaps can be set in ambient air over several hours and then placed back in the dessicator until the epoxy cures. Once the struts are installed in the dewar, the vacuum bakeout at 340 K for several weeks will remove the residual moisture that was readsorbed prior to pumpdown, bringing the gap setting back to where it was during assembly.

Microcracking is not predicted for this tube because the critical transverse stress going from 422 K (tube cure temperature) to 2 K is 16.4×10^6 N/m^2 (2387 psi). This is less than the 34.5×10^6 N/m^2 (5000 psi) transverse strength predicted for a ± 15-deg wind angle laminate. To be safe, two immersions of the tube in liquid nitrogen were included prior to assembly (Section 5) to eliminate this variable.

Creep under load shows very low values when cold but significantly higher values when at room temperature. This creep effect is not completely reversible. Typically 50 percent of the creep value remains after load removal. A simple creep test was conducted on the strut fabricated in Task 6. A 14-kg (31-lb) weight was hung on the strut for 138 h at ambient humidity and temperature. No measurable change (< 0.6 percent) in the tension

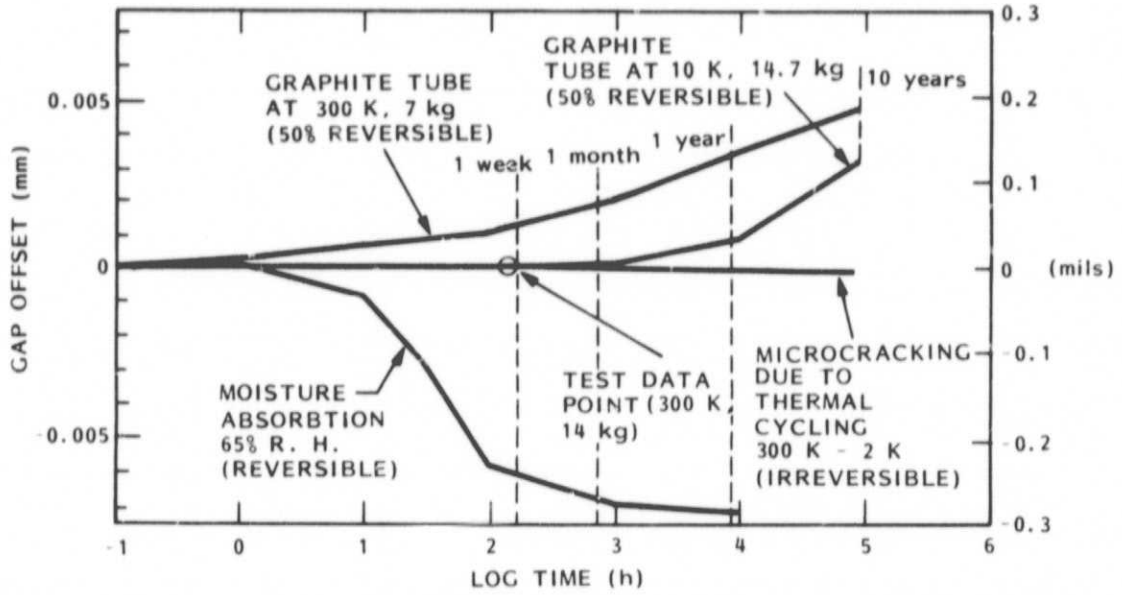

Fig. 3-17 Dimensional Stability of the Graphite/Epoxy Tube

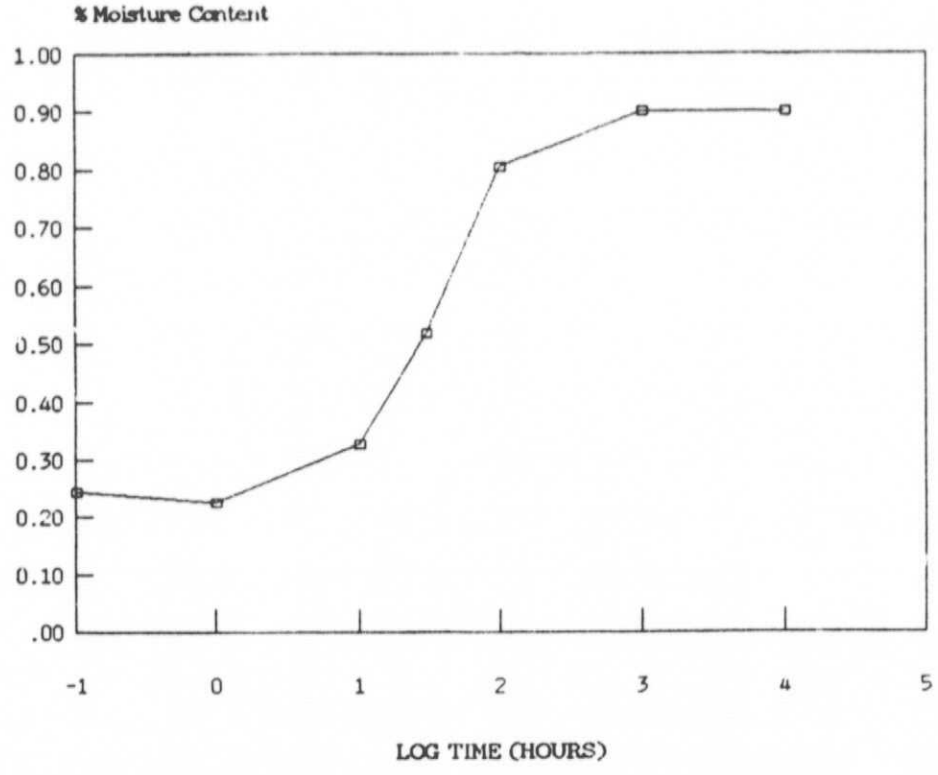

Fig. 3-18 Moisture Absorbtion Rate, Graphite/Epoxy Tube

shorting weight was recorded after load removable (within the accuracy of the measurement).

3.3 THERMAL ANALYSIS

A conduction network (Fig. 3-19) was programmed to predict the heat rates through the PODS-III strut at the cold end. This network includes only conduction, since radiation heat transfer between the body and stem amounts to less than 2 percent of the solid conduction at 40 K, the highest temperature the body will run when vapor-cooled. The contact resistances of the epoxy-bonded gold-coated threaded body/adjustment bushing and the threaded stem/rod end were assumed to be zero. The length of resistors R_3 and R_4, 0.0417 m (1.64 in.), was divided by a cos 15-deg term to take into account the winding angle of the graphite filaments, effectively increasing the filament or epoxy lengths and decreasing the heat rate down the tube.

The cross-sectional area of the graphite was obtained by multiplying the tube cross-sectional area by the volume fraction of graphite 0.595. The cross-sectional area of epoxy was obtained by multiplying the tube cross-sectional area by the volume fraction of epoxy, 0.405. Thermal conductivity values used in the analysis are provided in Table 3-4. Data on S-2 glass and boron are also provided for comparison.

The calculated heat leak per strut for minimum wall thicknesses is shown in Fig. 3-20 for the orbit tube using both S-2 glass/epoxy and graphite/epoxy. Typically, the vapor-cooled body will run near 20 K. At this temperature, the heat leak is cut in half using graphite in place of S-2 glass. Prior thermal tests at T_C = 4 K and T_H up to 40 K (Ref. 2) have shown that this model predicts heat rates that are 10 to 16 percent higher than the measured rates for an S-2 glass/epoxy tube.

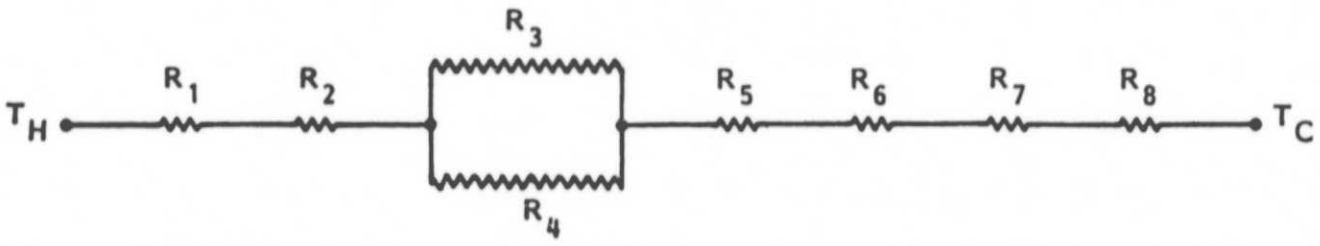

Part	Resistor	Material	Area (m^2)	Length (m)	A/L (m)
Body/Adjustment Bushing	R_1	Invar	1×10^{-4}	0.013	0.0077
Bond Line	R_2	Epoxy	3.7×10^{-4}	0.00013	2.85
Graphite/Epoxy	R_3	Graphite	0.083×10^{-4}	0.0431	0.000193
Graphite/Epoxy	R_4	Epoxy	0.057×10^{-4}	0.0431	0.000132
Bond Line	R_5	Epoxy	3.7×10^{-4}	0.00013	2.85
Stem	R_6	Invar	2.0×10^{-4}	0.0295	0.0068
Rod End	R_7	Inconel 718	0.6×10^{-4}	0.0066	0.009
Rod End	R_8	Inconel 718	0.3×10^{-4}	0.0089	0.0034

Fig. 3-19 PODS-III Test Article Conduction Nodal Network

Table 3-4 THERMAL CONDUCTIVITY VALUES

Temp (K)	THERMAL CONDUCTIVITY (W/m-K)								
	828 Epoxy (Ref. 14)	S-2 Glass (Ref. 15)	Graphite Thornel 300 (Ref. 14)	Boron (Ref. 16)	S-2 Glass/ Epoxy 0.64 Volume Fraction 10-deg Wind Angle	Graphite/ Epoxy 0.60 Volume Fraction 15-deg Wind Angle	Boron/ Epoxy 0.48 Volume Fraction 0-deg Wind Angle	Invar (Ref. 17)	Inconel 718 (Ref. 21)
2	0.034	0.036	0.019		0.03	0.02	-	0.10	1.7
4	0.046	0.110	0.032		0.09	0.04	-	0.23	1.8
6	0.046	0.173	0.045		0.13	0.05	0.22	0.40	1.9
8	0.047	0.219	0.058		0.16	0.05	0.36	0.60	2.2
10	0.051	0.243	0.067		0.17	0.06	0.50	0.80	2.3
15	0.070	0.296	0.15		0.22	0.12	0.85	1.3	2.7
20	0.083	0.326	0.25		0.24	0.17	1.16	1.8	2.9
25	0.093	0.357	0.39		0.25	0.26	1.43	2.2	3.3
30	0.107	0.371	0.52		0.27	0.34	1.65	2.7	3.5
35	0.115	0.382	0.70		0.28	0.45	1.80	3.2	3.9
40	0.122	0.411	0.90		0.30	0.57	1.91	3.7	4.2
50	0.128	0.48	1.3		0.35	0.80	2.02		4.8
100	0.15	0.70	3.4		0.49	2.0	1.94		7.1
150	0.16	0.94	5.4		0.65	3.2	1.90		8.3
200	0.19	1.09	7.1		0.76	4.2	1.86		9.0
250	0.23	1.21	8.3		0.84	4.9	1.85		9.6
300	0.26	1.32	8.5	20 (Crystal-line)	0.92	5.0	1.87		11.1

Notes: 1. Volume fractions and wind angles shown are typical
2. Composite conductivities can be calculated using the conductivities of the individual components

$$k_{composite} = \text{Cos wind angle}[V_{fiber}k_{fiber} + (1 - V_{fiber})k_{epoxy}]$$

Limits on this equation:
S-2 Glass/Epoxy - Good over entire range
Graphite/Epoxy - Good down to 15 K predicts too high below 15 K
Boron/Epoxy - Crystalline conductivity not applicable since boron filament is amorphous. Large variations in conductivity can occur from batch to batch, i.e., 50 percent due to differences in the amorphous state

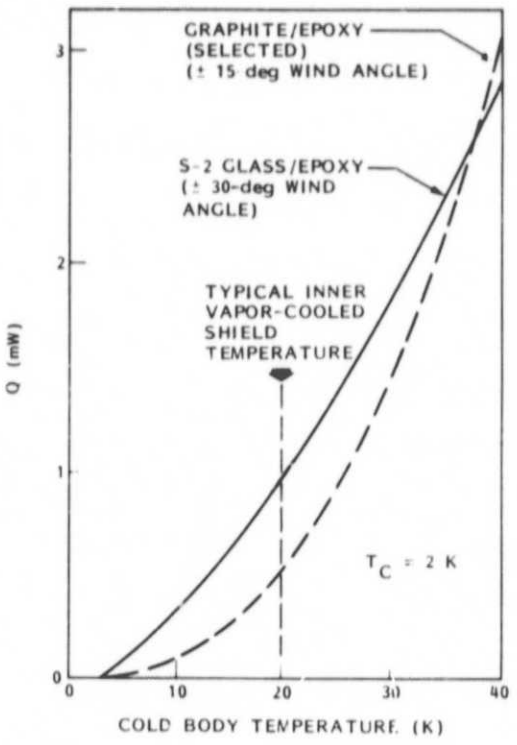

Fig. 3-20 PODS-III Heat Rate Versus Fiber Type

Section 4
DEVELOPMENT TESTS

A series of development tests characterized the graphite/epoxy orbit tube and the fiberglass/epoxy launch tube.

4.1 GRAPHITE/EPOXY ORBIT TUBE TESTS

4.1.1 Graphite/Epoxy Tube Properties

Dimension, weight, and volume measurements were made on the graphite/epoxy tubes as shown in Table 4-1. The figure also shows the tests or struts where the tubes are used. Density is obtained by weighing the tube in air and then in water to determine the tube volume. The average wall thickness is determined by knowing the tube volume (from the water displacement weighings), inside diameter, and length. The inside diameter is measured by using a series of calibrated cylinders that change diameter by 0.001 in. The graphite weight fraction is determined by a sulfuric acid/hydrogen peroxide method. The graphite volume fraction is calculated as follows:

$$\text{Volume Fraction} = \frac{(\text{Weight Fraction})(\text{Density of Composite})}{(\text{Density of Graphite})}$$

4.1.2 Modulus Tests (Graphite/Epoxy Tube)

Precision strain gages, Model EA-13-062TV-350 from Micro-Measurements, were epoxy bonded on opposite sides of the center of graphite/epoxy tube No. 1. Threaded Invar fittings were epoxy bonded into each end of the tube; spherical bearing rod end fittings, SWRMLH-4-100 from Southwest Products, were threaded into the ends; and the specimen was placed in a load machine. The distance between rod end centers was 9.80 cm (3.86 in.).

Table 4-1 ORBIT GRAPHITE/EPOXY TUBE PROPERTIES

Tube No.	1	2	4	6	8	9	11	12	13	Average
Used On:	Side Load Test	Strut 2	Axial Shorting Test	Strut 3	Strut 1	Strut 5	Fatigue Test	Strut 6	Strut 7	
Density (g/cm^3)	1.57	1.56	1.57	1.56	1.57	1.57	1.57	1.57	1.57	1.57 ± 0.004
Wall Thickness (mm)	0.276	0.284	0.269	0.297	0.284	0.279	0.292	0.292	0.297	0.287 ± 0.010
(mil)	10.9	11.2	10.6	11.7	11.2	11.0	11.5	11.5	11.7	11.3 ± 0.4
Cross-Sectional Area ($10^{-5}m^2$)	1.35	1.39	1.31	1.45	1.39	1.36	1.43	1.45	1.45	1.40 ± 0.05
($in.^2$)	0.0209	0.0216	0.0203	0.0224	0.0215	0.0211	0.0221	0.0221	0.0225	0.0216 ± 0.0007
Length (m)	0.05692	0.05692	0.05692	0.65695	0.05692	0.05687	0.05692	0.05687	0.05687	0.05691 ± 0.00003
(in.)	2.241	2.241	2.241	2.242	2.241	2.239	2.241	2.239	2.239	2.242 ± 0.001
Inside Diameter (m)	0.01524	0.01528	0.01525	0.1521	0.01524	0.01524	0.01521	0.01524	0.015240	0.1524 ± 0.00002
(in.)	0.600	0.6015	0.6003	0.599	0.600	0.600	0.599	0.600	0.600	0.600 ± 0.0007
Outside Diameter (m)	0.01579	0.01585	0.01579	0.01581	0.01581	0.01580	0.01580	0.01582	0.01583	0.01581 ± 0.00002
(in.)	0.6218	0.6239	0.6215	0.6224	0.6224	0.6220	0.6220	0.6230	0.6234	0.6225 ± 0.0008
Weight Fraction Graphite	0.67	0.67	0.67	0.67	0.67	0.67	0.67	0.67	0.67	0.67
Volume Fraction Graphite	0.595	0.595	0.595	0.595	0.595	0.595	0.595	0.595	0.595	0.595
	First Batch			Second Batch				Third Batch		

Notes: Tubes 1 and 4 used in development tests (Section 4)
Tube 11 used in single strut tests (Section 6)
Tubes 2, 6, 8, 9, 12, 13 used in six strut tests (Section 7)

Modulus tests were conducted at 0.12 percent strain and 295 (ambient air) and 78 K (immersed in liquid nitrogen). Table 4-2 shows the results.

4.1.3 Ultimate Compression Load Test (Graphite/Epoxy Tube)

With the same setup as that used for the modulus tests, graphite/epoxy tube No. 1 was failed in compression while immersed in liquid nitrogen. The failure load of 4,272 N (961 lb_f) compares to a predicted value of 5,650 N (1,270 lb_f) based on shell buckling.

The ultimate stress is 3.2×10^8 N/m^2 (46.0 ksi), and ultimate strain is 0.30 percent. Visual examination of the failed tube (Fig. 4-1) shows a crack 0.5 cm (0.2 in.) long running parallel to the +15-deg fibers and adjacent to the edge of one of the strain gages. At the gage, the crack angles back -15 deg a distance of 0.1 cm (0.05 in.), again parallel to the fibers. The rest of the tube is undamaged. It appears that the failure started where the graphite fibers overlap at the ± 15 deg intersection at the edge of the strain gage.

Table 4-2 GRAPHITE TUBE MODULUS VALUES

Temperature	Modulus, N/m^2 (psi)	
	Tension	Compression
295 K	11×10^{10} (16.0×10^6)	10.8×10^{10} (15.7×10^6)
78 K		10.4×10^{10} (15.1×10^6)
4 K (extrapolated from Ref. 18)		10.4×10^{10} (15.1×10^6)

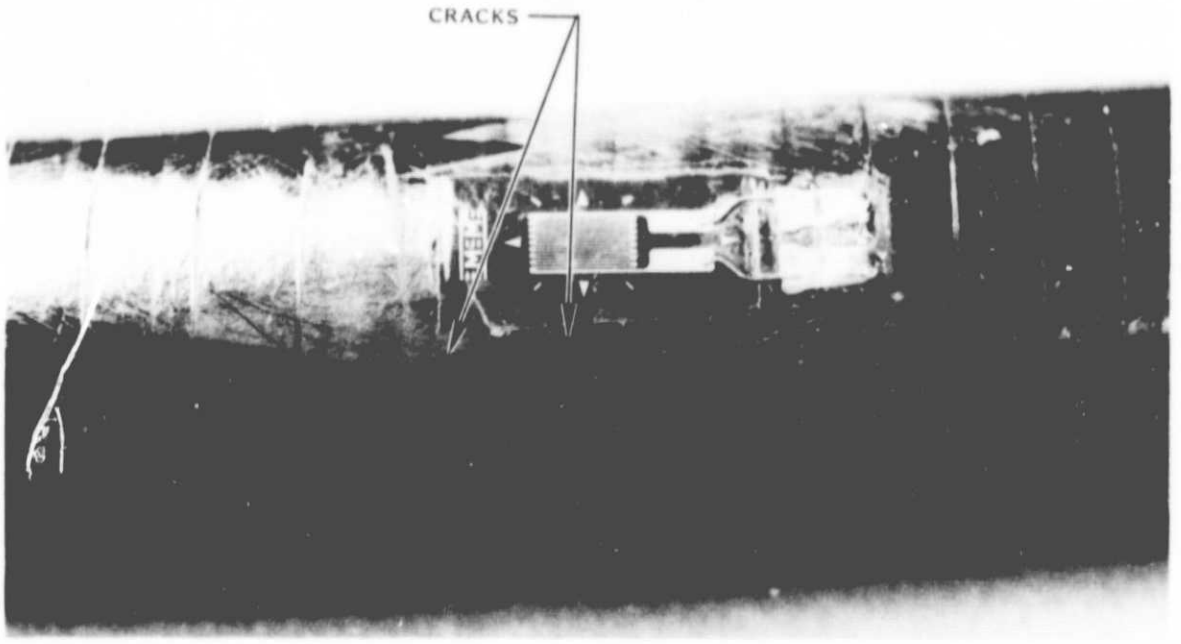

Fig. 4-1 Failed Graphite/Epoxy Tube After Ultimate Compression Load Test

4.1.4 Thermal Expansion Tests

Thermal expansion measurements were made over the range 394 K to 103 K for the bonded Invar adjustment bushing-orbit graphite/epoxy tube-Invar stem assembly. Previously measured Invar ΔL values for the adjustment bushing and stem length were subtracted from the ΔL values for the assembly to obtain the graphite/epoxy tube ΔL values. The $\Delta L/L$ values for the graphite/epoxy tube are given in Table 4-3 and plotted in Fig. 4-2. The graphite/epoxy expands slightly as the tube cools. Some $\Delta L/L$ values for Invar from two sources are plotted in Fig. 4-3. Below 90 K, the data do not agree very well.

Since the load gaps are set at room temperature, it is necessary to offset these gaps so they are equal at operating temperature. The amount of this offset was calculated from data in Figs. 4-2 and 4-3 according to the following formula.

$$\text{Gap Offset} = L\left[\left(\frac{\Delta L}{L}\right)_{\frac{T_H + T_C}{2},\ Gr} + \left(\frac{\Delta L}{L}\right)_{T_H,\ Invar}\right]$$

where

$$L = 4.17 \text{ cm } (1.64 \text{ in.})$$

Table 4-4 provides a comparison using both of the $\Delta L/L$ Invar curves from Fig. 4-3.

Table 4-3 GRAPHITE/EPOXY THERMAL EXPANSION, AXIAL DIRECTION

Tube No. 4		
Temperature (K)	Run 1 (percent)	Run 2 (percent)
102.6		0.0065
116.5	0.0065	0.0060
130.4	0.0074	0.0058
144.3	0.0054	0.0054
158.2	0.0060	0.0043
172.1	0.0049	0.0034
185.9	0.0045	0.0025
199.8	0.0036	0.0013
213.7	0.0034	0.0004
227.6	0.0020	-0.0004
241.5	0.0013	-0.0013
255.4	0.0009	-0.0009
269.3	0.0004	-0.0004
283.2	0	0
292.6	0	0
297.1	0.0002	0.0002
310.9	0.016	0
324.8	0.022	0
338.7	0.022	0.0002
352.6	0.022	0.0002
366.5	0.027	0.0007
380.4	0.0025	0.0007
394.3	0.0002	-0.0007

Prior experience with graphite/epoxy laminates indicates that the second cycle provides data that are more representative of future cycling data than the first cycle does.

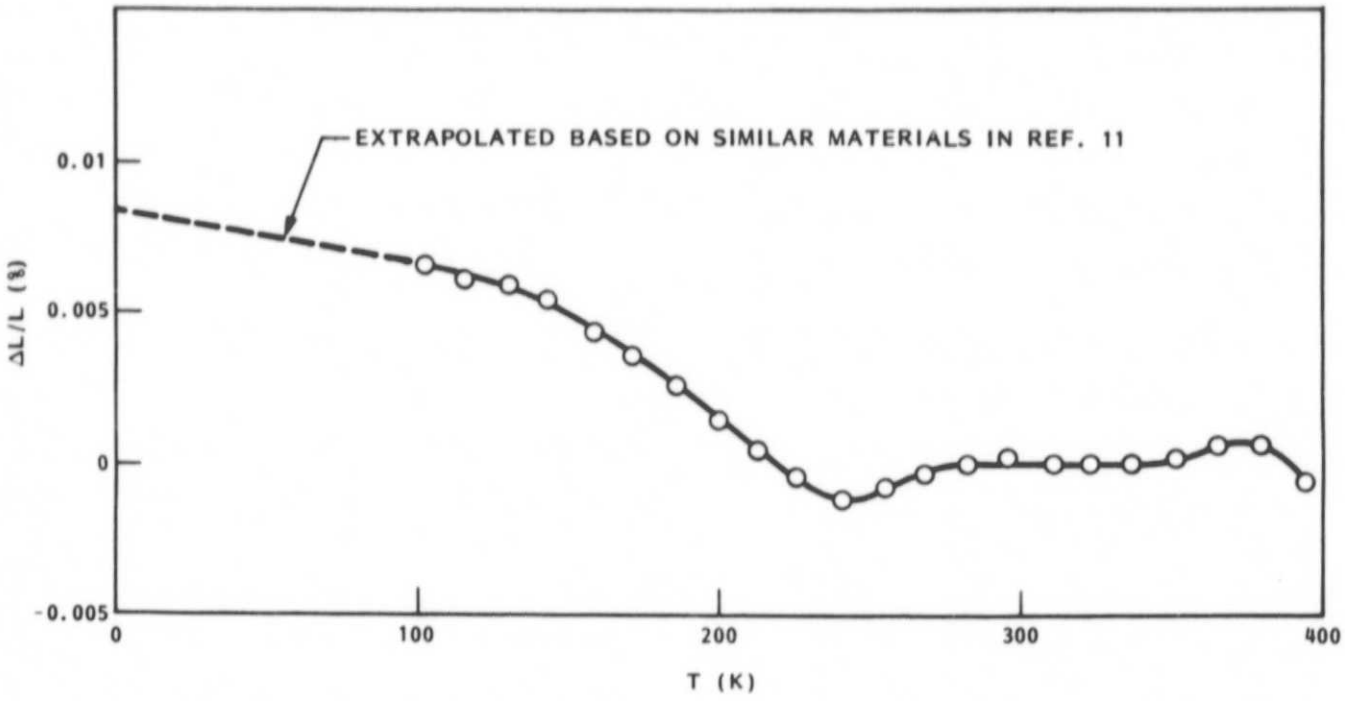

Fig. 4-2 Graphite/Epoxy Tube Thermal Expansion, Axial Direction

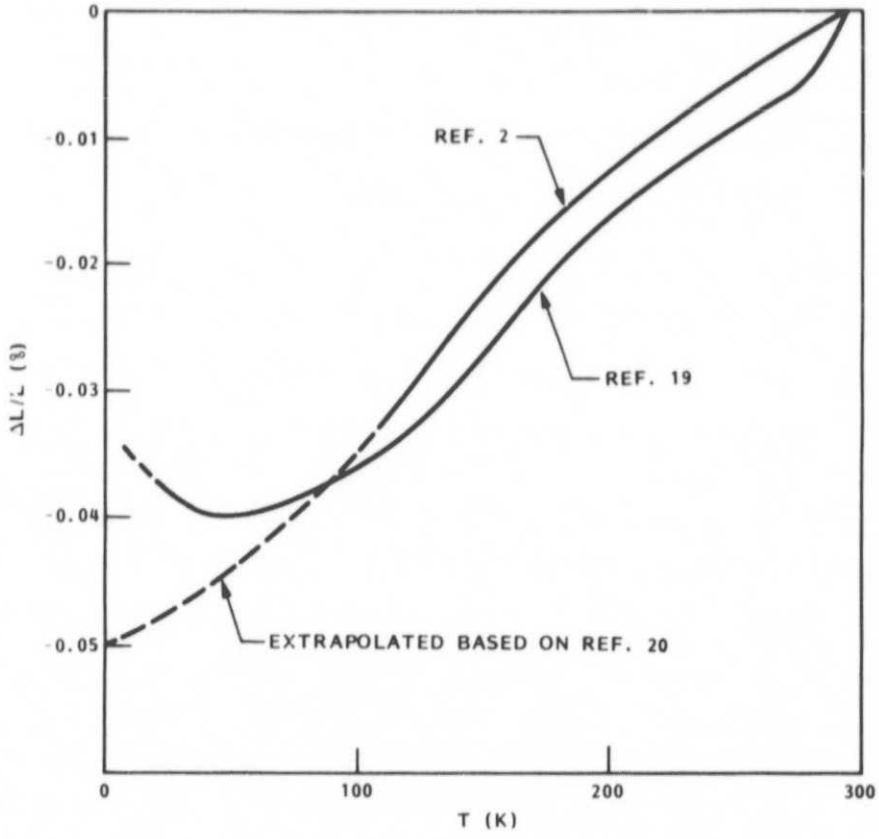

Fig. 4-3 Invar Thermal Expansion Data

Table 4-4 AXIAL GAP OFFSET REQUIREMENTS

Temperature (K)		Axial Gap Offset, mm (mil)	
T_C	T_H	Invar Curve Ref. 2	Invar Curve Ref. 19
1.7	15	0.0185 (0.73)	0.0236 (0.93)
1.7	20	0.0188 (0.74)	0.0234 (0.92)
1.7	25	0.0193 (0.76)	0.0231 (0.91)
1.7	30	0.0196 (0.77)	0.0229 (0.90)
1.7	35	0.0198 (0.78)	0.0226 (0.89)
1.7	40	0.0201 (0.79)	0.0224 (0.88)

The maximum discrepancy using the two different Invar curves is 0.0051 mm (0.2 mil) or 7 percent of the gap setting. A gap offset of 0.018 mm (0.7 mil) was selected for assembling the load strut tested in Task 6. The gap was changed to 0.020 mm (0.8 mil) based on the Task 6 results for the six struts tested in Task 7. The shim size used in the assembly is (3.0 - 0.8) cos 30 deg = 1.9 mil for the compression gap and (3.0 + 0.8) cos 30 deg = 3.3 mil for the tension gap. The cos 30 deg term takes into account the stem wedge angle.

4.2 S-2 GLASS/EPOXY LAUNCH TUBE TESTS

4.2.1 Test Specimens and Setup

An S-2 glass/epoxy tube was filament wound per the drawing shown previously in Fig. 3-2, except that the S-2 glass/epoxy tube had a thicker wall - 1.03 mm (0.0405 in.). Dummy Invar end fittings that simulated actual parts were machined. The tube was epoxy bonded onto the end fittings per the procedure described in Section 5. Axial strain gages were bonded at both sides of the tube center, and rod end fittings were threaded into the Invar ends. The length of strut was set at 59.1 cm (23.25 in.) between spherical bearing centers. Figure 4-4 shows the test setup.

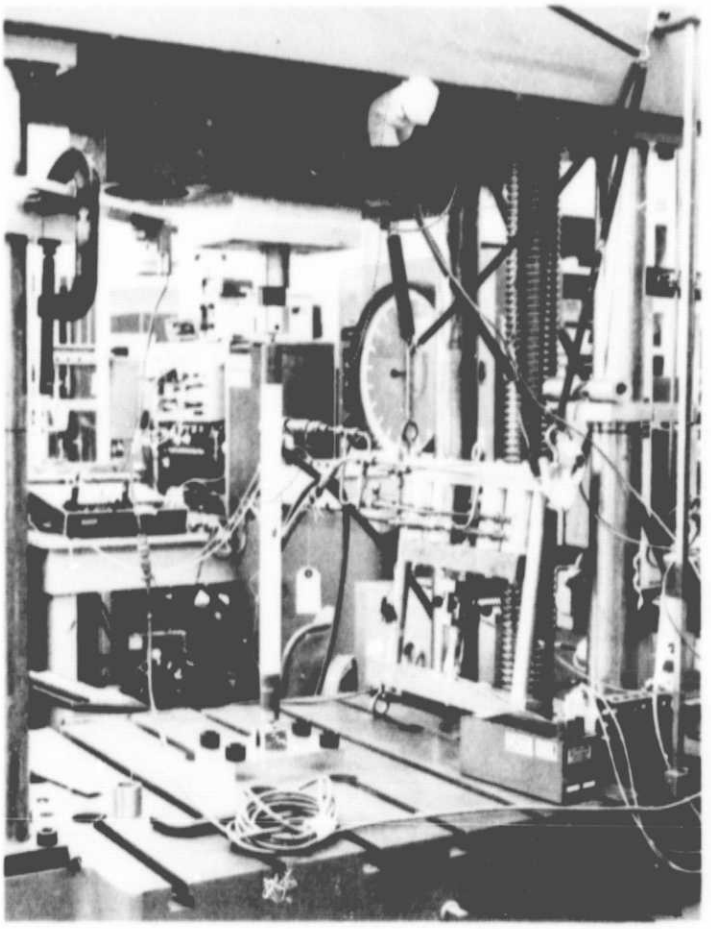

Fig. 4-4 Fiberglass Tube Axial Load Test Setup

4.2.2 Modulus and Ultimate Compression Load Tests (1.03-mm Wall)

The strut was loaded in tension three times to 11,125 N (2,500 lb_f) and compression three times to 4,450 N (1,000 lb_f). The measured modulus values are shown in Table 4-5.

Table 4-5 FIBERGLASS TUBE MODULUS VALUES (1.03-mm WALL)

Temperature (K)	Modulus, N/m^2 (psi)	
	Tension	Compression
295	5.6×10^{10} (8.2×10^6)	5.6×10^{10} (8.2×10^6)
4*	5.7×10^{10} (8.3×10^6)	5.7×10^{10} (8.3×10^6)

*Extrapolated from similar data in Ref. 18

The strut was then loaded in compression until the column buckled elastically. The test was repeated two more times. Table 4-6 shows the test results.

Table 4-6 STRUT COMPRESSION TEST RESULTS (1.03-mm WALL)

Test No.	Ultimate Compressive Buckling Load	
	N	lb_f
1	16,430	3,694
2	16,667	3,747
3	16,631	3,739

Using the Euler column buckling formula, strut dimensions, and measured modulus values, the predicted buckling load is 16,493 N (3,708 lb_f). This agrees with the measured values. The unsupported fiberglass tube length was assumed to be the rod end to rod end length. Consequently, the predicted value should be slightly lower then the measured value.

The strut end was immersed directly in liquid nitorgen ten times. No visible microcracking or damage to the bond line was evident.

Based on the measured high modulus values, the wall thickness of the tube was reduced, and eight more tubes were filament wound at reduced wall thicknesses as shown in Table 4-7. Tube dimensions, density, and weight fraction of glass were also measured.

4.2.3 Modulus and Ultimate Compression Load Tests (0.70-mm Wall)

The compression, tension, and ultimate compression load tests were repeated on tube No. 2 (Table 4-5) with the same dummy Invar end fittings plus rod ends. The S-glass/epoxy wall thickness is 0.70 mm (27.5 mil). The length of the strut is 59.1 cm (23.256 in.) between spherical bearing centers. The strut is loaded in tension three times to 8,900 N (2,000 lb_f) and compression three times to 4,450 N (1,000 lb_f). Table 4-8 presents the measured modulus

Table 4-7 LAUNCH FIBERGLASS/EPOXY TUBE PROPERTIES

Tube No.	2	8	9	10	11	12	13	14	Average
Used on:	E, F_{cu}	Strut 2	Strut 5	Strut 6	Fatigue Test	Strut 1	Strut 7	Strut 3	
Density (g/cm^3)	2.05	2.05	2.05	2.05	2.05	2.05	2.05	2.05	2.05
Wall Thickness (mm)	0.699	0.693	0.683	0.696	0.688	0.681	0.683	0.678	0.688 ± 0.008
(mil)	27.5	27.3	26.9	27.4	27.1	26.8	26.9	26.7	27.1 ± 0.3
Cross-Sectional Area ($10^{-5} m^2$)	6.29	6.24	6.16	6.27	6.19	6.11	6.16	6.10	6.19 ± 0.07
(m^2)	0.0974	0.0967	0.0955	0.0972	0.0960	0.0947	0.0954	0.0945	0.0959 ± 0.0011
Length (m)	0.4572	0.4572	0.4573	0.4570	0.4573	0.4572	0.4573	0.4573	0.4572 ± 0.0001
(in.)	18.001	17.999	18.003	17.993	18.003	17.999	18.005	18.002	18.001 ± 0.004
Inside Diameter (m)	0.02795	0.02795	0.02795	0.02799	0.02796	0.02795	0.20795	0.02795	0.02796 ± 0.00001
(in.)	1.1005	1.1005	1.1005	1.1018	1.1006	1.1004	1.1004	1.1002	0.02796 ± 0.0005
Outside Diameter (m)	0.02935	0.02934	0.02932	0.20938	0.02933	0.2931	0.2932	0.02930	0.2933 ± 0.00003
(in.)	1.1555	1.1551	1.1544	1.1566	1.1548	1.1539	1.1543	1.1536	1.1548 ± 0.00096
Weight (g)	58.9	58.5	57.7	58.7	58.1	57.3	57.7	57.2	58.0 ± 0.6
Fraction Glass By Weight	0.783	0.783	0.783	0.783	0.783	0.783	0.783	0.783	0.783
By Volume	0.65	0.65	0.65	0.65	0.65	0.65	0.65	0.65	0.65

Notes: Tube 2 used in development tests (Section 4)
Tube 11 used in single strut tests (Section 6)
Tubes 8, 9, 10, 12, 13, 14, used in six strut tests (Section 7)

Table 4-8 FIBERGLASS TUBE MODULUS VALUES (0.70-mm WALL)

Temperature (K)	Modulus, N/m2 (psi)	
	Tension	Compression
295	5.3 x 10^{10} (7.73 x 10^{6})	5.4 x 10^{10} (7.78 x 10^{6})
4*	5.4 x 10^{10} (7.8 x 10^{6})	5.4 x 10^{10} (7.8 x 10^{6})

*Extrapolated from similar data in Ref. 18

values. These modulus values are approximately 6 percent lower than for the 1.03-mm (0.0405-in.) wall thickness tested previously.

The strut was then loaded in compression until the column buckled elastically; the test was repeated three more times. Table 4-9 shows the test results.

Table 4-9 STRUT COMPRESSION TEST RESULTS (0.70-mm WALL)

Test No.	Ultimate Compressive Buckling Load	
	N	lb_f
1	12,317	2,769
2	11,841	2,662
3	11,921	2,680
4	11,814	2,656

The buckling load calculated using the measured modulus value, wall thickness, and rod end to rod end length with fittings is 10,264 N (2,308 lb_f). This calculation assumes that the unsupported fiberglass tube length is the rod end to rod end length. Consequently, the predicted value should be slightly lower than the measured value, as is the case.

The epoxy bond lines (Invar to fiberglass) were thermally shocked in liquid nitrogen ten times. No evidence of microcracking or other bond-line damage was visible.

Section 5
PODS-III STRUT ASSEMBLY PROCEDURES

5.1 INTRODUCTION

Figure 5-1 shows the parts of the PODS-III strut. Figure 5-2 shows the assembled adjustment bushing/thin-wall graphite tube/stem, and Fig. 5-3 presents the completely assembled strut. The remaining figures and the text of this section describe the strut parts and steps required to assemble the strut based on the development test results.

5.2 REQUIRED PARTS AND ASSEMBLY MATERIALS

5.2.1 Strut Parts (See Section 3.1)

Fig. No.	Qty		
-	1	2 BREM-5A-009	Rod end, warm
-	1	LS8819-6	Jam nut
3-12	1	SFH-173	Jam nut
3-9	1	SFH-170	Length adjustment
3-5	1	SFH-166	Body, warm end
3-10	2	SFH-171	Clamshell, large
3-2	1	SFH-163	Large tube, fiberglass/epoxy
3-3	1	SFH-164	Small tube, graphite/epoxy
3-11	2	SFH-172	Clamshell, small
3-8	1	SFH-169	Adjustment bushing
3-4	1	SFH-165	Body, cold end
3-7	1	SFH-168	Nut
3-6	1	SFH-167	Stem
-	1	LS8819L6	Jam nut
-	1	2 BREMLH-5A-009	Rod end, cold
3-13	2464	SFH-208	Dexiglas discs, Dexter Paper Co.

Fig. 5-1 PODS-III Parts

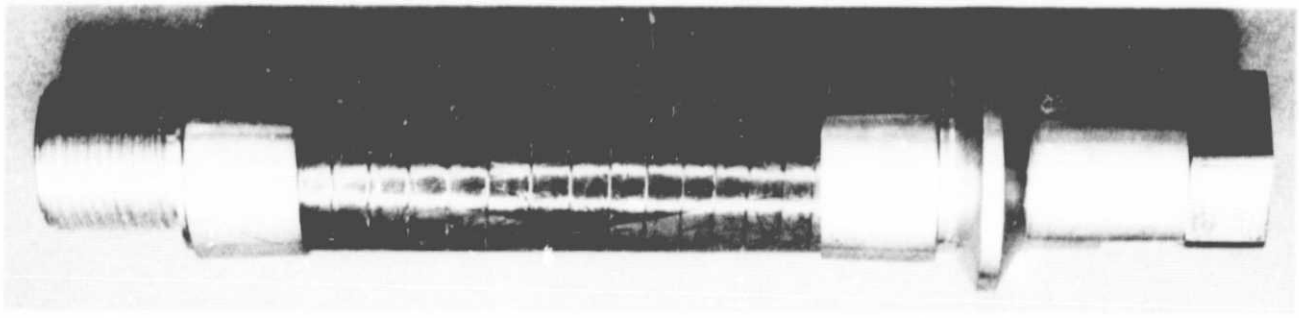

Fig. 5-2 Graphite/Epoxy Tube Subassembly

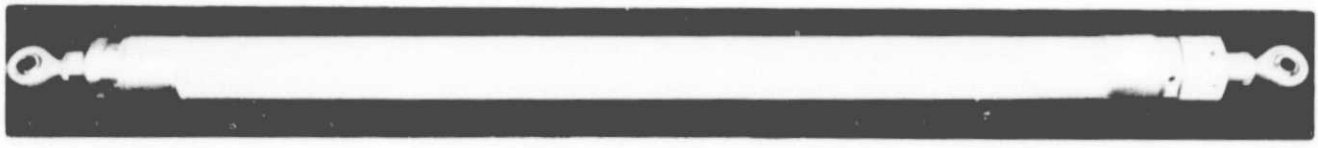

Fig. 5-3 Assembled PODS-III Strut

Fig. No.	Qty		
3-13	123	SFH-208	Double aluminized Mylar discs (1/4 mil)
3-13	1	SFH-208	Silk net
-	AR	1210-A/9615-10 100 parts by wt/ 50 parts by wt	Epoxy adhesive Furane Plastics, Inc.
-	AR	4-mil Diameter	Glass beads
-	AR	3 μm	Alumina, Norton Precision Alumina

5.2.2 Assembly Tools

Fig. No.	Qty		
5-4	1	HE 0015	Orbit tube assembly tool
5-5	1	HE 0025	Dexiglas and silk net disc cutters
5-5	1	HE 0025	Double aluminized Mylar disc cutter
5-6	1	HE 0027	Length adjustment bar
5-7	1	HE 0028	Holding block
5-8	1	HE 0029	Assembly spacer
5-9	2	HE 0030	Plug gages
5-10	1	HE 0033	Assembly rod
5-11	1	HE 0034	Toroidal weight and 14-lb weight

5.2.3 Miscellaneous Equipment

Qty	
1	Lathe
1	Side load test apparatus (see section 6.1.2)
1	Micrometer (accurate to 0.001 in.)
1	Scale, to 1000 g, accurate to 0.01 g
1	Pan scale for weighing epoxy, glass beads
1	Small vacuum pump and 1/8-in. diameter tube 20 in. long

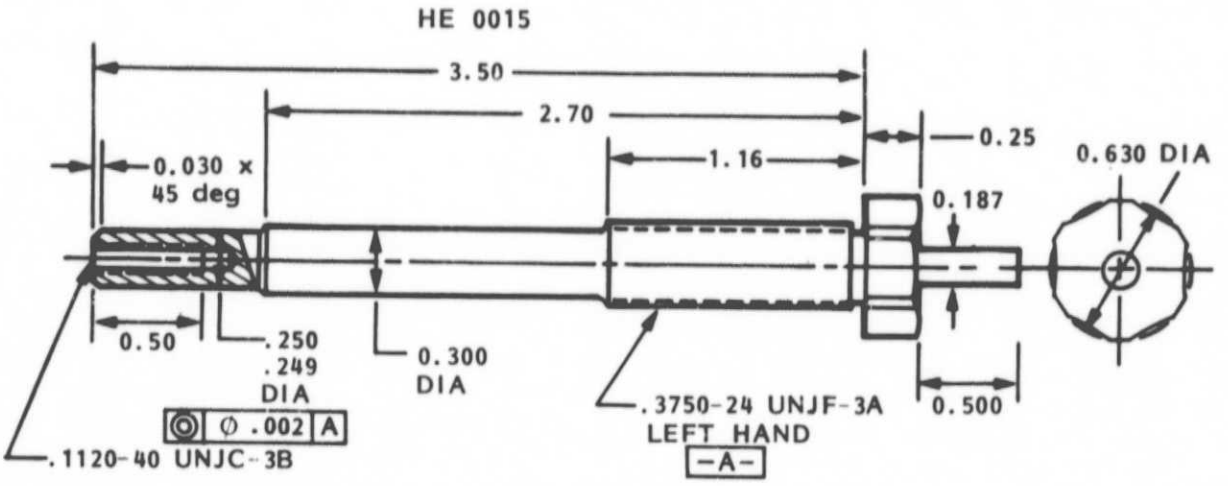

Fig. 5-4 Assembly Tool

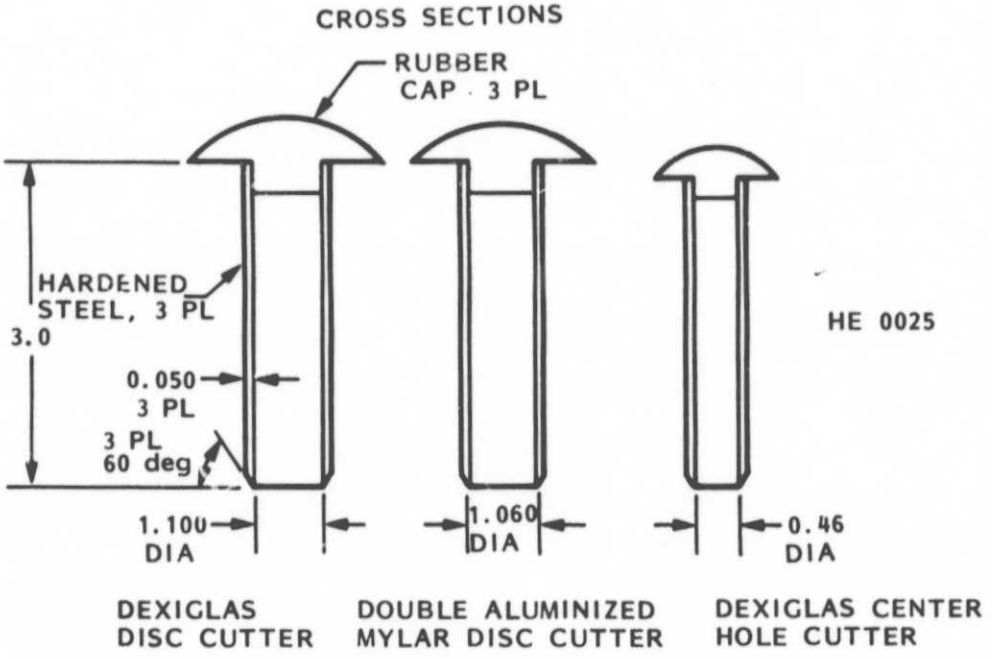

Fig. 5-5 Disc Cutters

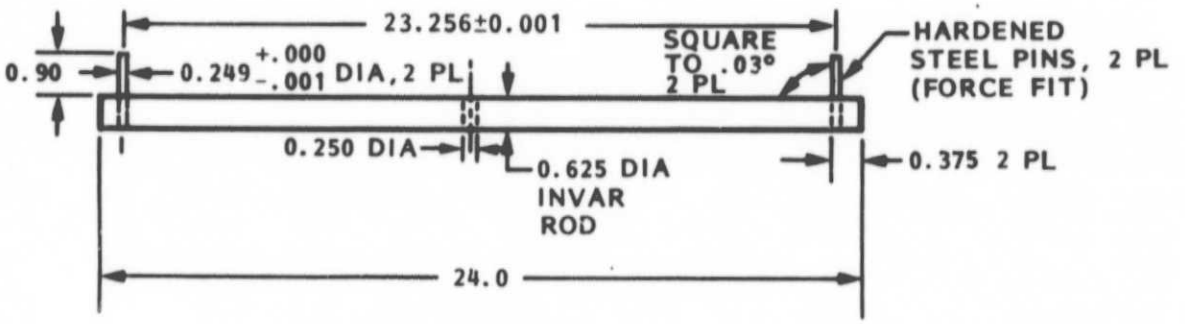

HE 0027

DIMENSIONS IN in.

Fig. 5-6 Length Adjustment Bar

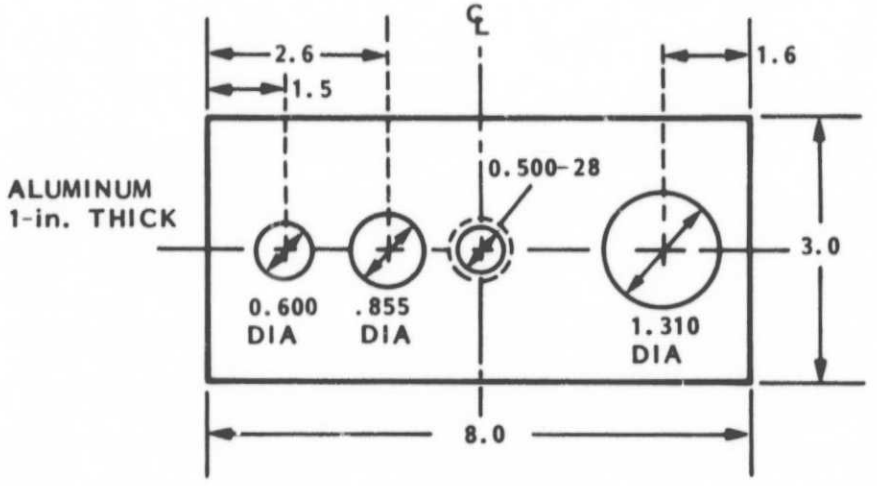

HE 0028

DIMENSIONS IN in.

Fig. 5-7 Holding Block

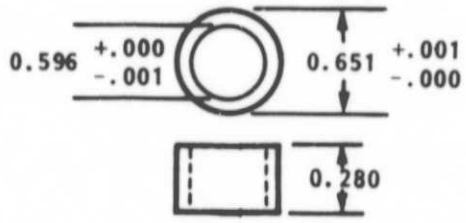

HE 0029

DIMENSIONS IN in.

Fig. 5-8 Assembly Spacer

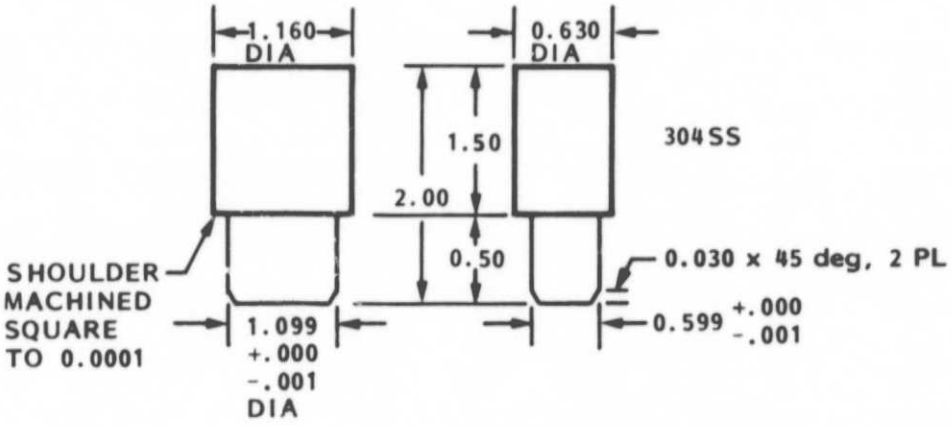

FOR FIBERGLASS TUBE, 1 EACH

FOR GRAPHITE EPOXY TUBE, 1 EACH

HE 0030

DIMENSIONS IN in.

Fig. 5-9 Plug Gages

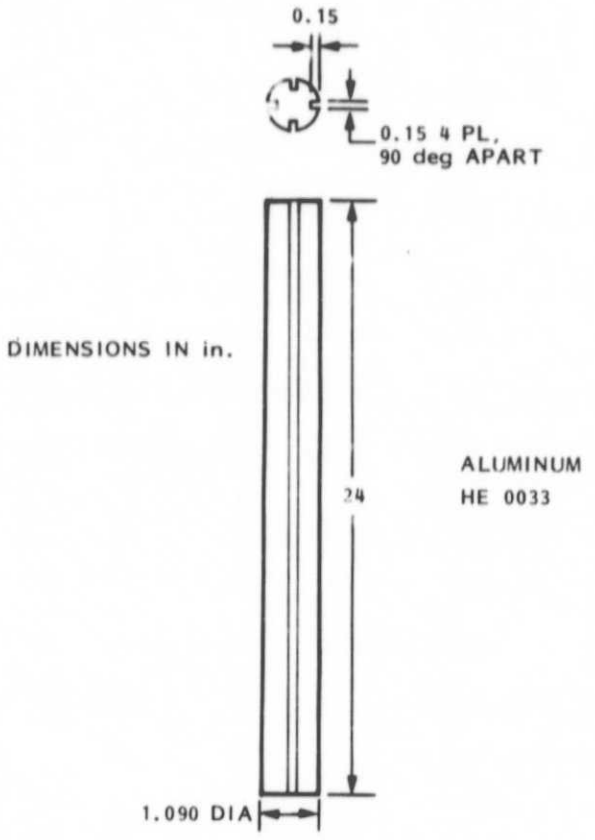

Fig. 5-10 Assembly Rod

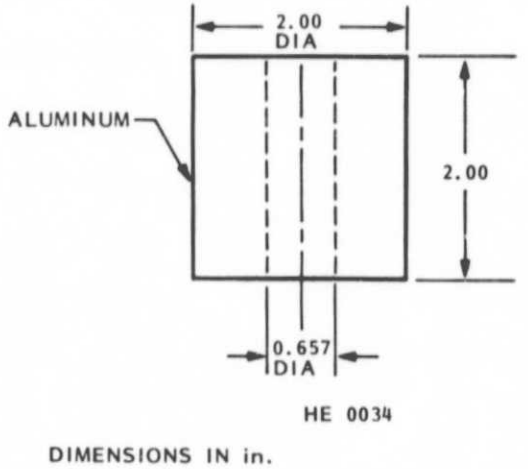

Fig. 5-11 Toroidal Weight

Qty	
	Open-end wrenches (in.)
1	0.500
1	0.688
1	0.750
1	0.813
1	1.00
1	Allen wrench (1/4 in.)
1	Straight edge
1	Metal spatula
AR	White lint-free Dacron gloves
3	Shims 0.0019 x 0.060 x 2 in., s.s.
3	Shims 0.0033 x 0.060 x 2 in., s.s.
1	Test tool HE 0035

5.2.4 Miscellaneous Materials

Qty	
AR	Distilled water
AR	Isopropyl alcohol
AR	MEK
AR	Trichloroethane
AR	Aluminum cups
AR	Kapton tape LAC 24-4450C
AR	320 and 600 grit emery paper
AR	Q-tips
AR	20-mil safety wire
AR	Glennel Diamond Compound Type UB, Grade HVY
AR	Clover Lapping Compound A
AR	Lightweight lubricating oil

5.3 SPECIAL FABRICATION STEPS

Prior to gold coating the Invar parts, perform steps 1 through 3.

1. Check the following threaded parts for seizing.
   - Cold end body SFH-165/adjustment bushing SFH-169
   - Cold end body SFH-165/nut SHF-168
   - Warm end body SFH-166/length adjustment SFH-170
   - Length adjustment SFH-170/2 BREM-5A-009 rod end
   - Stem SFH-167/2 BREMLH-5A-009 rod end

   Back off at the first sign of seizing and clean up the threads as required.
2. Dimensionally verify that all parts meet drawing requirements. Fit check all parts that go together. Ensure the 125 surfaces are suitably roughened for good epoxy bonding. The conical surface dimensions, angles, and concentricity called out in Note 9 on the following parts are particularly critical.
   - Stem SFH-167
   - Nut SFH-168
   - Body, cold end SFH-165
3. (Procedure A) The mating conical surfaces of the stem (SFH-167) versus nut (SFH-168) and stem versus body (SFH-165) must match to within 0.0001 in. over their facing areas. A lapping method has been developed to achieve this level of accuracy. Since these parts must be assembled as a unit, a set identification number must be engraved on each part in noncritical areas that are still visible after assembly (including the adjustment bushing, SFH-169) to ensure that they are not mixed up with other parts of the same type. The setup used for the lapping is shown in Fig. 5-12. The parts required for the lapping are shown in Fig. 5-13. The following steps a through n are required.
   a. Screw the 3/8 - 24L nut halfway up the threaded length of the assembly tool (HE 0015).

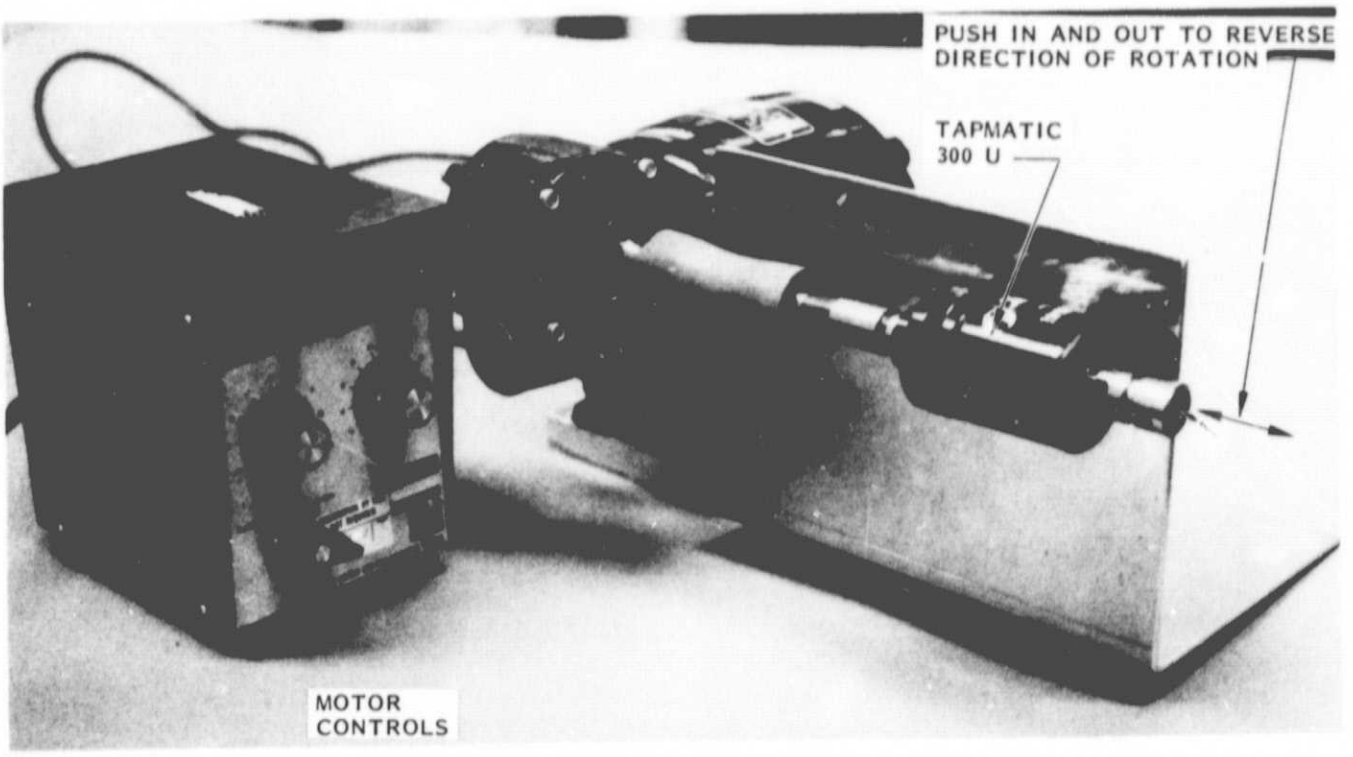

Fig. 5-12 Lapping Setup

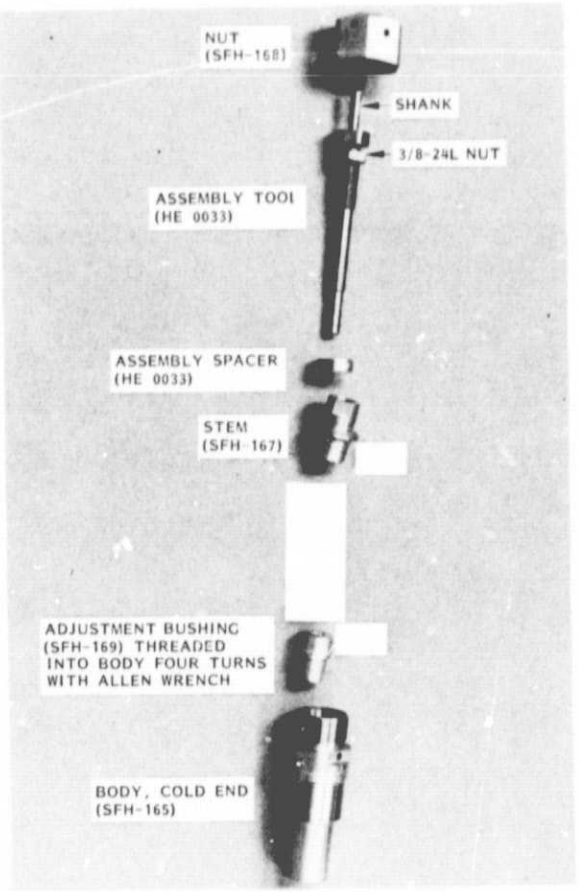

Fig. 5-13 Parts Required for Lapping Procedure

b. Oil both surfaces of the assembly spacer HE 0029 (inside and out) and slip it over the guide end and threads of the assembly tool up to the nut. Keep the assembly spacer free of the grinding compounds that are used later.

c. Screw the stem (SFH-167) onto the assembly tool CCW up to the 3/8-24 L nut and lock together. Make certain the stem is oriented as shown in Fig. 5-13. Also make certain the assembly spacer slides freely onto the stem down to the conical surface.

d. Place small amounts of grinding compound (Clover Compound A)* on both conical surfaces of the stem. Place the assembly tool with assembly spacer and stem down into the body (SFH-165) until the guide end of the assembly tool slips into the adjustment bushing (SFH-169) and the conical surfaces of the stem and body mate.

e. Place the nut (SFH-168) over the shank end of the assembly tool and screw onto the body CW until all conical surfaces contact each other, then back the nut off 1/8 turn, CCW.

f. Insert the shank of the assembly tool into the chuck of the Tapmatic 300 U and lock tight with wrenches.

g. When the switch is turned on at the motor control, there will be a few seconds delay before the motor starts to turn. Grasp the body in one hand and the nut in the other. After the motor starts, do not let the body turn. Adjust the nut CW until you feel a light tension and hear a grinding noise.

h. If you screw the nut too tight, the complete assembly will start turning. If this occurs, remove both hands and turn off the motor drive. Again loosen the nut CCW and start the lapping again. With practice, you will soon find the right pressure to apply by adjusting the nut for the right feel and sound.

---

* Start with Glennel Diamond Compound Type UB, Grade 15 HVY. If the surfaces mate to approximately 80 percent after minimal lapping, do not use Clover Compound A. Only use the Clover Compound A if there are large mismatches.

i. Allow the Tapmatic chuck to rotate CCW in the inward position for 3 to 4 turns. Then pull outward on the assembly reversing the rotation to CW; again allow 3 to 4 turns. Repeat the above in-out cycle ten times.

j. Remove the assembly from the Tapmatic chuck, disassemble the parts to expose the lapped conical surfaces, and rinse with isopropyl alcohol.

k. Repeat procedures d through j until the conical surfaces are approximately 80 percent lapped. At this point, change the grinding compound to Glennel Diamond Compound Type UB, Grade 15 HVY. Use this compound until the conical surfaces are 100 percent lapped.

Note: On the final lapping with the diamond compound, complete only three in-out cycles, then disassemble, rinse, and check visually for a correct finish without any gouge marks, etc.

l. When the surfaces are 100 percent lapped, machine 0.005-in. grooves in the stem per Drawing HE 0009, Note 10. These grooves eliminate any potential ridges left by the lapping procedures.

m. Assemble the clean nut, stem, and body. Place three 1.9 mil shims between the nut and body and three 3.3-mil shims between the stem and body. Screw down the nut until all six shims are snug.

n. If any of the shims are loose, even after several tries, repeat steps k and l until all six shims are snug.

4. After gold coating the Invar parts, heat treat to 600°F for 1 h in a dry helium atmosphere and allow to cool to room temperature. Then heat back up to 203°F and hold for 49 h in a helium atmosphere. Allow to cool back down to room temperature. This heat treatment stabilizes Invar dimensionally over long periods of time.

5. The glass/epoxy and graphite/epoxy tubes split parallel to the fibers unless the following cutting technique is used. Insert a close-tolerance plug (diameter to within 0.002 in.) inside the tube for support. Cut the tube ends square with a diamond saw on a lathe. Insert the plug gage HE 0030 in the end of the tube and

inspect the end cut under a 100X stero microscope to ensure that the end cut is square to 0.001 in. and there are no splits or chips in the tube ends.

6. For the fiberglass tube (SFH-163) and graphite tube (SFH-164), record a weight on a scale accurate to 0.01 g, I.D. with plug gages that change diameter by 0.001 in., and O.D. with a micrometer accurate to 0.001 in. (with the plug gage inserted).
7. Perform a sulfuric acid/hydrogen peroxide analysis on a graphite/epoxy tube from the same lot to determine the weight fraction of graphite and epoxy. Wet ash a separate fiberglass/epoxy tube from the same lot to determine the weight fraction of glass and epoxy.

5.4 ASSEMBLY STEPS

After gold coating the nut, body, and stem, remove any traces of gold from the mating conical surfaces with 600 grit emery paper and degrease in MEK.

1. Handle all gold-coated parts with clean white lint-free gloves in Steps 1 through 18. Vapor degrease the following parts; all SFH-XXX; LS8819-6, LS8819L6, rod ends, and all tools used in the assembly.
2. Seal the cut ends of the graphite/epoxy tube as follows: wipe the ends clean with trichloroethane. Put parallel strips of 2-mil thick tape on a flat aluminum sheet spaced 1 in. apart. Mix the epoxy adhesive and place on the aluminum plate between the tape pieces. Using a flat edge, scrape off excess epoxy so a 2-mil thick layer is left between the tape strips. Heat the epoxy momentarily with a hot air gun and press one end of the graphite tube into the epoxy at a fresh spot. Turn 1/4 turn. Place the tube on a vertical rack so the epoxy is up. Allow the epoxy to cure overnight. Repeat the next day for the other end. This procedure serves two purposes. The epoxy prevents the graphite fiber ends from cracking apart during subsequent handling, and it prevents the electrically conductive graphite ends from shorting out to the Invar. (Electrical isolation

is required as a check to see if the gaps are maintained between the PODS stem and the body or nut.) Hand sand the inside and outside surface of both ends of the graphite/epoxy tube (0.4 in. axially) with 320 grit emery paper to remove the surface gloss. Sand so that the marks form circumferentially around the part. Measure the average wall thickness of the tube by weighing the tube in air and water. Calculate the tube volume from the amount of water displaced; calculate the wall thickness and cross-sectional area knowing the I.D. and length.

3. Place the graphite/epoxy tube into trichloroethane (immersed in an ultrasonic bath) for 1 min. Remove and rinse the tube with distilled water and air dry. No water break shall occur in the sanded areas upon rinsing within 1 min after withdrawal from the water.
   The graphite/epoxy tube dimensions may be affected by microcracking during thermal cycling (permanent change) and moisture absorbtion/desorbtion (reversible change) from atmospheric exposure to vacuum. The following steps are designed to remove these variables from the assembly procedure: Immerse the graphite/epoxy tube in liquid nitrogen. After boiling subsides, remove the tube and air dry. Wipe off excess moisture and repeat the liquid nitrogen immersion sequence. Place the tube in a vacuum oven and vacuum bakeout ($< 10^{-3}$ torr) at 150°F for 1 week. Backfill the oven with nitrogen, remove the tubes, and place the tubes in a dessicator until ready for bonding. Important: the graphite/epoxy tube must be kept in a dessicator between bonding steps through step 7.
4. Steps 4 and 5 must be completed within 1 h. Cover the O.D. of the stem (SFH-167) where shown and the I.D. of both ends of the graphite/epoxy tube (SFH-164) with a thin layer of epoxy with 5 percent by weight of glass beads added.

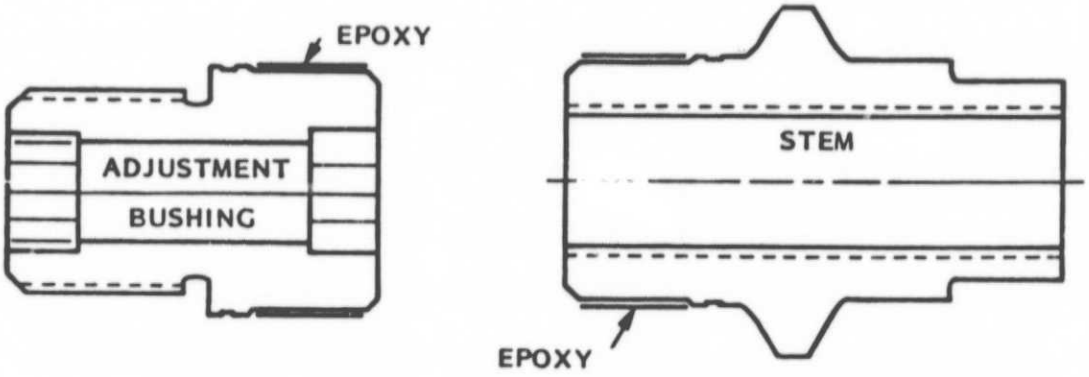

Cover an area 0.3 in. from each end of the tube. Push the tube slowly onto the stem. Cover the O.D. of the adjustment bushing (SFH-169) with an epoxy/glass bead mixture where shown and push onto the other end of the tube. Place the assembly spacer (HE 0029) over the stem, and screw the assembly tool (HE 0015) into the stem. Place a screw/washer/rubber hex in the other end of the assembly tool to hold the assembly together. Remove all excess epoxy with a spatula.

5. Place the cold body (SFH-165) in the holding block (HE 0028) in a vertical position with the smaller female threaded end pointing down. Lower the bonded assembly (stem, tube, adjustment bushing, assembly tool) into the body. Screw the adjustment bushing part way into the body using the hex on the assembly tool. Keep screwing in the bushing until the stem seats in the body. Back off 1/8 of a turn. Screw on the nut (SFH-168) until it seats against the stem. Place three 1.9-mil shims through holes in the nut so they slip between the body and stem conical surfaces. The shims slant upward. Tighten the assembly tool using the external hex (9/16-in. open-end wrench) until the three shims are snug. Tighten the nut (HE 0010) until it seats snugly against the stem. The time elapsed from first mixing the epoxy until this point in the assembly should be less than 1 h. Place the assembly in a dessicator, and allow the epoxy to cure overnight.

6. This step must be accomplished in 1 h. Remove the nut (SFH-168), unscrew the adjustment bushing (SFH-169) with a 1/4-in. Allen wrench, and remove the bonded part (Fig. 5-14). Using 320 grit paper, sand both ends of the tube circumferentially over a 0.3-in. length to remove the gloss from any new epoxy. Wipe the sanded area of the tube with a trichloroethane soaked cloth and air dry. Screw the adjustment bushing into the threaded hole in the holding block. Degrease the small clamshell parts (SFH-172) in MEK and air dry. Coat the inside surfaces of the clamshell parts (SFH-172) and the mating graphite tube/groove area on the bonded bushing/graphite tube/stem assembly with a thin layer of epoxy plus 5 percent by weight of glass beads. Place each clamshell (SFH-172), making certain to match pairs, on top of a 1-in.-high block. Pick up the bonded graphite tube assembly and guide the clamshell lip into the adjustment bushing (SFH-169) or stem (SFH-167) groove. Assemble the small clamshell halves (SFH-172) on each end so that the joint is rotated 90 deg with respect to the other clamshell. Hold the small clamshells (SFH-172) in place with safety wire wrapped twice and then twisted. Remove excess epoxy with a metal spatula followed by a Q-tip. Allow to cure overnight in a dessicator. Remove the safety wire. Remove excess epoxy with a scalpel. Remove the assembly tool. Place the assembly back in the dessicator until ready for the next step.
7. Step 7 must be completed in less than 1 h. Mix the epoxy and add alumina powder (3 parts to 4 parts by weight respectively). The high modulus alumina powder greatly stiffens the epoxy adhesive, minimizing elastic movement of the bonded threads under load. Place a thin layer of the epoxy/alumina mix on the internal body threads (SFH-165). Screw the bonded graphite tube assembly (with the assembly tool and assemby spacer installed) into the body using a 1/4-in. Allen wrench in the adjustment bushing hex, and then remove. Inspect the threads on both the body and adjustment bushing to make sure they are fully covered with epoxy (except in the key slots on the adjustment bushing). Use more epoxy mix and a hot air gun, if

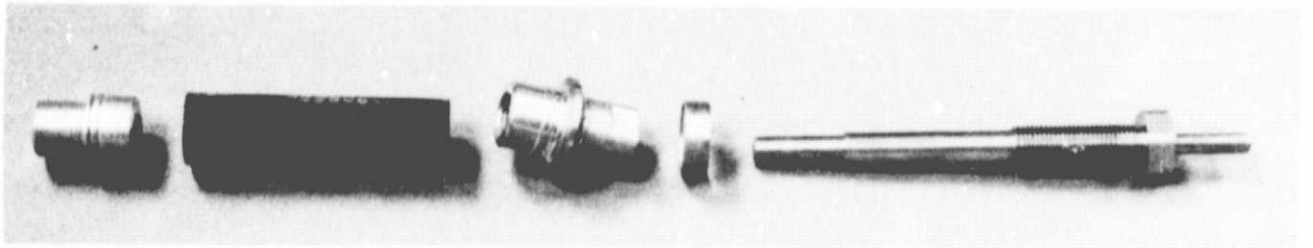

A. Parts Plus Assembly Tool (HE 0015) and Assembly Spacer (HE 0029)

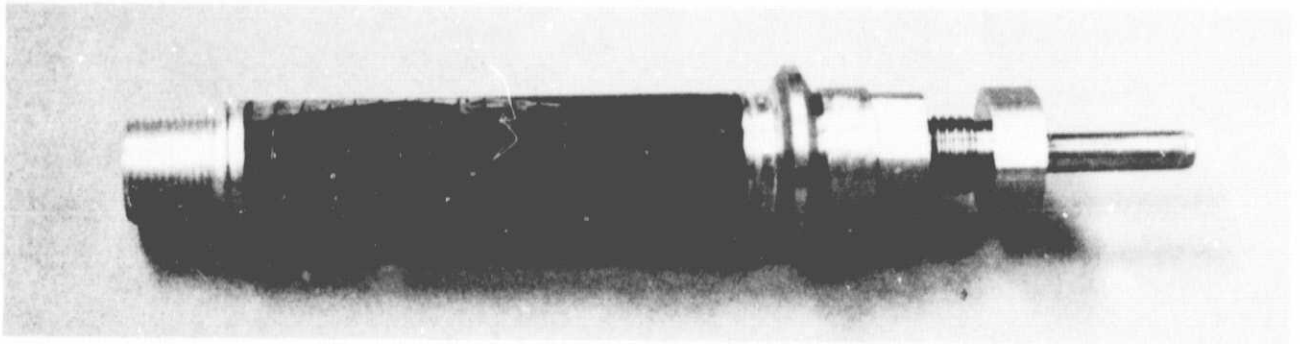

B. Graphite Tube Bonding

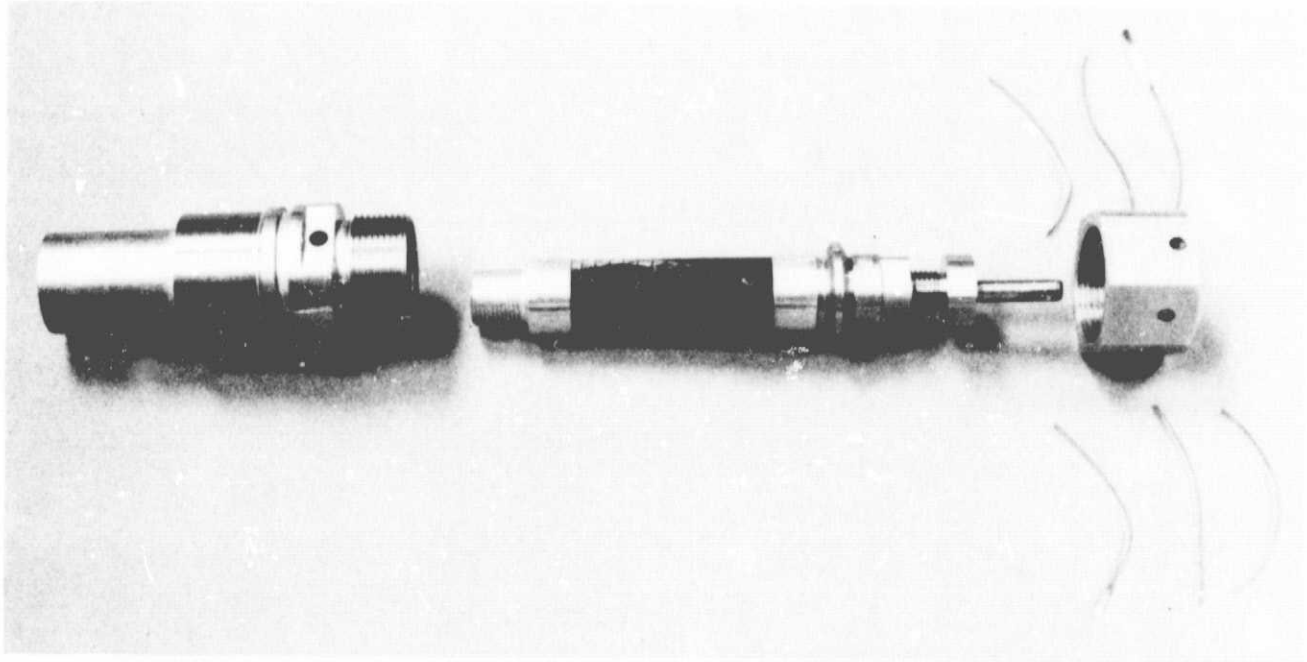

C. Clamshell Bonding Plus Body (SFH 165) and Nut (SFH 168) Bonding

Fig. 5-14 Assembly Sequence for Graphite Tube Subassembly

required, to get the viscous epoxy mix to wet the threads. Again screw the bonded graphite tube assembly into the body using a 1/4-in. Allen wrench in the adjustment bushing hex. Be careful not to get epoxy on the I.D. of the body when inserting the tube. After the stem seats, back off 1/8 turn. Place a thin layer of the epoxy/alumina mix on the body external threads (but not in the slots) starting at the top of the key slots located 0.2 in. from the conical end surface. Keep the epoxy away from the body's conical surface. Use a hot air gun to get the viscous epoxy mix to wet the body threads. Carefully thread on the nut (SFH-168) until it bottoms against the stem. Remove the nut and add more epoxy/alumina mix to the nut or body threads if required. Clean the epoxy out of the keys and 0.2 in. off the threads away from the nut and body conical surfaces. Place assembly spacer HE 0029 over the stem and screw on the nut. Back off the nut 1/8 turn. Place three 1.9-mil shims between the conical surfaces of the stem and body (through the holes in the nut). Place three 3.3-mil shims between the conical surfaces of the stem and the nut (through the holes in the nut). Use a 1/4-in. Allen wrench in the adjustment bushing hex to snug the three 1.9-mil shims between the stem and body. Hand tighten the nut until one or more of the 3.3-mil shims are snug. Place the body, nut end up, in the holding block. Slip the toroidal weight (HE 0034) over the assembly spacer so its weight rests on the nut. Carefully place a 14-lb weight on top of it. Pull gently on the three 3.3-mil shims to make certain they are all snug. Allow the epoxy to cure overnight in a dessicator. Remove the 14-lb weight and toroidal weight assembly. Remove the shims. Check to make certain the assembly is not shorted by touching the body/nut and stem with ohmmeter leads on the 100,000-ohm scale. After curing the epoxy for 48 h, place the PODS mechanism in the test assembly (HE 0035) as shown in Fig. 5-15. Tighten the clamp. Place rod ends in the test tool and PODS mechanism as shown, lock the jam nuts, and mount in a tensile test machine (with close fitting yokes and bolts) as shown in Fig. 5-15. The PODS compression shorting load

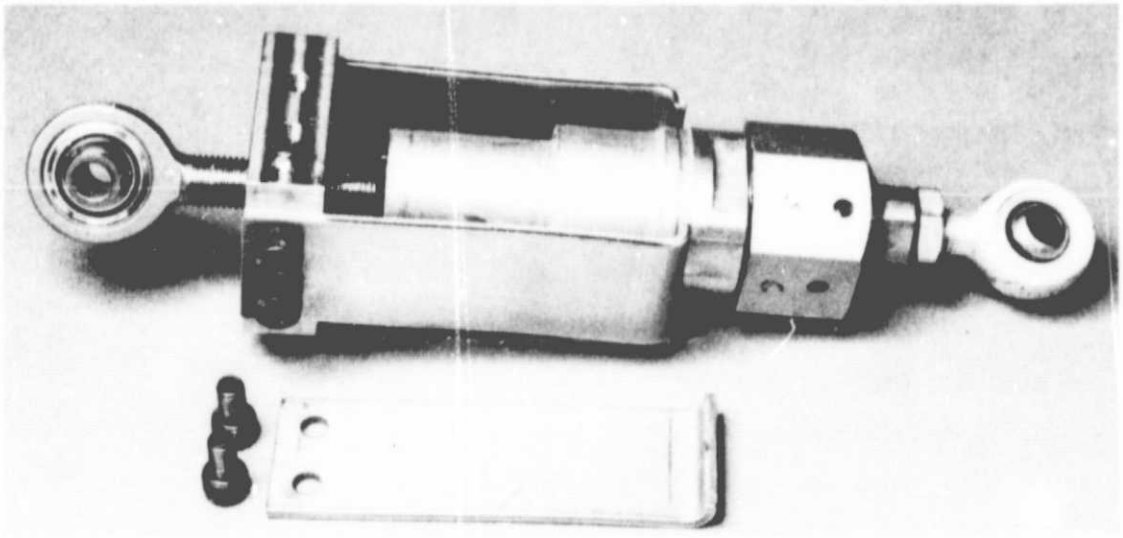

A. HE0035 Parts and PODS Mechanism

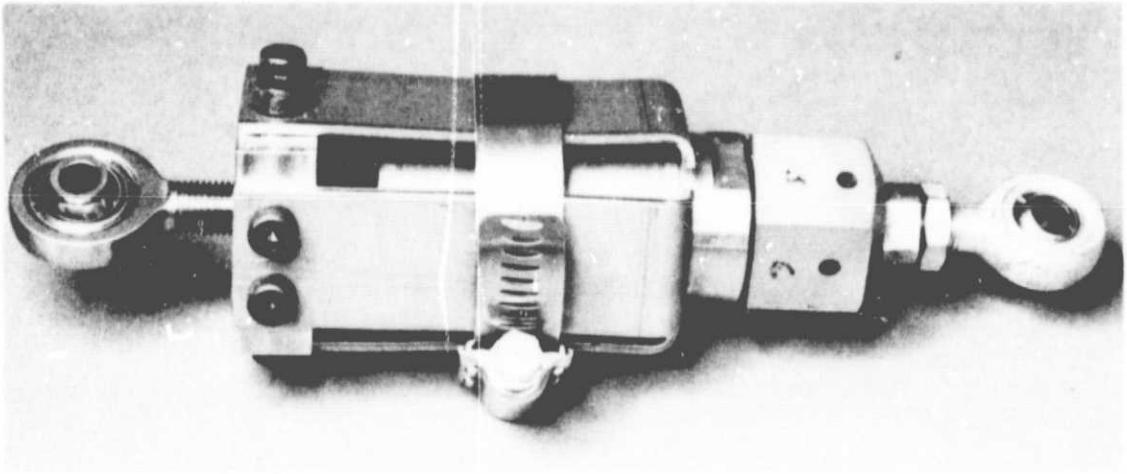

B. Assembled HE 0035 and PODS Mechanism

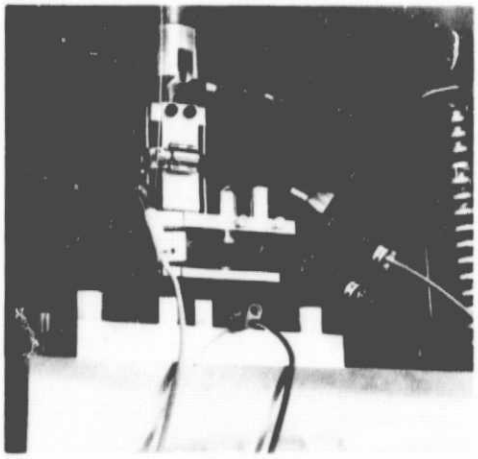

C. PODS Mechanism in Load Test

Fig. 5-15 Test Fixture for Quality Check of Load Gap Setting

must exceed 200 lb_f and the tension shorting load exceed 500 lb_f, or the PODS mechanism is rejected.

8. Hand sand the inside and outside surfaces of both ends of the S-2 glass/epoxy tube (SFH-163) 0.8 in. axially with 320 grit emery paper to remove the surface gloss. Sand so the marks form circumferentially around the part.
9. Place the tube ends (SFH-163) into tricholoroethane (immersed in an ultrasonic bath) for 1 min. Remove and rinse the tube with distilled water and air dry. No water break shall occur in the sanded areas upon rinsing within 1 min after withdrawal from the water.
10. Punch out radiation shields on a Teflon surface using disc cutter HE 0026. Handle discs with tweezers to prevent getting fingerprints on them. These discs can also be cut in large quantitites with a CO_2 laser. Stack the Dexiglas layers either four or eight deep and punch out on a Teflon surface using disc cutter HE 0025A for the outside diameter and HE 0025B for the centrally located 0.46-in. diameter vent hole. Clamp assembly rod HE 0033 in a vertical position. Place a piece of masking tape axially along the fiberglass tube, stopping 0.75 in. from one end and 1.70 in. from the other, with 1/8-in. markings between. Place the first "sandwich" of Dexiglas and double aluminized mylar (Fig. 5-16) on top of the assembly rod. Carefully lower the fiberglass tube over the discs with the 1.70-in. end up until the top of the Dexiglas reaches the 1.70-in. mark. Slowly remove the fiberglass tube. The sandwich should occupy 3/16 in. of space. The Dexiglas diameter is large enough to hold the discs in place by friction. Insert the second, third, etc. sandwiches (per Fig. 5-16) as shown. It is important that the discs occupy the approximate spaces shown even if there are slight gaps between the sandwiches. The last sandwich includes a silk net layer. If the layers start to cock during the insertion process, remove the fiberglass tube and straighten the discs with a small 1/8-in. diameter tube by pushing on the side of the discs. If the discs become badly cocked, it may be necessary to remove a few of the discs with the small 1/8-in. diameter tube connected to a small vacuum pump.

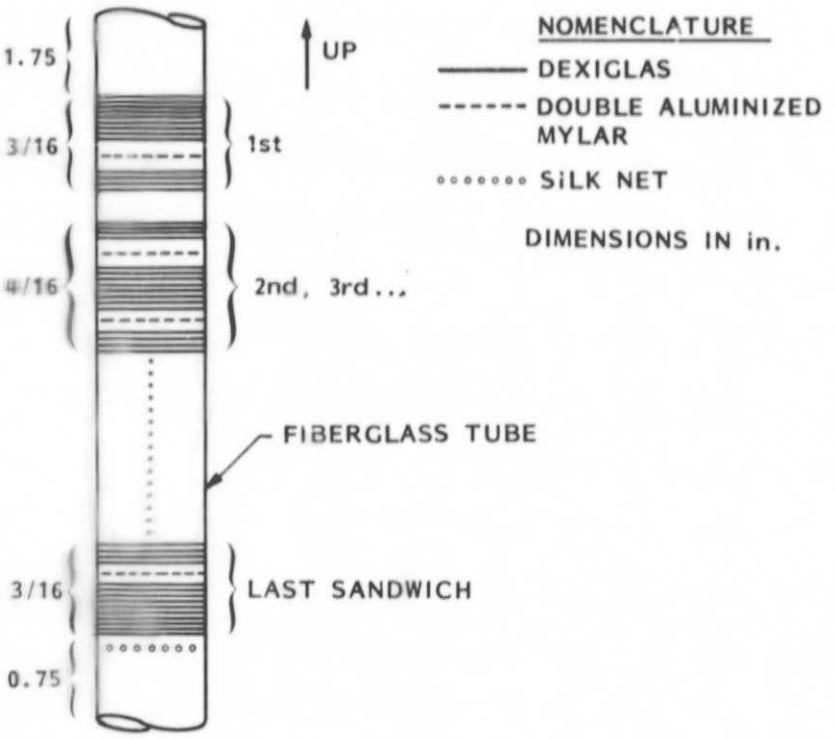

Fig. 5-16 Radiation Shield/Spacer Stacking Order

11. Step 11 must be accomplished in less than 1 h. Mix the epoxy and add 5 percent by weight glass beads. Using a metal spatula, spread a thin layer of epoxy on the warm and cold body assemblies in the areas shown.

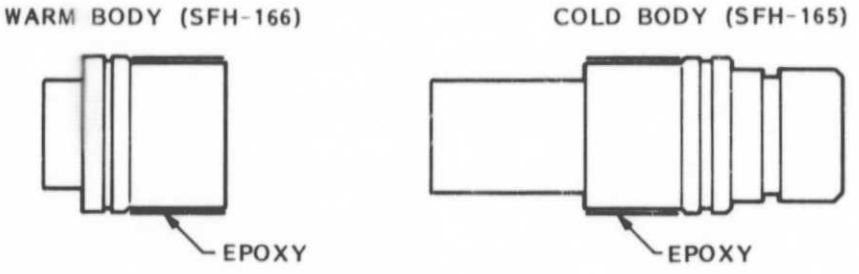

Spread a thin layer of the epoxy bead mixture inside both ends of the fiberglass tube to a depth of 0.75 in. Push the fiberglass

tube very slowly onto the bodies with the 0.75-in. open end onto the warm body part and the 1.75-in. open end onto the cold body part. Push the body parts onto the tubes slowly so the radiation shields and spacers do not move. Check the bond line for gaps or bubbles, and repeat if required. Enough excess epoxy should be available on the warm body so that the silk net spacer is bonded around the edge inside the fiberglass tube. Remove any external excess epoxy with a spatula. Place the strut in a lathe with the nut on the cold body supported in a chuck. Run the lathe dead center tip against the warm body to center it and apply slight pressure while the epoxy cures overnight.

12. Remove the strut from the lathe. Using 320 grit paper, sand any new epoxy on the fiberglass tube to remove the surface gloss. Clean the sanded areas with a trichloroethane rinse and air dry.

13. Step 13 must be accomplished in less than 1 h. Mix epoxy with 5 percent by weight glass beads. Using a metal spatula, spread a thin layer of epoxy on the inside surfaces (including the lip) of the two pairs of matched, large clamshells (SFH-171). Spread a thin layer of epoxy on both ends of the fiberglass tube to a length axially of 0.8 in.; also spread epoxy on both bodies over the lip and into the grooves as shown.

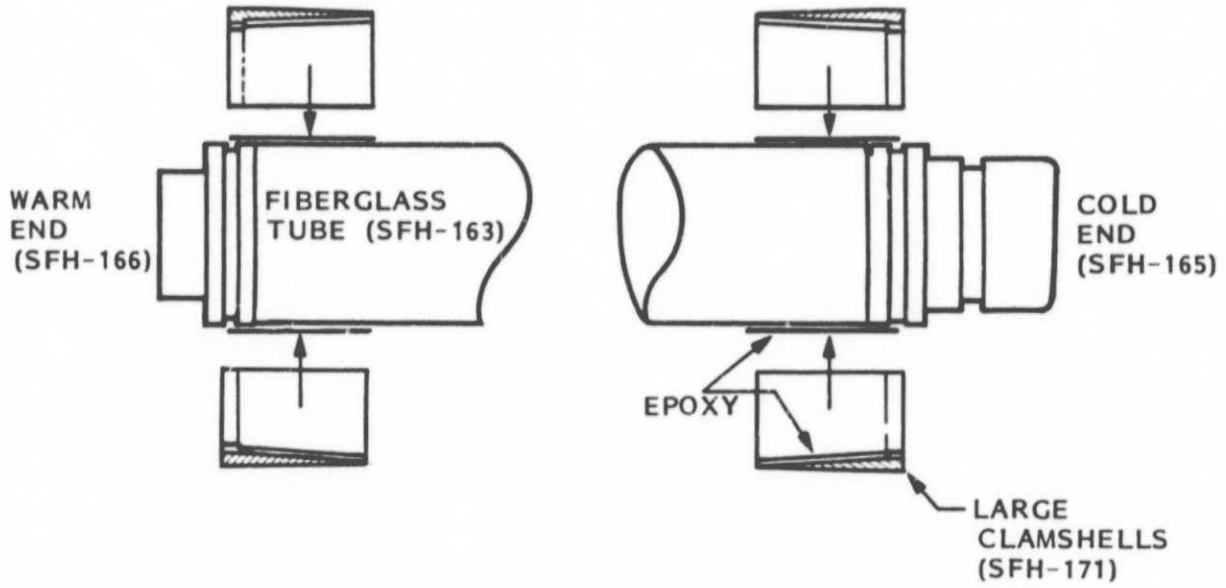

Snap the matching clamshells in place with the clamshell lip fitting into the body grooves. Hold the large clamshells with safety wire wrapped twice and then twisted. Remove excess epoxy with a metal spatula. Allow to cure overnight.

14. Cut off the safety wire. Remove excess epoxy with a scalpel.
15. Screw the jam nut (SFH-173) onto the length adjustment (SFH-170). Screw the length adjustment into the warm end body (SFH-166) so the end of the length adjustment is 0.70 in. from the warm body. Screw jam nut LS 8819-6 onto rod end 2BREM-5A-009. Screw the rod end into the length adjustment (SFH-170) so that the centerline hole of the rod end is 1.05 in. from the end of the length adjustment.
16. Screw jam nut LS8819L6 onto rod end 2 BREM-5A-009. Screw the rod end into the stem (SFH-167) so that the centerline hole of the rod end is 1.05 in. from the end of the stem.
17. Rotate the length adjustment so that the spherical bearings slip freely over the pins of the length adjustment bar (HE 0027). Tighten jam nuts SFH-173, LS8819-6, and LS8819L6. A further fine length adjustment may be required when installing all six struts. When final length adjustment is made, place a small spot of epoxy adhesive on one edge of all three jam nuts to lock them. Allow the epoxy to cure overnight.
18. Place the strut in a load machine. Take the load to 8000 N (1800 lb_f) in both compression and tension without tube SFH-163 buckling. Using an ohmmeter connected to the stem and body/nut, note at what load the strut shorts in tension (nut) and compression (body). The minimum allowable tension load is 500 lb_f. The minimum allowable compression load is 200 lb_f. Place the strut on the length adjustment bar (HE 0027). Using the side load test setup described in Section 6.1.1 with the strut in a horizontal (0 deg) attitude, hang weights on the fiberglass tube a distance of 9.3 in. from the centerline of the cold body, rod end hole. Rotate the strut and repeat the tests six times at 60-deg increments around the circumference. The minimum allowable shorting load at any of these six locations is 4.0 lb. If the strut fails any of these tests in step 19, it is rejected.

Section 6
LOAD TESTS ON A SINGLE PODS-III STRUT

A complete PODS-III strut was assembled per Fig. 3-1. The assembly procedure is described in Section 5. An axial load gap offset of 0.018 mm (0.7 mil) was used. Fiberglass/epoxy tube no. 11 from Table 4-6 and graphite/epoxy tube no. 11 from Table 4-1 were installed. The strut is 59.07 cm (23.256 in.) long from center to center of the rod end fittings, and the strut weighs 0.604 kg (1.33 lb). Side-load tests were conducted first, followed by evacuation rate tests, axial-load tests, and fatigue tests at LN_2 temperature.

6.1 SIDE-LOAD TESTS

Vapor-cooled shields attached to the struts plus installed MLI place side loads on the struts in 1-g. The side-load tests determine the maximum loads that can be tolerated as a function of load angle and location without shorting out the strut on the ground. In orbit, weight is no longer a factor.

6.1.1 Test Setup

The length adjustment bar (Fig. 5-6) supports the strut for these tests. The Invar bar has two 0.64-cm (0.250-in.) diameter press fit pins located 59.07 cm (23.256 in.) apart that slip into the rod end fittings. The bar is supported off a plate at 0 (horizontal), 15, 30, 45, 60, and 75 deg as shown in Fig. 6-1. Weights are hung on the strut at different locations (including lead shot for fine weight adjustment) until the PODS-III mechanism "shorts" as determined by an ohmmeter measurement between the body and stem. The strut can be rotated so that the shorting loads are measured at 60-deg increments around the circumference to determine how well the stem is centered between the body and nut.

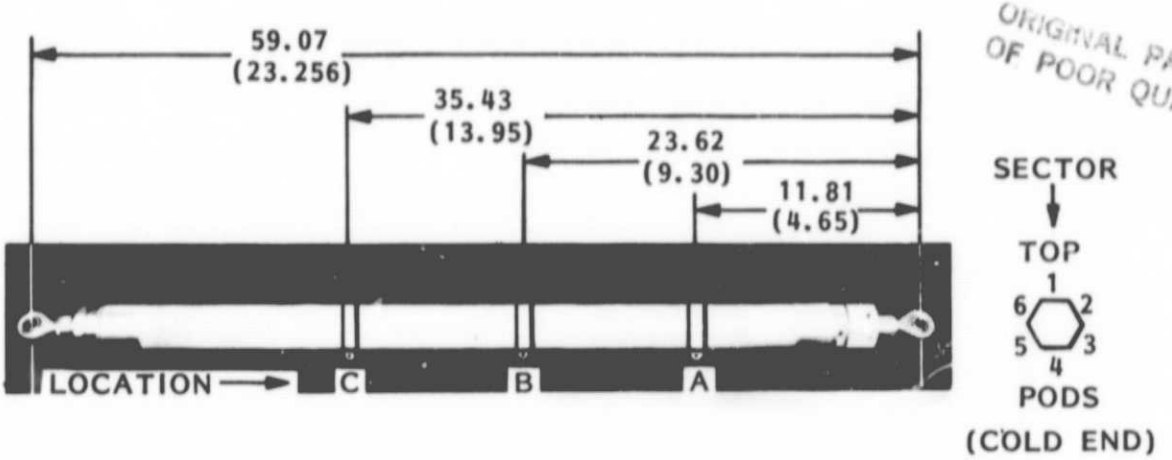

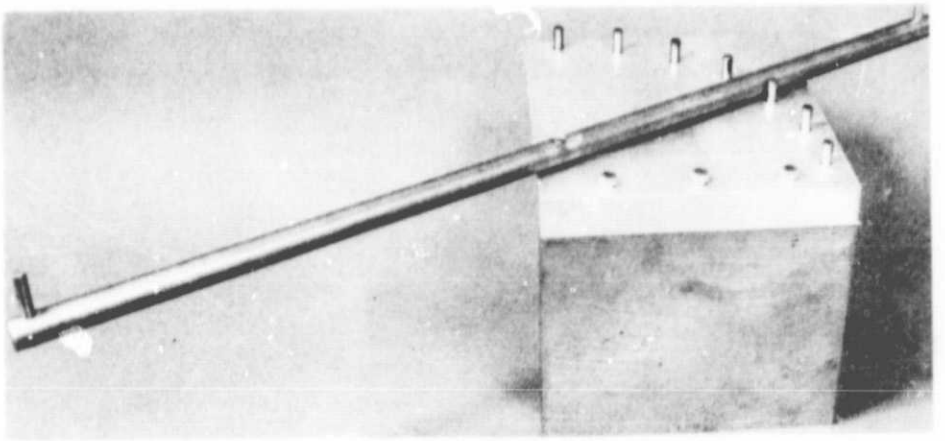

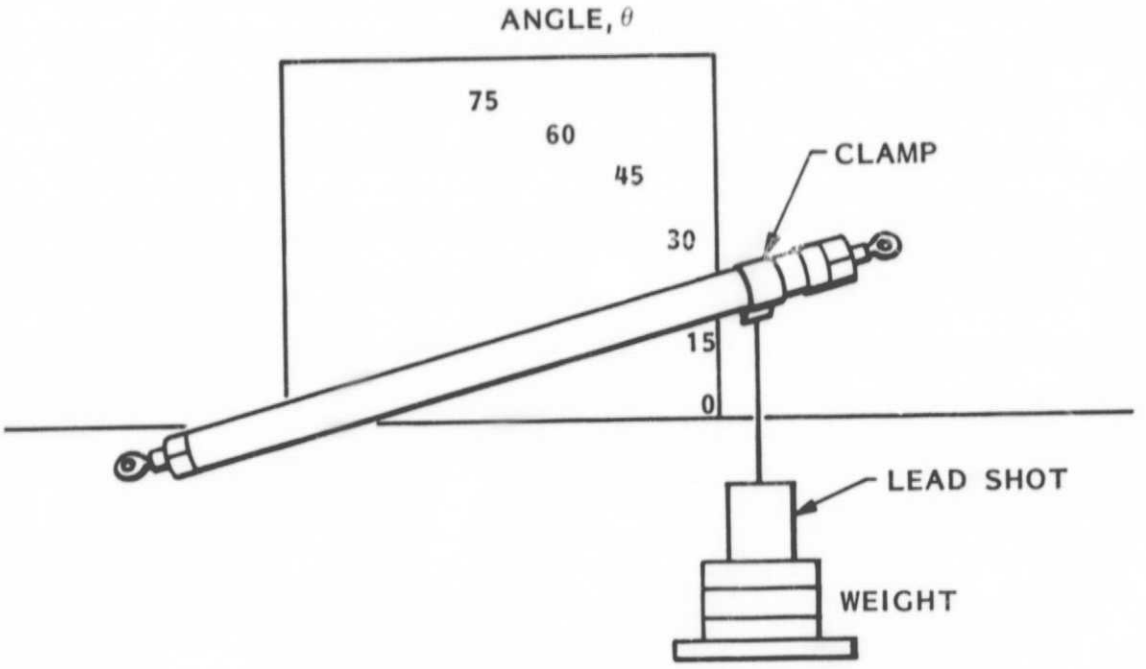

Fig. 6-1 Side-Load Test Setup

6.1.2 Test Results

The test results are tabulated in Table 6-1. The shorting measurements around the circumference with the strut horizontal were somewhat inconclusive . At some of the locations, in particular sector 6, the results were widely scattered. Perhaps a small amount of epoxy flowed onto the stem's conical surfaces, partially insulating the stem electrically and causing the erratic results. However, if the average value from sector 6 is compared to the other five sectors, the standard deviation is still only ± 12 percent for all six sectors, indicating that the stem is reasonably well centered inside the cold body and nut.

The effects of angle and load locations are plotted in Fig. 6-2. The strut angle and length relationships are given by the equations in Fig. 6-2. The empirical constant in the equation will change with the load gap setting, stem angle, and graphite tube dimensions and properties.

6.2 EVACUATION TESTS

The loosely packed radiation shields and spacers located inside the fiberglass tube can be displaced as the strut is evacuated. The purpose of this test is to determine what the maximum allowable pumpdown rate is without shield or spacer movement.

6.2.1 Test Setup

The assembled strut is placed vertically in a glass bell jar with the PODS end down. Pressure is plotted on a strip chart recorder; a variable orifice valve in the pumping line is used to control the pumpdown rate from 760 to 1 torr. A separate variable valve was used to bring the bell jar back up to atmospheric pressure. The fiberglass/epoxy tube is translucent so that movement of the shields or spacers can be detected visually.

Table 6-1 SIDE-LOAD TEST RESULTS

Angle (deg)	Sector 1 kg	1 lb	2 kg	2 lb	3 kg	3 lb	4 kg	4 lb	5 kg	5 lb	6 kg	6 lb	
	Location A												
0	1.58	3.48	1.63	3.6	1.32	2.9	1.53	3.37	1.17	2.58	2.45	5.4	
0			1.77	3.9	1.63	3.6	1.54	3.4	1.27	2.8	1.62	3.58	
0			1.88	4.15	1.27	2.8					0.77	1.7	
Average	1.58	3.48	1.76	3.88	1.41	3.10	1.54	3.39	1.22	2.69	1.61	3.56	1.52 ± 0.19 (3.35 ± 0.41)
30			2.13	4.7									
45			2.67	5.88									
60			3.65	8.05									
	Location B												
0			2.34	5.15									
30			2.69	5.94									
45			3.54	7.80									
60			4.96	10.93									
	Location C												
0			3.54	7.80									
30			4.06	8.95									
45			5.21	11.48									
60			7.03	15.50									

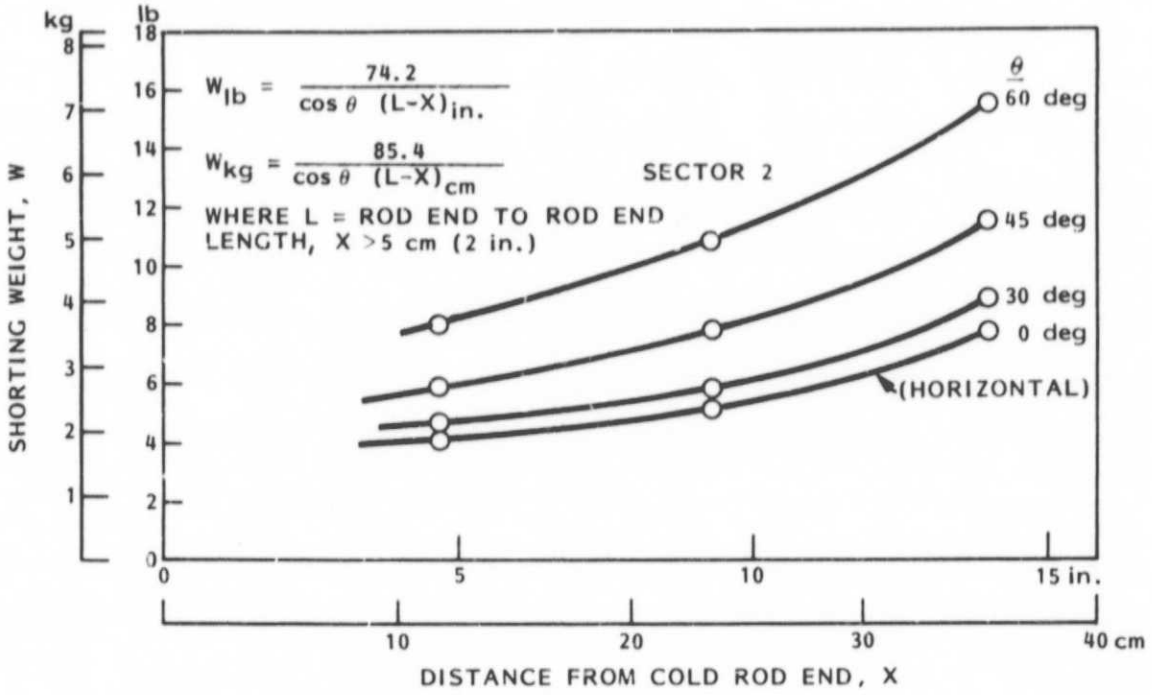

Fig. 6-2 Shorting Side Loads as a Function of Location and Angle

6.2.2 Test Results

The initial pumpdown rate from 760 to 50 torr was varied from 127 to 100 torr/min with progressively lower rates down to 1 torr. No movement of the shields or spacers was noticed. During air backfill to 760 torr, the letup rate was inadvertently increased to 540 torr/min. At this rate, the shields and spacers packed toward the PODS end of the strut, leaving an empty gap of approximately 9.9 cm (3.9 in.) at the other end of the strut. The shields and spacers were compressed approximately 24 percent. The safe pumpdown rate or letup rate is therefore somewhere between 127 and 540 torr/min. In practice, the maximum dewar pumpdown rate is held to 0.5 torr/min.

6.3 AXIAL LOAD TESTS

6.3.1 Test Setup

The strut was mounted in a load machine enclosed inside a foam insulated box as shown in Fig. 6-3. Two strain gages each were mounted in the middle and on opposite sides of both the fiberglass and graphite tubes. Thermocouples were located at both ends and in the middle of the strut. Shorting leads from the stem and body were connected to an ohmmeter. A LN_2 fill line was connected to the lower end of the foam container with an overflow line 10 cm nigher. This allowed the PODS mechanism to be immersed in LN_2 while the cold N_2 vapor cooled the fiberglass strut. The cold rod end fitting was enclosed in a shroud and purged with GN_2 to prevent frost formation. The warm rod end was heated periodically with a hot air gun when frost appeared.

6.3.2 Test Results

The strut was loaded three times in both tension and compression to 8000 N (1800 lb_f). The strut was then cooled with LN_2, and the tests were repeated. The strut withstood the load cycles without buckling. Typical temperature profiles along the strut were:

78 K	cold end
161 K ± 20 K	middle
237 K ± 6 K	warm end

The loads at which shorting occurred (as determined by the ohmmeter and by a change in slope of the load/strain plots for the graphite tube) are given in Table 6-2.

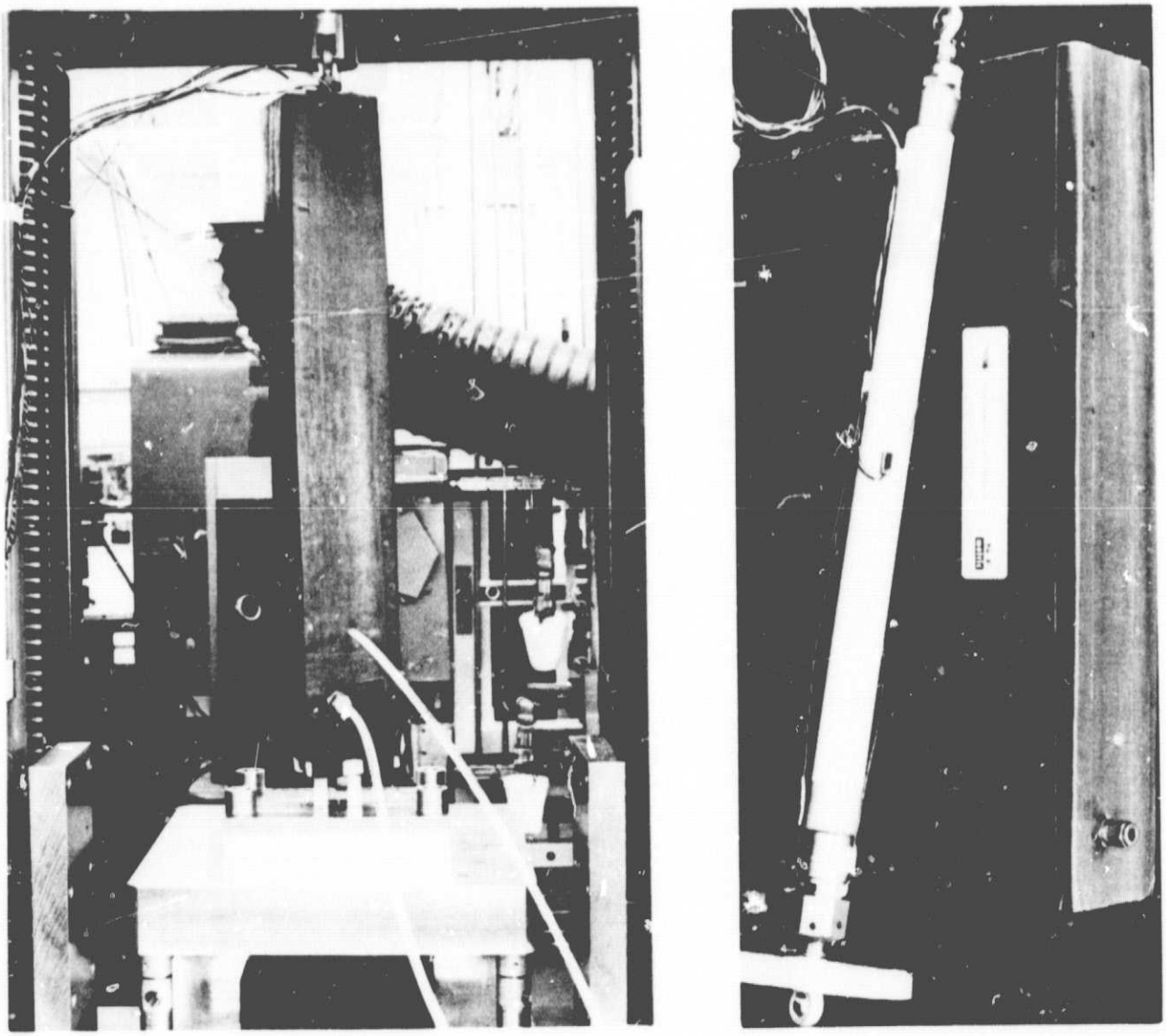

Fig. 6-3 Axial-Load Test Setup

Table 6-2 SHORTING WEIGHT
kg (lb)

Load	Temp	Ohmmeter		Change of Slope of Stress-Strain Plot	
		Short	Unshort	First Variation from Straight Line	Straight Line Intersections
Compression	Amb	114 (251)	140 (309)	136 (300)	161 (355)
Tension	Amb	243 (535)	234 (516)	236 (520)	232 (555)
Compression	LN_2	248 (547)	223 (492)	245 (540)	258 (568)
Tension	LN_2	186 (409)	177 (390)	163 (360)	175 (385)

6.4 FATIGUE TESTS

6.4.1 Fatigue Loads

Preliminary analyses were performed on the limit load as a function of the effective weight the PODS-III struts can support in an STS combined quasistatic/dynamic launch acceleration environment.

The limit load is calculated as follows:

$$W_{\text{limit load}} = W_{\text{eff}}(g_{\text{dynamic}} + g_{\text{quasistatic}})$$

where

W_{eff} = effective supported weight, total

g_{dynamic} = dynamic acceleration from Fig. 6-4 for $C/C_c = 0.00$ and effective supported weight (no critical damping)

$g_{\text{quasistatic}}$ = 3.17

The results are plotted parametrically in Fig. 6-5. For a strut angle of 45 deg from the horizontal, the axial limit load for six PODS-III struts per the design given in Section 3 is (1800 lb_f)(6)(sin 45 deg) = 7640 lb_f where the design limit load per strut is 1800 lb_f or a safety factor of 1.5 over the ultimate load of 2769 lb_f. From Fig. 6-5, the effective supported weight is 584 lb_f. Fatigue loads are determined by the quasistatic accelerations, so the selected loads for the fatigue test per strut are given by:

$$\text{Fatigue Load per Strut} = \frac{584\ lb_f(4.448\ \frac{N}{lb_f})(3.17)}{6 \sin 45\ deg} = 1941\ N\ (436\ lb_f)$$

6.4.2 Fatigue Test Setup

Two fatigue tests were conducted on the PODS-III strut with the cold end held at 78 K and instrumented as described in the axial load tests. The first test alternately loaded the strut in tension and compression to load values given in section 6.4.1. The second test alternately loaded the strut in tension and compression to failure at design limit loads. The test setup is shown in Fig. 6-6.

6.4.3 First Fatigue Test

For the first test, a 10-Hz sinusoidal fatigue load of ± 1980 N (± 445 lb_f) was applied (slightly above the calculated value). The fatigue tests were stopped at 35,000, 100,000, 240,000, 350,000, and 500,000 cycles. Stress-strain curves were plotted for both the fiberglass/epoxy and graphite/epoxy tubes to the design limit load of ± 8000 N (± 1800 lb_f). These tests were conducted both with a cooled strut and at ambient temperature. The strut was warmed to ambient temperature after 35,000, 240,000, 350,000, and 500,000 cycles. Following each ambient-temperature load-strain test, the strut was cooled down for additional fatigue cycles.

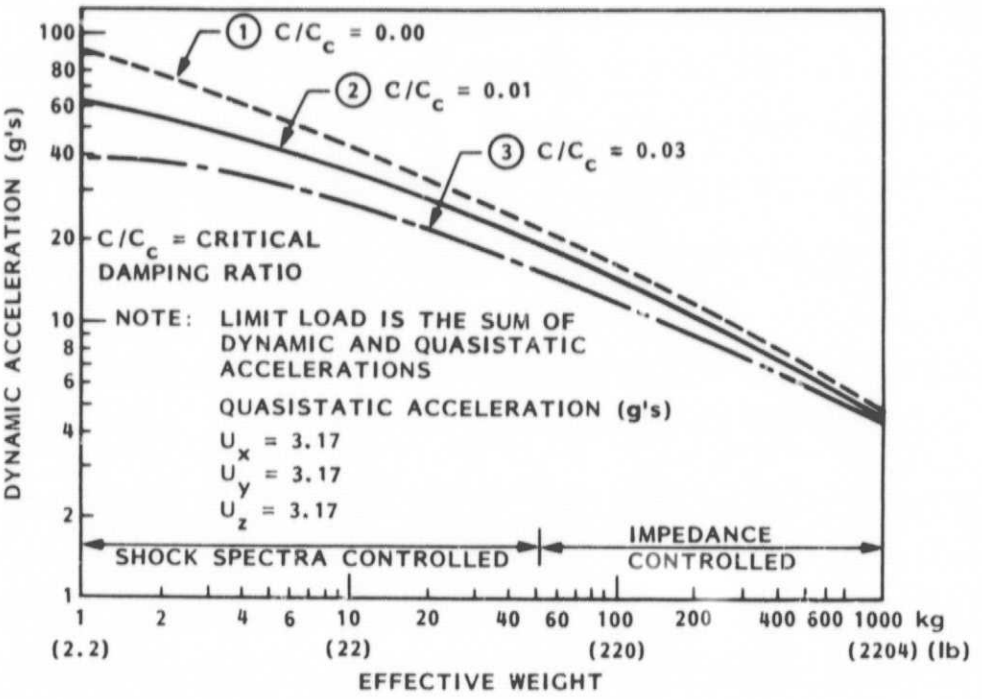

Fig. 6-4 STS Dynamic and Quasistatic Acceleration

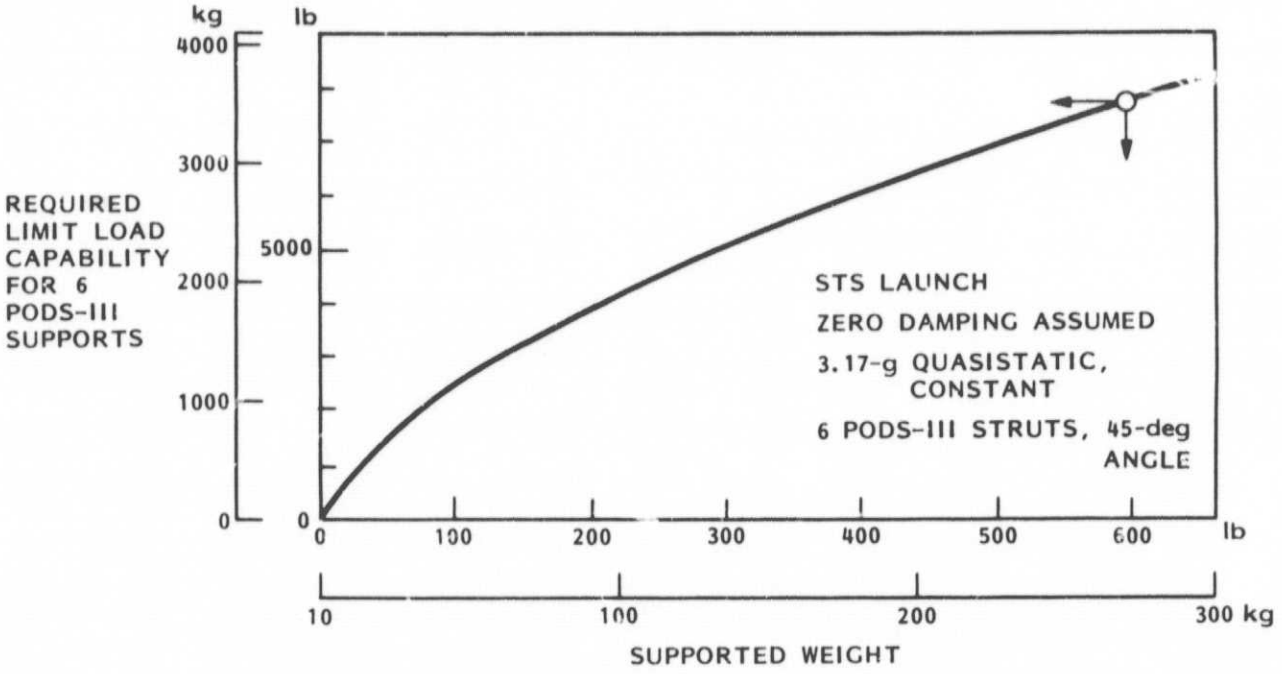

Fig. 6-5 Limit Load Requirement Versus Supported Weight

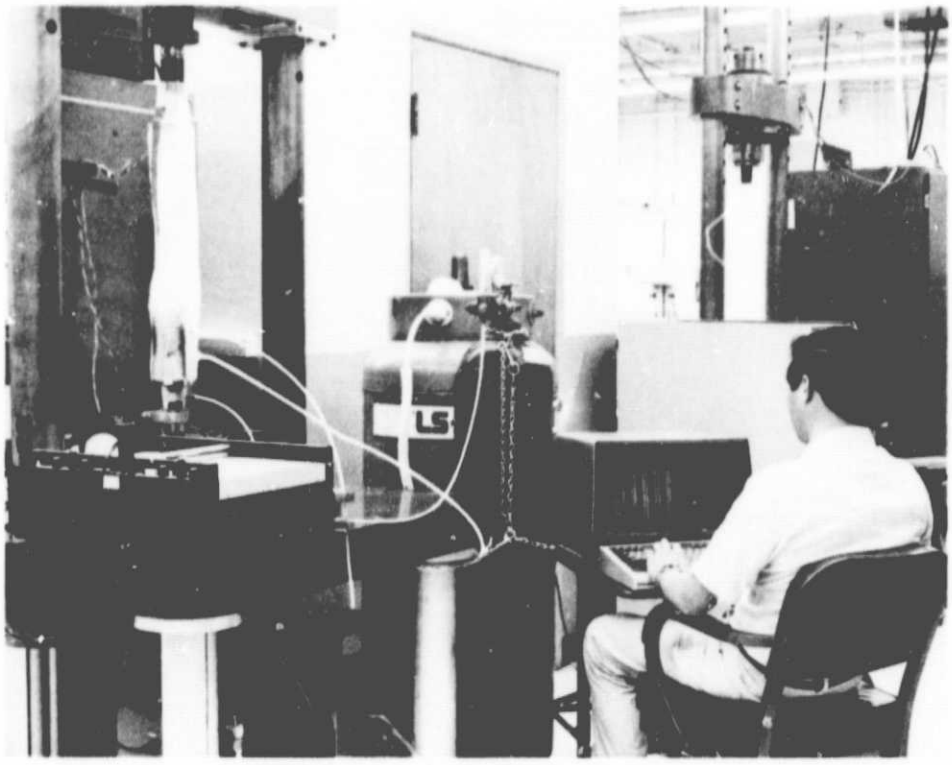

Fig. 6-6 Fatigue Test Setup

The total number of applied load cycles was 1,000,000: 500,000 in tension and 500,000 in compression.

The temperature history of the strut is shown in Fig. 6-7. At 35,000 cycles, the design of the foam-insulated box was modified to allow the warm end of the strut to run at a higher temperature. There is relatively good temperature contol after 80,000 cycles at both ends of the strut, but there is a wide temperature band in the middle of the fiberglass tube.

Figure 6-8 shows the modulus for each tube, calculated from the load-strain plots and cross-sectional area, as a function of the number of load cycles. No apparent change in modulus is noted up to 500,000 cycles for the fiberglass/epoxy tube. The strain gages on the graphite/epoxy tube failed open at 100,000 cycles and read intermittently in compression at 240,000 cycles and room temperature. No apparent change in graphite modulus is noted within the experimental accuracy of the measurement.

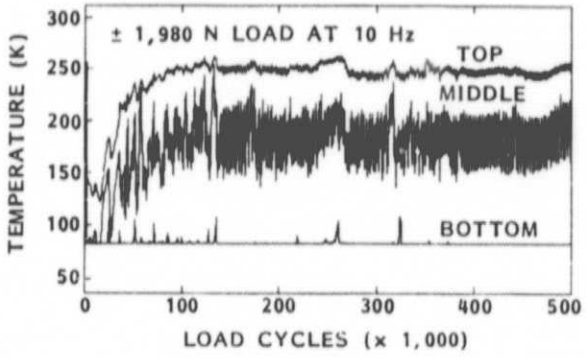

Fig. 6-7 PODS-III Temperature During First Fatigue Test

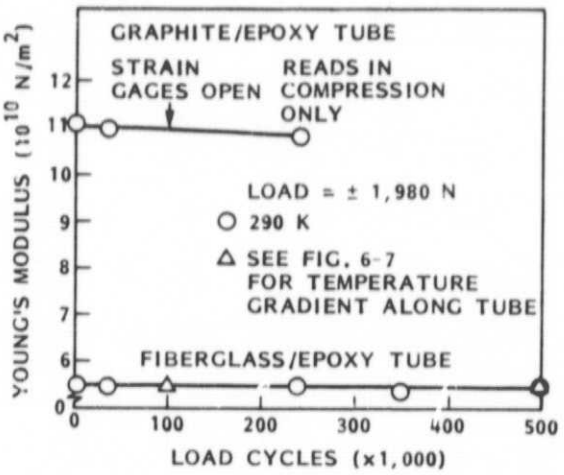

Fig. 6-8 Effect of Load Cycles on Modulus

This conclusion is verified by the results of the electrical shorting measurement (Fig. 6-9). The shorting weight is constant up to 500,000 cycles in both tension and compression and at 290 K and 78 K, except for one point in compression at 78 K and 500,000 cycles. It may be that ice forming in the gap caused this high result. The same compression point at ambient temperature shows no change. These data indicate that the graphite tube modulus and load gap setting have not changed after 500,000 load cycles.

6.4.4 Second Fatigue Test

The strut used in the first fatigue test was fatigue cycled in the same test setup to destruction at the limit design load of ± 8,000 N (± 1800 lb_f). A 10-Hz sinusoidal loading cycle was used as in the first test, with the cold end held at 78 K. This loading is much more severe than the strut will ever experience in an STS launch environment.

The epoxy bond at the cold end of the fiberglass/epoxy tube failed at 16,200 load cycles (16,200 compression and 16,200 tension cycles). The fiberglass tube end had minor damage due to the pounding it absorbed during the several seconds it took to shut the load machine down. An ohmmeter resistance check of the body to stem indicated that the graphite/epoxy tube was not damaged.

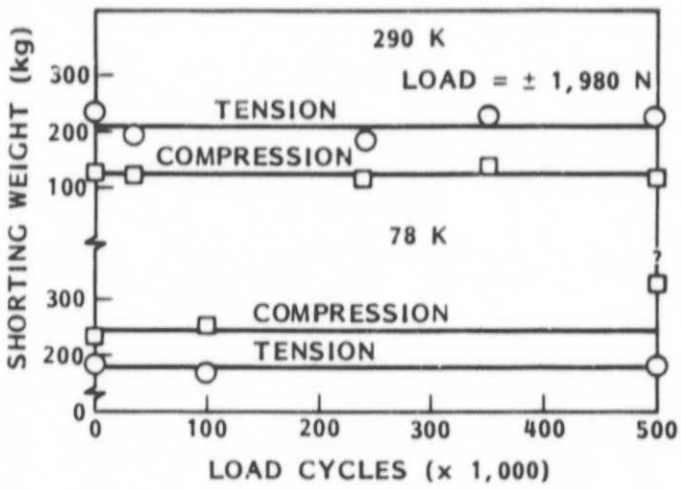

Fig. 6-9 Effect of Load Cycles on Shorting Weight

The bond between the clamshell and the outside of the fiberglass/epoxy tube failed at the Invar/gold-coating interface. The bond between the cold body and the inside of the fiberglass/epoxy tube failed at the epoxy/gold-coating interface. Epoxy remained bonded to both the outside and the inside of the fiberglass/epoxy tube.

The strut was repaired by eliminating the gold coating in the bond area and roughening the Invar surfaces to a greater degree to improve adhesion. After test resumption, the warm rod end fatigued and separated at 110,360 cycles (Fig. 6-10).

Failure of the Southwest Products Co. rod end bearing SWREM-4-100 was initiated by fretting (a small-amplitude ocsillating motion). This action is observed on the inner body and outer race mating surfaces by the dark spotty color (Fig. 6-10). This fretting action then instituted a classical thumb-nail fatigue crack, as can be seen on one side of the body. The fatigue crack grew, as cycle loading progressed, until it became critical and was followed by catastropic tensile/bending failure.

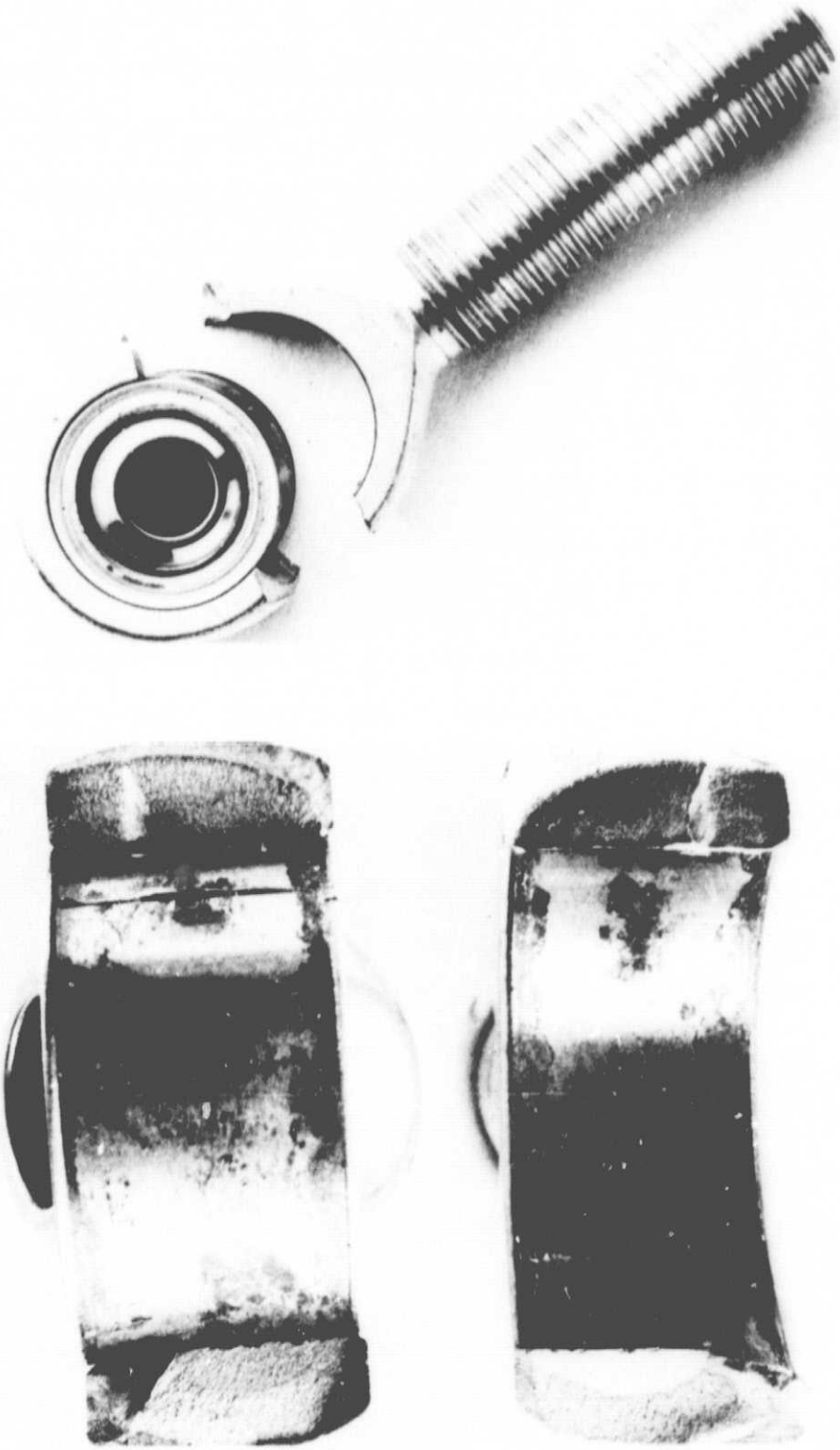

Fig. 6-10 Failed Rod End Bearing

Southwest Products has recommended switching to a two-piece rod end design from the current three-piece design and from their SWPCO-9 super alloy steel to Inconel 718 to improve the fatigue life. Inconel 718 has excellent mechanical properties down to helium temperatures. The part number for the new rod end is 2BREM-5A-009. Fatigue testing of this rod end should be performed before it is used in flight dewars.

The shorting weight at 293 K following all fatigue testing is 129 kg (284 lb) in compression and 154 kg (339 lb) in tension. The compression load is unchanged when compared to prefatigue load measurements (Fig. 6-9). The tension shorting weight is somewhat lower than the average 205 kg (451 lb) value measured previously (Fig. 6-9). The strut has been cooled nine times from the ambient to 78 K during the structural test program.

The strut was heated in an oven to 475 K to soften the epoxy, and the nut was removed from the cold body. Examination of the contacting conical surfaces of the stem and nut shows a polished, slightly fretted circular ring on both parts where the load transfer occurred as shown in Fig. 6-11.

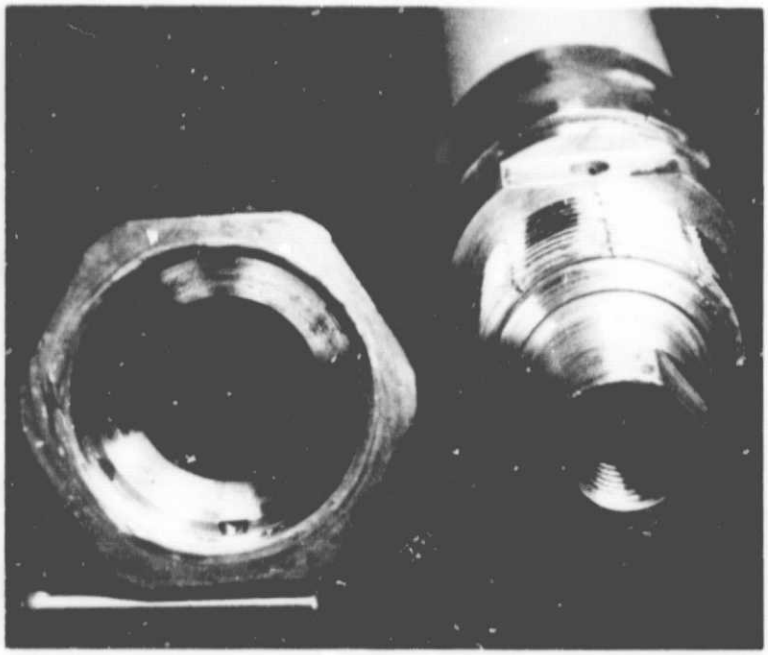

Fig. 6-11 Conical Load Surfaces After the Second Fatigue Test

Section 7
LOAD TESTS ON SIX PODS-III STRUTS

Six PODS-III struts were assembled per the procedure given in Section 5, except that rod end fittings SWREM-4-100 were used. Future applications of the struts should use the BREM-5A-009 rod ends. Characteristics of the graphite/epoxy and fiberglass/epoxy tubes used in the struts are given in Tables 4-1 and 4-7 respectively.

Before installing the six struts in the dewar simulator, each strut was loaded individually three times in tension and three times in compression (per the procedure described in Section 6.3) to the design limit load of 8000 N (1800 lb_f) without failure. The average measured shorting weights are given in Table 7-1. These values are used as references against which the six-strut performance can be compared.

Table 7-1 MEASURED SHORTING WEIGHTS FOR SIX STRUTS

Strut	Shorting Weight kg (lb)	
	Tension	Compression
1	249 (550)	109 (240)
2	237 (522)	108 (237)
3	262 (577)	131 (288)
5	244 (538)	114 (252)
6	271 (598)	114 (252)
7	277 (611)	131 (288)
Average	257 ±16 (566 ±35)	118 ±10 (260 ±23)
Axial Load Gap at 290 K mm (mil)	0.097 (3.8)	0.056 (2.2)

The good agreement shows that the load gap was held to within 0.005 mm (0.2 mil) of the desired value between all six struts.

7.1 DEWAR SIMULATOR

A dewar simulator was designed so that simulated ground hold, launch, and orbit loads can be applied. These include loads from the weight of the tank, helium, vapor-cooled shields, and insulation. In addition, loads due to temperature changes in the tank and vacuum shell can be simulated.

The simulator was fabricated and installed in a three-post load machine as shown in Figs. 7-1 and 7-2. A 56-kg (123.5-lb) triangular aluminum plate and six adjustable clevis fittings (Fig. 7-3) simulate the aluminum tank attachments. Each clevis can be adjusted along the radius to simulate temperature changes. Three aluminum blocks are attached to the three load posts. Six adjustable clevis fittings (Fig. 7-4) attached to the blocks simulate the vacuum shell attachments. Each clevis can be adjusted along the radius to simulate temperature changes. The six struts are installed as shown at a 55-deg angle from the horizontal. (This angle was changed from 45 deg to 55 deg to match a dewar that is currently being designed.)

Axial compression or tension hydraulic loads were applied at the geometric center of the simulated tank through a load cell and large spherical bearing (Fig. 7-1). For some tests, the weight of the simulated tank was taken off the struts by suspending the weight from a pinned clevis on the top center of the triangular aluminum plate. All struts were electrically wired using six light bulbs and a power supply to indicate when each strut shorted.

For the side-load tests, the loads were applied through a center post and three rigid arms as shown in Fig. 7-5 to simulate the weight of the vapor-cooled shields and insulation. The center post was attached to the load machine hydraulic actuator through a spherical bearing and load cell. Each arm was attached to the center of a bar through a spherical bearing.

The end of each bar was attached to one strut through double-ended spherical bearings and a rubber-lined clamp secured around the strut. The setup was designed so that the strut attach points can be varied along the length of the

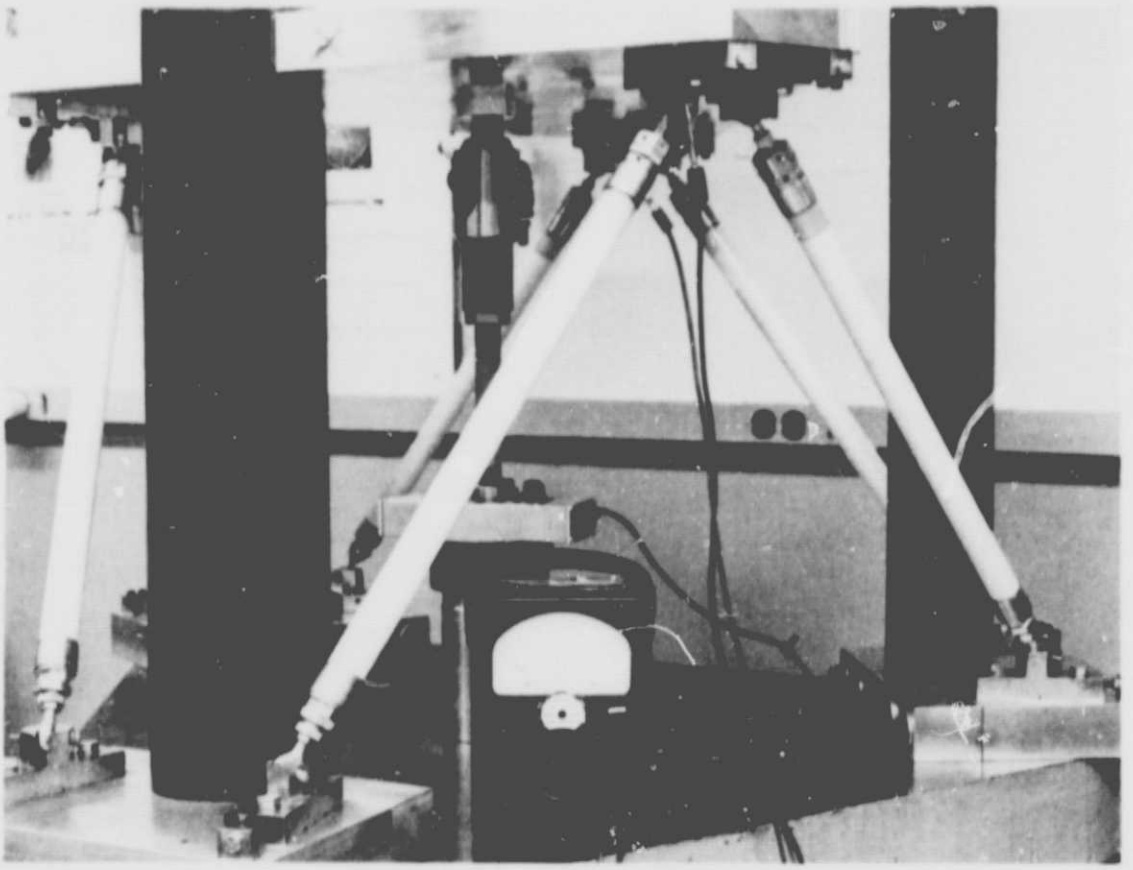

Fig. 7-1 Dewar Simulator

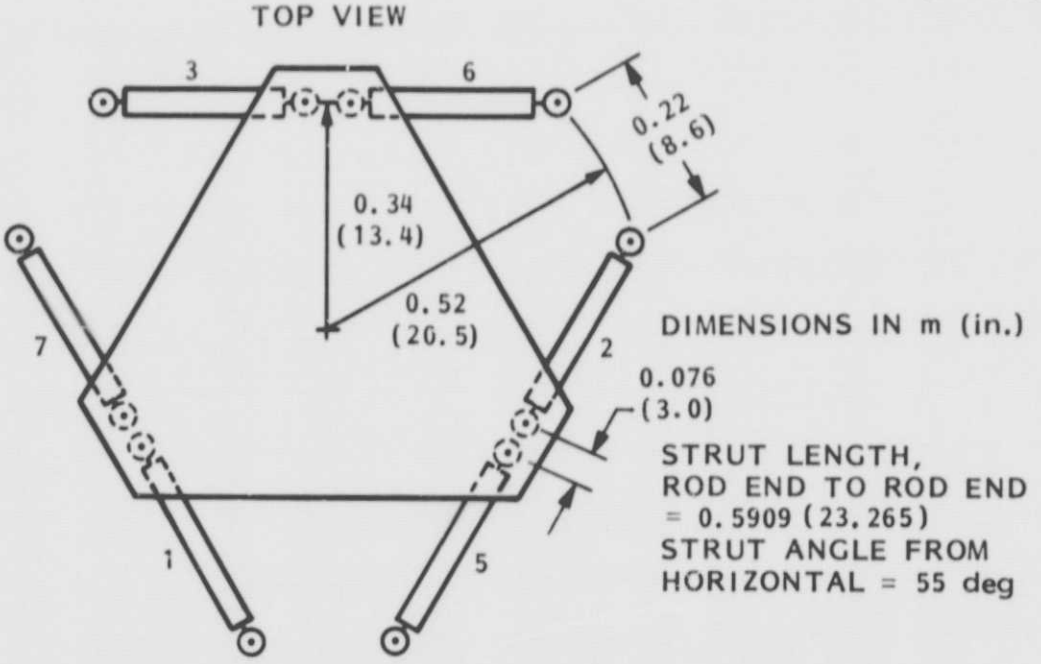

Fig. 7-2 Dewar Simulator Dimensions

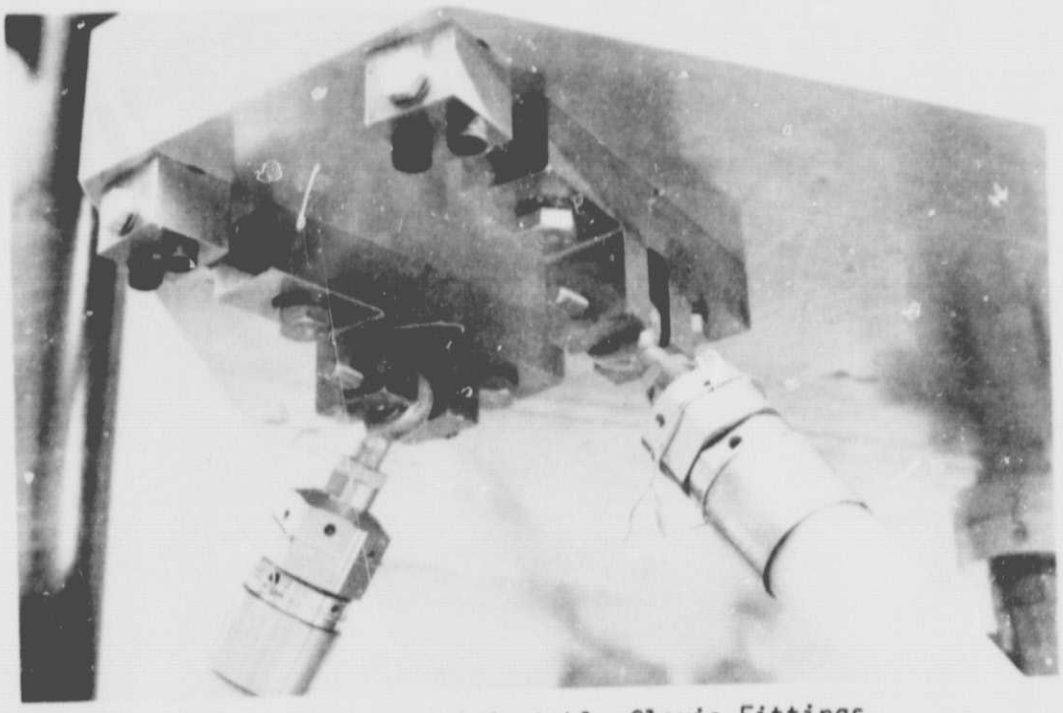

Fig. 7-3 Tank Adjustable Clevis Fittings

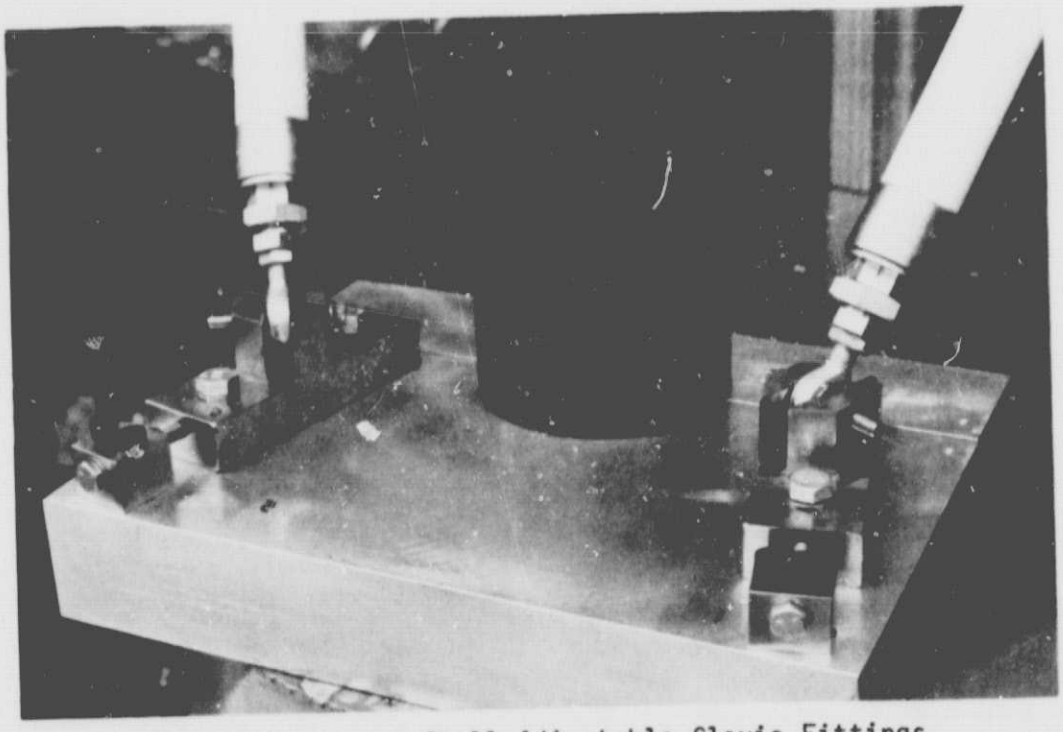

Fig. 7-4 Vacuum Shell Adjustable Clevis Fittings

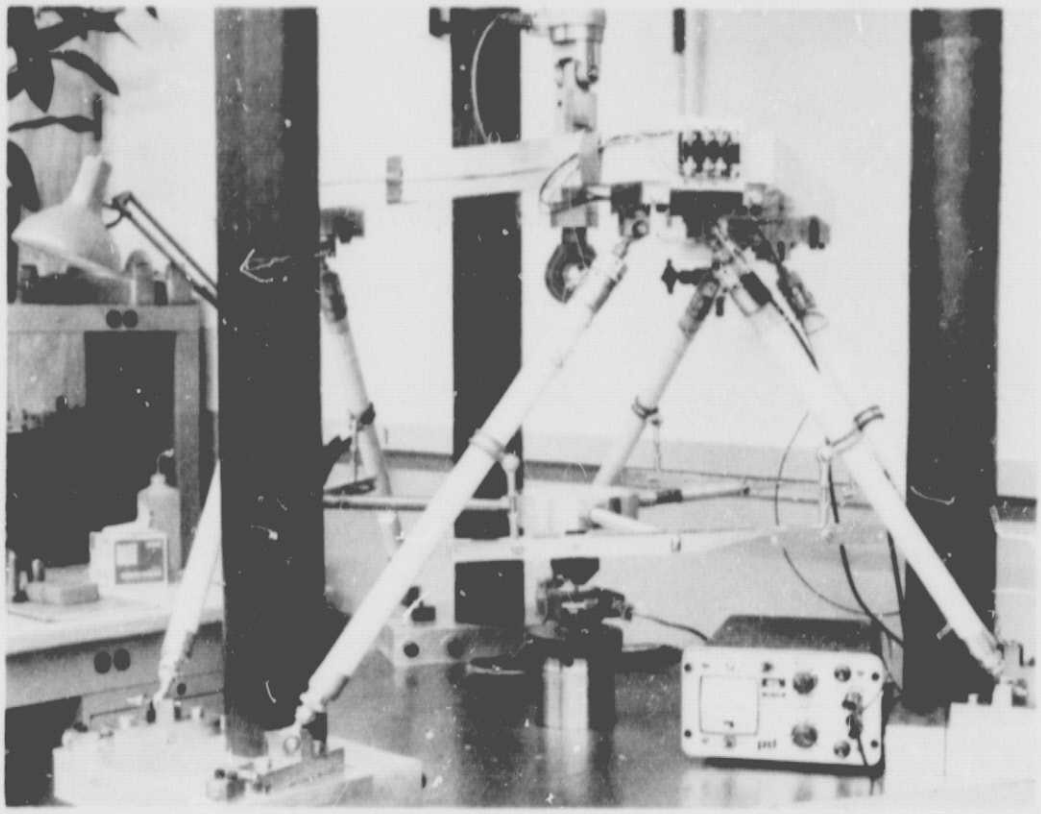

Fig. 7-5 Side-Load Test Setup

strut. With this setup, equal compression side loads can be applied to all six struts at the same time.

7.2 STRUT INSTALLATION PROCEDURE

The simulated tank was supported from the top center clevis. The length of all six struts, rod end to rod end center, was set accurately to 0.5907 m (23.256 in.) using the length adjustment bar HE 0027. Initially all six struts were attached to the tank clevises with Expando bolts to remove play. Three struts were attached to the vacuum shell clevises with close-tolerance bolts undersized on the diameter by 0.013 mm (0.5 mil). The remaining three struts were installed and slight length adjustments made as required using the warm-end length adjustment feature.

By iterating the installation procedure around all six struts and monitoring the load cell and the six light bulbs, it was determined that less than a 2-N

(0.5-lb_f) load was put into any one strut. The six close-tolerance bolts were then removed one by one from the vacuum shell and replaced with Expando bolts. Even though these bolts removed all play between the rod end and the clevis, there was still play in the rod end itself between the spherical bearing and the rod end. This play allowed slightly uneven loading of the struts as shown by the axial test results in Section 7.3.

7.3 AXIAL-LOAD TESTS

Axial loads were applied to the six struts through the large central spherical bearing in both tension and compression. The weight at which each strut shorted is shown in Fig. 7-6 after four load cycles. From these curves, it appears strut number five picks up the load first and strut number six is loaded last in both tension and compression. The average tension shorting load falls 4 percent below the average shorting loads of individual struts (Table 7-1). The 55-deg strut angle was accounted for in this comparison. The average compression load is 29 percent lower.

The axial load was then increased to 90 percent of the design limit load of 35,600 N (8000 lb_f) in both tension and compression. Ninety percent was selected to account for the slightly uneven loading measured in the struts. This cycle was repeated four times. No strut failure was noted. The average measured shorting loads were also measured and compared to those from the previous test. No change in the shorting load was evident as shown in Fig. 7-7.

7.4 SIDE-LOAD TESTS

Figure 7-5 presents the test setup. Tests were conducted with the load attached at different points along the strut. In addition, the weight of the triangular aluminum plate, 56 kg (123.5 lb), was applied simultaneously for all but one of the tests. Seven load cycles were performed. The results for the 0.36-m (14-in.) attach point are shown in Fig. 7-8 (axial weight of 56 kg) and Fig. 7-9 (minimal axial weight). Strut 6 shorts at a higher load than the

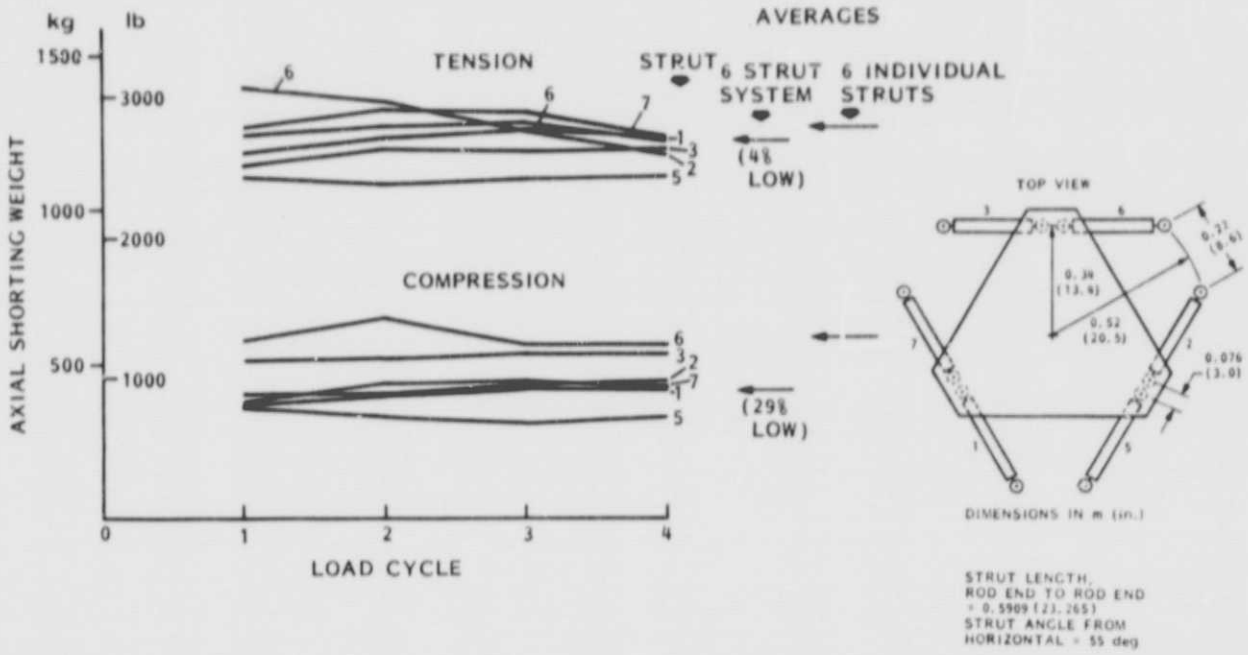

Fig. 7-6 Axial Shorting Loads

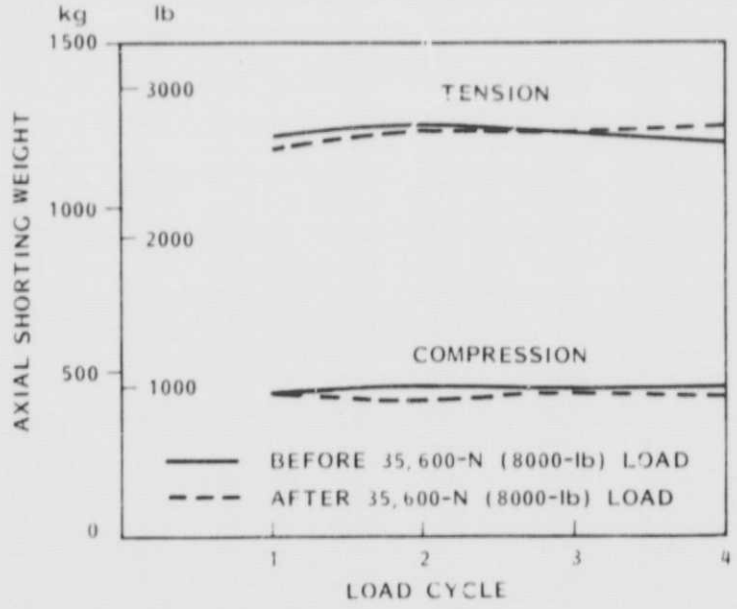

Fig. 7-7 Axial Shorting Loads Before and After 90 Percent of Design Limit Load

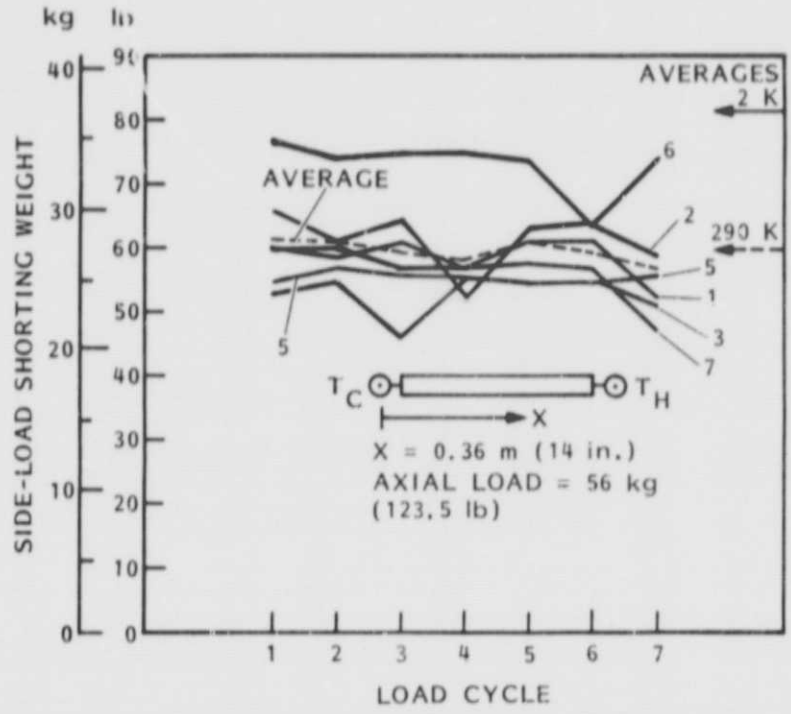

Fig. 7-8 Side-Load Shorting Test With Axial Load (X = 0.36 m)

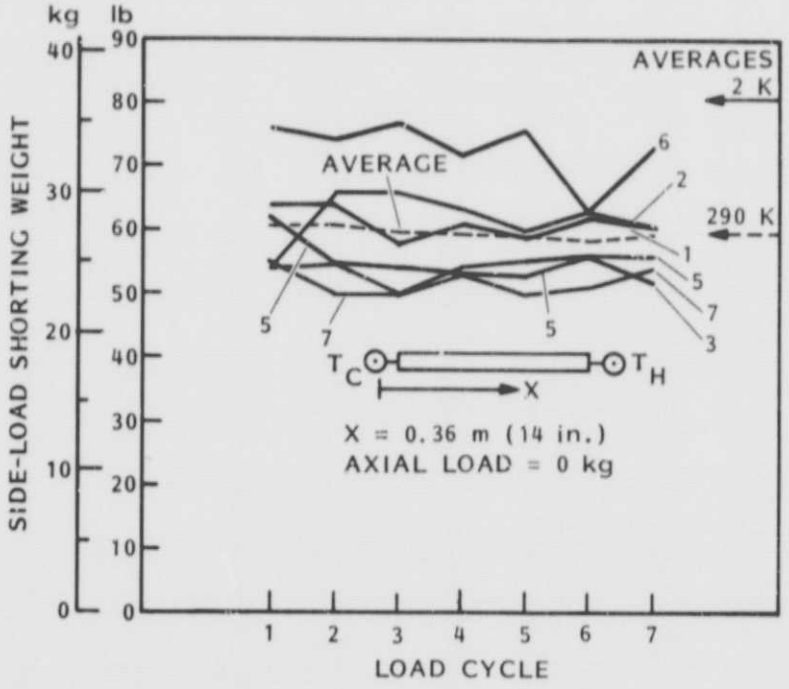

Fig. 7-9 Side-Load Shorting Test With No Axial Load (X = 0.36 m)

remaining five struts. The average value for all struts is the same whether an axial weight of 65 kg is applied or not applied.

Data taken at the 0.25-m (10-in.) and 0.15-m (6-in.) attach points are shown in Figs. 7-10 and 7-11. Again, strut 6 is the highest, with the remaining five struts grouped together. Apparently strut 6 has a larger axial- and side-load clearance than the remaining five struts.

In Fig. 7-12 the side-load shorting weight is plotted as a function of the attach point distance from the cold end. The results are compared to tests performed previously on a single strut (Fig. 6-2). The slight differences in load gap setting and the differences in strut angle were accounted for in this curve. The predicted side-load shorting weights at operating temperature (2 K) are also shown where the tension and compression load gaps are equal.

If a substantially larger side-load shorting capability is required, i.e., for very large dewars such as SIRTF (4000L) or GP-B (1600L), a modified version of the PODS design is recommended. The Invar nut is modified and a titanium collar added; six graphite filament "spokes" with equal pretension loads are epoxy bonded to the nut and collar as shown in Fig. 7-13. The equal pretension load technique was developed for and demonstrated on the PODS-I design. Titanium was chosen for the collar to ensure that the filament preload does not go slack when the strut is cooled to operating temperature; i.e., the strain increases only 0.02 percent in the graphite filament upon cooldown.

Preliminary analyses show that the graphite epoxy strands can be sized so the total support conductance increases only 10 percent or less while the side-load shorting resistance increases nearly a factor of 10. The thermal contact resistance between the collar and stem will be high at low temperature, thus decreasing the conduction heat leak down the fibers even further. It is recommended that a design, fabrication, and test effort be initiated to demonstrate this PODS-IV version of the strut.

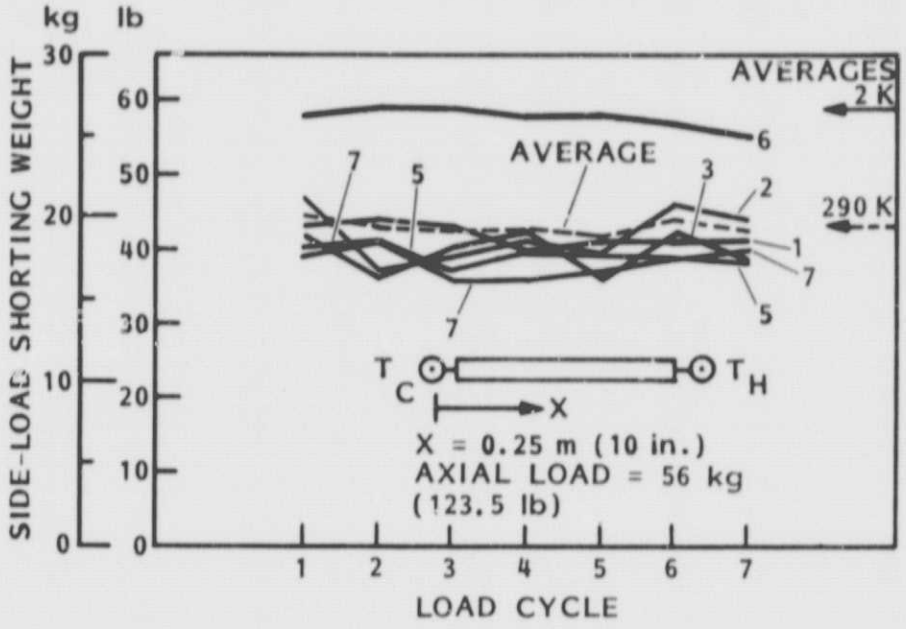

Fig. 7-10 Side-Load Shorting Test With Axial Load (X = C.25 m)

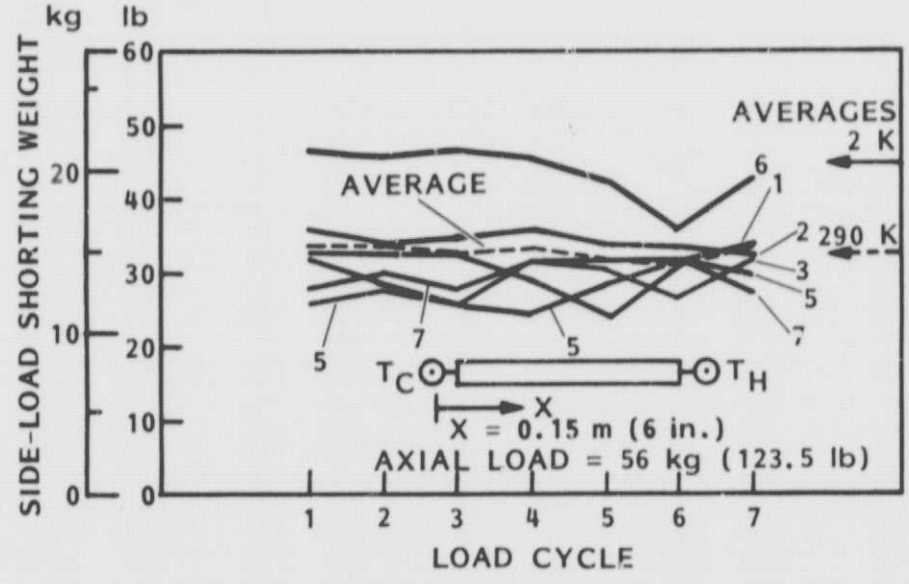

Fig. 7-11 Side-Load Shorting Test With Axial Load (X = 0.15 m)

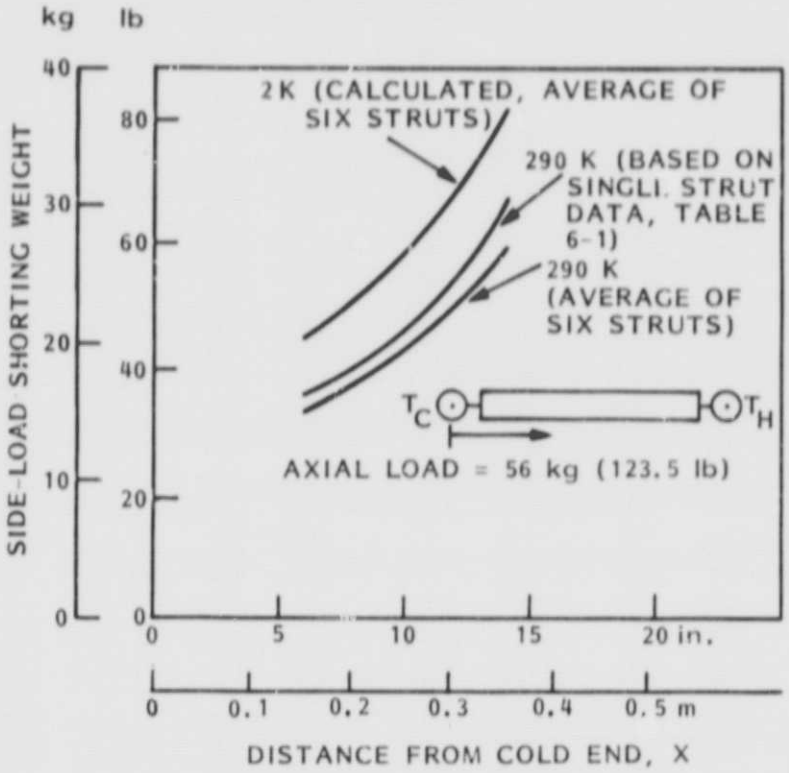

Fig. 7-12 Side-Load Shorting Versus Attachment Location on the Struts

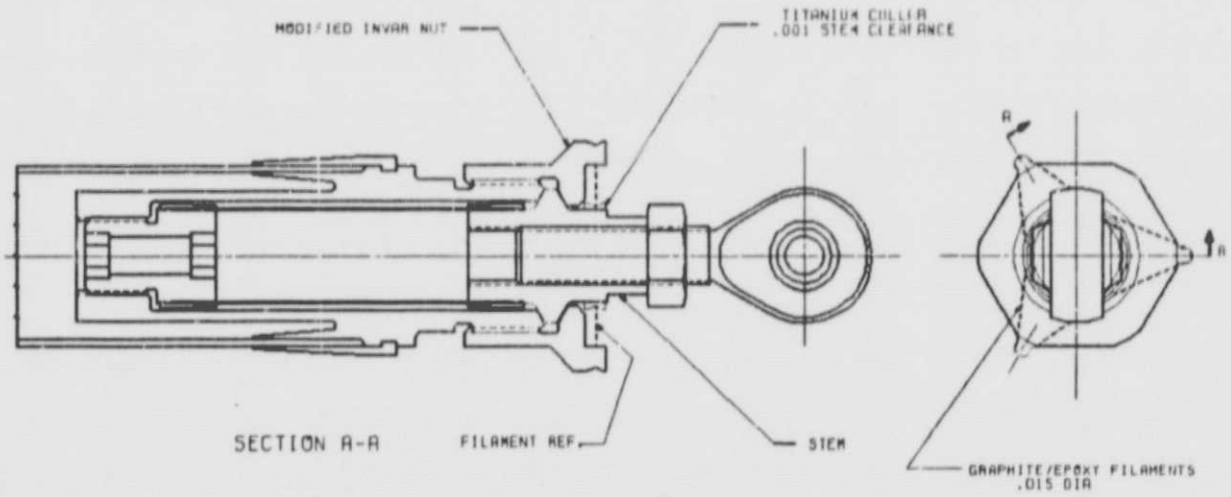

Fig. 7-13 PODS-IV Design Concept

7.5 ASYMMETRIC TEMPERATURE DISTRIBUTION TESTS

In orbit, a temperature gradient can exist around the circumference of the 6061 aluminum vacuum shell, placing uneven loads into the struts. This test simulates a temperature gradient of 0 K at one point(s) on the shell and 300 K at other point(s), much more severe than could ever occur in orbit. For this test, the aluminum plate (simulated tank) was suspended so that there was a minimal axial load on the struts.

The clevis attachment of individual struts (Fig. 7-4) was moved inward radially a distance of 0.22 cm (0.086 in.), simulating a temperature change from 300 to 0 K on a radius of 0.52 m (20.5 in.). Figure 7-14 shows combinations of strut movements. At no time did any of the struts short out. This demonstrates that asymmetric temperature distributions of the vacuum shell in orbit are not a problem for a six-strut support system.

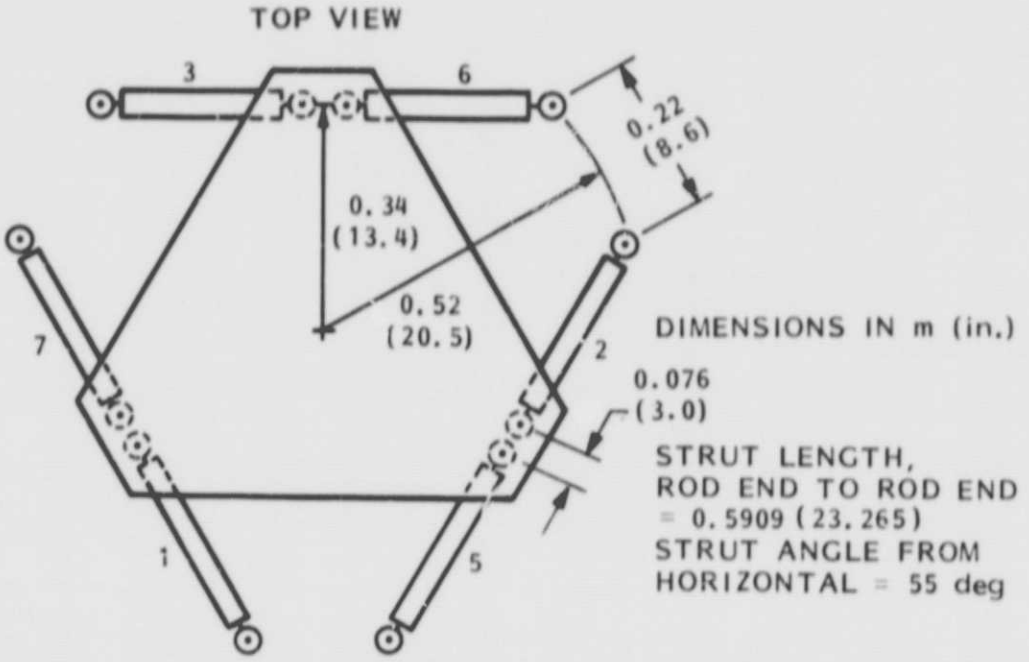

Vacuum Shell Strut End(s) Moved Inward on Radius, Back Out X = 0.22 cm (0.086 in.)	Simulated Vacuum Shell Temperature At Strut Clevis (K)						Shorting Noted on Any of the Six Struts
	1	2	3	5	6	7	
1	0	300	300	300	300	300	No
1,5 Simultaneously	0	300	300	0	300	300	No
1,7 Simultaneously	0	300	300	300	300	0	No
2	300	0	300	300	300	300	No
2,6 Simultaneously	300	0	300	300	0	300	No
3,6 Simultaneously	300	300	0	300	0	300	No

Fig. 7-14 Shorting Effect of Temperature Distributions Around the Vacuum Shell Circumference

Section 8
CONCLUSIONS AND RECOMMENDATIONS

8.1 CONCLUSIONS

The structural test results from this program plus the thermal test results from Reference 2 verify the adequacy of the design concept. Consequently, superfluid helium dewar lifetimes of 3 years are obtainable as predicted previously in Reference 1. The struts perform structurally as designed under all load conditions from ground hold through launch and orbit environments. Test data, analysis, and procedures are available for designing and fabricating the struts. Analytical methods are available for predicting strut shorting loads for a six-strut system under all load and temperature conditions. For very large dewar applications requiring a higher side-load shorting capability, a PODS-IV design modification is recommended that increases the side-load capability by a factor of 10 while increasing the strut conductance 10 percent or less.

8.2 RECOMMENDATIONS

The following recommendations resulted from this test program:

1. Use the PODS-III design concept shown in Section 3 if the side-load shorting capability is adequate. Increase the load gap spacing to 4 mil (from 3 mil) to increase the shorting load capability by 33 percent if needed. Use the PANDA-DEWAR program described in Reference 1 (or suitable modifications for specific designs) to optimize the struts.
2. Develop the PODS-IV design concept shown in Fig. 7-13 for large dewars with side loads up to ten times higher than the PODS-III concept can handle.
3. Use the manufacturing and assembly procedure specified in Section 5.

4. Substitute a two-piece rod end for the current three-piece design. Use Inconel 718 material for all parts and specify minimum free play in the rod ends. Perform a low-temperature fatigue test on the rod end before using in a flight application.
5. Use the procedure in Section 7.2 for installing six struts between the tank and vacuum shell.
6. Use Expando bolts on both the tank and vacuum shell attachments to minimize free play.

Section 9
REFERENCES

1. Parmley, R.T., Feasibility Study for Long Lifetime Helium Dewar, NASA-CR166254, Dec 1981
2. Parmley, R.T., Passive Orbital Disconnect Strut (PODS-III) Structural and Thermal Test Program, NASA-CR166473, Mar 1983
3. Owens/Corning Fiberglas Data Sheet on E, S, and S2 glass
4. Union Carbide Technical Bulletin 465-227 on Thornel 300 carbon fiber, Grade WYP 15 1/0
5. Internal Communication, R. Johnson
6. Handbook on Materials for Superconducting Machinery
7. Internal Communication, E. N. Yoshioka
8. Hust, J. G., "Materials Research for Superconducting Magnets - IV," Semi-Annual Report Mar 1, 1975 - Sep 1, 1975, NBS ADA019230
9. Kasen, M. B., Schramm, R. E., and Read, D. T., Fatigue of Filamentary Composite Materials, ASTM STP 636, 1977, pp 141-151
10. Bansemir, H. and Weiss, W., "Fibre Composites for Aerospace Structures," Cryogenic Engineering Conference, Aug 15-19, 1983
11. Hartwig, G., "Reinforced Polymers at Low Temperatures," Advances in Cryogenic Engineering, Vol 28, 1982, pp 179-189
12. Tobler, R. L. and Read, D.T., "Fatigue Resistance of a Uniaxial S-Glass/Epoxy Composite at Room and Liquid Helium Temperatures," J. Composite Materials, Vol 10, Jan 1976, pp 32-43
13. Gauchel, J. V., Olinger, J. L., and Lupton, D. C., "Characterization of Glass Reinforced Composites for Cryogenic Applications," Advances in Cryogenic Engineering, Vol 28, 1982, p 214
14. Radcliffe, D. J. and Rosenberg, H. M., "The Thermal Conductivity of Glass-Fibre and Carbon-Fibre Composites from 2 to 80 K," Cryogenics, May 1982, pp 245-249
15. Hust, J. G. and Arvidson, J. M., Thermal Conductivity of Glass Fiber/Epoxy Composite Support Bands for Cryogenic Dewars, NBS Report 275.03-78-2

16. Reed, R. P., and Clark, A. F., Materials at Low Temperature, ASME 1983, p 414
17. Thermal Conductivity of Solids at Room Temperature and Below, NBS Monograph 131, p 257
18. Kasen, M. B., "Cryogenic Properties of Filamentary-Reinforced Composites: An Update," Cryogenics, Jun 1981, pp 323-340
19. Reed, R. P., and Clark, A. F., Materials at Low Temperature, ASME 1983, p 95
20. Thermal Expansion of Technical Solids at Low Temperatures, NBS Monograph 29, May 19, 1961.
21. Cryogenic Materials Data Handbook, Vol II, AFML-TDR-64-280, Jul 1970